NASA Contractor Report 165513

External Fuel Vaporization Study

Phase II Final Report

E.J. Szetela
J.A. TeVelde

UNITED TECHNOLOGIES RESEARCH CENTER
East Hartford, CT 06108

November 1981

NASA
National Aeronautics and
Space Administration

Lewis Research Center
Cleveland, Ohio 44135

External Fuel Vaporization Study

TABLE OF CONTENTS

FOREWARD

This report describes the work done in the Phase II experimental effort of the study of external fuel vaporization for use in advanced aircraft gas turbine engines. The work was done under NASA Contract NAS3-21971. The Phase I analytical conceptual design effort was described in NASA Contractor Report 159850. In both Phases I and II, the NASA Program Manager was C. E. Baker and the UTRC Principal Investigator was E. J. Szetela.

SUMMARY

A major factor involved in the determination of the feasibility of external fuel vaporization in advanced aircraft gas turbine engines is the physical behavior of the fuel during the flash vaporization process. Of particular concern are the heat transfer rate in the heat exchanger and the performance of the orifice used in the throttling process. Experiments were run to determine key fuel properties including boiling points, dew points, critical temperature, critical pressure, heat transfer coefficients, deposit formation rates, and deposit removal in a flowing system. Three fuels were utilized in the experiments including Jet-A, Experimental Referee Broad Specification fuel (ERBS), and a premium No. 2 diesel fuel. Engine conditions representing the NASA Energy Efficient Engine (Ref. 1) at Sea Level Takeoff (SLTO), cruise and idle were simulated in the vaporization system and it was found that single phase flow was maintained in the heat exchanger and downstream of the throttle. Deposits encountered in the heat exchanger represented a thermal resistance as high as $1.3 \times 10^{-3} m^2$ K/watt and a deposit formation rate as high as $800 \mu gC/cm^2$ hr. These values are equivalent to a buildup of 0.055 cm of thickness in 36 hours resulting in a more severe fouling condition than originally anticipated. It was found that the deposit can be removed by cleaning with air at a temperature of 720 K for 10 minutes. The results indicate that the conceptual design of the vaporization system formulated in Phase I of the program is valid with the exception that more maintenance will be required because of a substantially greater cleaning frequency.

INTRODUCTION

Lean premixed/prevaporized (LPP) combustion is a technique for reducing flame temperature and luminosity, thus providing the potential for improving combustor durability, reducing the airflow required for combustor wall cooling, and reducing NO_x emissions. Catalytic combustion promises the same benefits along with the potential of greater combustor stability and additional emissions reductions. A particular problem with LPP or catalytic combustion is the fuel prevaporization requirement. Premixing ducts must be sufficiently long to permit droplet vaporization to occur and at the high pressures and temperatures that exist in high performance engines like the NASA Energy Efficient Engine (E^3), the use of excessively long passages may result in autoignition upstream of the flame stabilizer. A potential solution is to provide a fuel vaporizer which is external to the premixing duct. Thus, premixing ducts need only be long enough to achieve the desired fuel distribution.

During Phase I of the External Vaporization Study (Ref. 2), an analytical investigation was carried out to select three candidate external vaporizer concepts for aircraft gas turbines and to make a feasibility determination based on the use of one or more of these concepts. The concepts were analyzed from the standpoint of fuel thermal stability (coking), integration of the vaporizer system into the aircraft engine, engine and vaporizer dynamic response, startup and altitude restart, engine performance, control requirements, safety and maintenance. The results of the Phase I study indicated that of the three concepts analyzed, one concept (Concept 1) was favored because it had the potential of improving engine performance in terms of increased thrust/weight ratio over 3 percent and a decrease in specific fuel consumption of about 0.5 percent without a major deterioration of engine dynamic response, ground start, or altitude restart. Concept 1 contains a vitiated air-to-fuel heat exchanger operating at a pressure high enough to maintain the fuel in its liquid state. A throttling orifice is used for flash vaporization at the fuel injector operating pressure.

A major factor entering the consideration of vaporizing Jet-A or alternative fuels is their properties: critical temperature and pressure, effect of pressure on boiling points and dew points, rate of deposit formation and thermal resistance of deposits, and ease of deposit removal. During Phase II, these properties were measured for Jet-A, Experimental Referee Broad Specification (ERBS), and premium diesel fuel, and the impact of the results on the design of the heat exchanger was evaluated. This report covers the work done during Phase II of the study.

THERMODYNAMIC CONSIDERATIONS

A schematic diagram of the selected vaporization system is shown in Fig. 1. A small amount of fuel is added to compressor bleed air in an auxiliary burner which produces vitiated air at approximately 1200 K. The remainder of the fuel is heated in the vaporizer to a temperature which is sufficient to produce complete vaporization when the fuel is flashed across the throttle. Flash vaporization permits the heat exchanger to operate with a single phase fluid which helps to avoid dynamic instability during heating. This process is shown in Fig. 2; a complete list of symbols is found on page 25.

In this example, the pressure at the fuel injector is P_1 and the dew point of the fuel is T_1. Complete vaporization can be attained at Point A. This condition can be reached by maintaining the fuel at pressure P_2, heating the liquid fuel to temperature T_2 (Point B), and passing the fuel through a throttling orifice. Throttling with adiabatic conditions is a constant enthalpy process which results in conditions corresponding to Point A downstream of the throttle. The pressure drop across the throttle is (P_2-P_1) and the temperature drop is (T_2-T_1).

The example cited is somewhat idealized because the process requires a precise control of conditions at Point B. For instance, if the upstream throttle pressure is P_2 and the temperature is between T_2 and T_3, the fuel is in a mixed phase, a condition which is to be avoided by the selection of the flash vaporization process. The two phase state can be avoided throughout the fuel vaporization system by meeting two simple conditions. The fuel will always be a liquid in the heat exchanger if the pressure upstream of the throttle is maintained at Pc (critical pressure) or greater. Having met that condition, it is then only necessary to heat the fuel to a temperature T_2 or greater for complete vapor to be specified by thermodynamic equilibrium in the fuel manifold. The special condition where P_2 is equal to or greater than P_c requires that T_2 is equal to or greater than T_c.

The throttle inlet and exit conditions are shown in the data listed in Fig. 1 for five engine conditions. The minimum throttle inlet pressure is the "idealized" pressure previously called P_2, except for SLTO, where it is equal to compressor discharge pressure plus injector pressure drop. The minimum pressure is equal to the critical pressure at cruise and only slightly lower than the critical pressure at approach and idle. The selected pressure is set at injector inlet conditions at SLTO and at the critical pressure at the other three conditions. At SLTO and cruise, the minimum temperature is the critical temperature. At approach, idle and altitude relight the minimum temperature corresponds to Point B in Fig. 2. The calculated throttle inlet (vaporizer exit) temperature at SLTO is equal to the minimum required temperature because SLTO is the vaporizer design point. At all other (off-design) conditions, the calculated throttle inlet temperature which was obtained in the output of the heat exchanger computer program, is above the minimum value.

The throttle exit pressure listed in Fig. 1 is equal to the compressor discharge pressure plus injector pressure drop. The exit temperature was determined from thermodynamic considerations, e.g., Fig. 2. At SLTO the throttle is wide open and there is no temperature drop. At approach and idle conditions, the temperature drop across the throttle is quite small, as would be expected from the increasing level of throttle inlet temperature; a higher temperature brings the fuel vapor closer to an ideal gas which has no temperature drop during throttling (Joule-Thompson coefficient = zero, Ref. 3). It can be seen that the throttle exit temperature at off-design conditions equals or exceeds the minimum required (dew point) temperature, which is Point A on Fig. 2.

It might appear that except at altitude relight, the throttling process does not involve much flash vaporization because at high engine power (cruise) the operating conditions (P_1 and P_2) are near the tip of the dome in Fig. 2 and at low power (idle) the calculated temperature indicates that the fuel is in the vapor state. However, the design status of the vaporizer system is only preliminary, and if the design more closely approaches a hardware stage, other operating modes could be selected. For instance, the table in Fig. 1 shows that at approach and idle, the calculated throttle inlet temperature is considerably above the minimum value. If a lower vaporizer inlet (auxiliary burner exit) gas temperature were assumed, the calculated throttle inlet fuel temperature would be closer to the minimum temperature.

FUEL PROPERTY CONSIDERATIONS

Fuel property variations were considered analytically by checking the effect of various properties on the projected size and performance of the heat exchanger and experimentally by including three fuels in the test matrix. A final analytical assessment of the experimental results and their impact on the vaporization system performance was made at the end of the program.

The fuel properties that were considered in this program include thermal stability, critical temperature and pressure, specific heat, volatility and viscosity. In reviewing the influence of these properties on heat exchanger performance it was found that critical temperature significantly affects the size requirements of the heat exchanger while critical pressure has minimal effect on heat exchanger performance. Specific heat is the slope of the enthalpy temperature curve, and hence changes in enthalpy are directly related to changes in specific heat. Thermal conductivity is not appreciably affected by fuel type while viscosity is appreciably affected.

The variation in critical temperature, enthalpy and volatility was defined by comparing Jet A with hypothetical fuels having the properties shown in Table 1. Fuel critical temperature and enthalpy can be calculated (Ref. 4) from specific gravity and the distillation curve; gravity and distillation range of the hypothetical fuels were chosen to obtain an increase in critical temperature and enthalpy.

Table 1

Properties of Selected Fuels

	Jet-A	Hypothetical Fuels		
		1	2	3
Gravity (API)	43	33.5	53.5	43
Distillation Range (K)				
10%	464	492	372	492
90%	520	520	575	520
Critical Temperature (K)	683	715	683	694
Enthalpy at T_{crit} (KCal/Kg)	319	319	346	341

Hypothetical Fuel No. 1 has the specific gravity and 10 percent distillation point of No. 2 heating oil, the 90 percent distillation point of Jet-A, a critical temperature higher than that of Jet-A but the same enthalpy at the critical temperature. Hypothetical Fuel No. 2 has the specific gravity and 10 percent distillation point of JP-4, the 90 percent distillation point of No. 2 heating oil, critical temperature the same as that of Jet A, and a higher enthalpy at the critical temperature. Hypothetical Fuel No. 3 is the same as Jet-A except that it has the 10 percent distillation point of No. 2 heating oil and a higher critical temperature and enthalpy than those of Jet A. To obtain the effect of changes in fuel viscosity, data were obtained (Ref. 5) for a premium diesel fuel which has a viscosity that is 50 percent higher than that of Jet-A at room temperature. It was assumed that the viscosity-temperature curve for the diesel fuel had the same shape as the Jet-A curve.

The assessment of the effect of fuel properties indicated that in comparison with Jet-A, future aircraft fuels will impose more stringent design requirements on the external fuel vaporization system. The details of the analytical study of fuel property variations are found in the Appendix.

The use of the critical temperature and pressure in the design of the heat exchanger and the use of the flashing process at off-design conditions necessitated experimental verification of these critical properties for Jet-A and alternative fuels. It was also important to establish the region of pressure and temperature containing the two-phase dome. The extent of deposit formation and the effect of deposit on the heat transfer rate also required experimental determination. Since the hypothetical fuels previously discussed are not available, three real fuels were used: Jet-A, ERBS and premium No. 2 diesel fuel. Specimens of the three fuels were analyzed and the results are contained in Table 2.

Table 2

Analysis of Test Fuels

	Jet-A	ERBS	Premium Diesel
Specific Gravity @ 15.5C	0.7932	0.8417	0.8308
Sulfur ppm	547	252	1758
Nitrogen ppm	85	68	74
Copper ppm	0.26	0.02	< 0.01
Aromatics %	23.67	29.96	19.47
Naphthalenes %	1.88	7.98	4.21
Olefins %	0.55	0.57	0.70
Initial Boiling Pt K	438	461	451
30% Recovered K	472	488	505
50% Recovered K	484	501	522
70% Recovered K	500	519	541
Final Boiling Pt K	547	600	616

The Jet-A values are normal except that sulfur is slightly higher and copper is much higher than expected. The ERBS values are as expected except for sulfur and aromatic which are slightly lower than anticipated. Naphthalene content is greater than in Jet-A and copper content is much lower than in Jet-A. Premium diesel was named so because of its low aromatics content; however, sulfur content is much greater than that of Jet-A or diesel. All three fuels are potentially prone to deposit formation, Jet-A because of copper content, ERBS because of aromatics, particularly naphthalenes, and diesel because of its sulfur content.

RANGE OF EXPERIMENTAL DATA

The experimental conditions were selected to simulate parameters in the heat exchanger over a portion of the E^3 flight spectrum; high flow conditions such as SLTO could not be simulated because of the immense requirements of fuel supply and handling. Typical engine and rig parameters are shown in Table 3.

Table 3

Engine and Rig Fuel Parameters

	Engine				Rig	
	SLTO	Cruise	Approach	Idle	Min	Max
Inlet Velocity m/sec	4.9	2.2	1.2	0.36	1.3	2.6
Reynolds No. x 10^{-3}	27	12	6.9	2.1	1.9	3.8
Exit Fuel Temp. K	683	683	750	780	700	780
Fuel Pressure atm	34.6	21.8	21.8	21.8	21.8	31.2
Throttle ΔP atm	0	5.8	9.2	17	0.2	22

It can be seen that all conditions except the highest engine fuel velocity and Reynolds No. were simulated in the rig.

EXPERIMENTAL APPARATUS

The apparatus which was used to determine critical temperature and pressure, boiling points and dew points, deposit formation and deposit removal was a flowing system containing an electrically heated tube and its associated equipment. The critical temperature and pressure of petroleum fractions have often been measured in a static apparatus in which a small quantity of fuel is viewed while its temperature and pressure are varied (Ref. 6). Bubble points (initial boiling point), and dew points are determined by observation and the critical point is determined by extrapolation of the boundaries of the two-phase dome. Because fuel decomposes at temperatures approaching the critical point, the results usually depend on the time expired during the experiment. In Ref. 7, the author noted that in the static apparatus, a color change which was termed "critical opalescence" occurred in the fuel at the critical point. He reasoned that decomposition can be avoided by using an alternative apparatus in which the fuel is constantly flowing. A flowing apparatus was constructed, and again critical opalescence was observed. The data of Ref. 7 which includes critical points of 100 petroleum fractions determined by an opalescence criterion were correlated in Ref. 8 and the correlation is presently used in a standard procedure for calculating critical temperature and pressure (Ref. 4).

A similar flowing apparatus was used in the present program to determine the critical temperature and pressure of the fuels. It consisted of an electrically heated tube for the study of deposit formation and a special observation section was added for the study of phase changes. The apparatus was located in a concrete test cell which was equipped with a separate control room. The apparatus was capable of continuous operation at a fuel flowrate of up to [illegible] Kg/hr at pressures as high as 68 atm. A 64 kW DC electrical power supply was used to provide power for electrically heating the stainless steel tubes.

The arrangement of the components used for the determination of fuel phase boundaries (e.g., bubble points, dew points and critical point) and throttle performance is shown schematically in Fig. 3. It consists of the following major components: (1) a fuel supply and delivery system (2) a series of filters used to remove solid particulate contamination, (3) a turbine-type flowmeter, (4) a large pressure drop orifice to render fuel supply insensitive to pressure changes in the test apparatus, (5) a resistance heated tube connected to a 64 kW DC power supply, (6) a temperature controller used to maintain fuel exit temperature by regulating input power, (7) a viewing section used to observe and photograph the outlet fuel stream, (8) a fuel condenser, (9) a back pressure regulator to control test pressure, (10) a fuel dump tank, (11) a nitrogen purge system and (12) a hot air supply system used for tube cleaning. The same arrangement was used for heat transfer and deposit removal tests with the exception that the viewing section was removed.

Heated Tube Fabrication and Instrumentation

Tubes used for fuel heating were of stainless steel material capable of withstanding the pressures and temperatures in the test matrix. Phase boundary determination and throttling tests were conducted using an 0.64 cm OD x 0.09 cm wall AISI 304 tube. The length of the tube was 3.6 m. A throttling orifice with a diameter of 0.10 cm was located at the exit of the tube. The throttling orifice and viewing assembly is shown schematically in Fig. 4. The throttle discharged into a 5.0 cm diameter stainless steel reservoir which contained two round quartz windows with diameters of 2.5 cm. The window ports were arranged to permit straight-through viewing of a 5.0 cm^2 area which included the throttle and the downstream region. A photograph of the viewing section installed in the test apparatus is shown in Fig. 5. For the heat transfer tests and deposit removal tests, 0.32 cm OD x 0.05 cm wall AISI 316 tubes of 2.4 m length were used.

Prior to testing, the tubes were prepared in the following manner: cleaned with trichlorethylene, rinsed with acetone and dried with nitrogen. Each tube was instrumented with thermocouples attached to the outer wall to measure tube wall temperature. A schematic of an instrumented tube assembly used for heat transfer tests is shown in Fig. 6. In order to obtain an accurate measurement of wall temperature, each thermocouple was electrically isolated from the tube by a thin layer of ceramic paint. The thermocouple junction, whose size was no greater than 0.04 cm, was tightly pressed against the tube and secured with ceramic cement. The tube was insulated with 20.0 cm of bulk Fiberfrax to minimize heat losses.

Fuel temperatures were measured at the tube inlet, at 3 equally spaced intermediate locations and at the tube exit. It was felt that thermocouples immersed into the heated fuel can cause preferential deposit sites in the vicinity of the thermocouple. This was avoided by inserting along the tube three 1.0 cm OD x 1.9 cm long stainless steel cylinders with inner diameters equal to the tube ID, at equally spaced locations. It was experimentally determined that because of their low electrical resistance, the wall temperature of the thick cylinders was very close to the local fuel temperature. Temporary immersed thermocouples were added in clean tubes and it was found that the wall temperature of the thick cylinders was within 5 K of the fuel temperature measured by the immersion thermocouples.

The tube assemblies used for heat transfer tests and deposit removal tests were silver-soldered to copper bus bars used for electrical connections. In the tube assembly used for phase boundary and throttle performance tests, a thick stainless steel bus bar made a part of the viewing reservoir. An intermediate bus bar was used to provide capability for bypassing electrical power (5, 15 or 25 percent) around the downstream end of the tube to avoid a possible over-temperature condition at the aft end of the test section. This provision was only used in deposit removal tests to obtain a more uniform wall temperature distribution along the tube when cleaning with hot air.

Flow measurement was made with a turbine-type flowmeter located upstream of the test section. Pressures were measured with strain-gauge type pressure transducers.

Data Acquisition and Control System

All test data were recorded using a microprocessor-controlled datalogger. The data system, capable of scanning 70 input channels at a scan rate of 35 channels per second, converted the output signals from thermocouples, pressure transducers, etc., to precisely scaled DC voltages for measurement and converted the voltages for display of the data in appropriate engineering units. The reduced data were logged on paper tape either on demand or by programmed interval logging at a rate of 6 channels per second. A built-in cathode ray tube (CRT) displayed key operating variables, thereby providing a continuous visual display of up to 13 channels. An alarm function was utilized to provide a continuous check of test conditions. The alarm function allowed up to six alarm set points per channel. In the event that any variable exceeded a set point automatic shutdown would occur by actuating a contact closure which would initiate the automatic shutdown process.

In order to assure safe and unattended operation, a failure analysis was performed. The results of the failure analysis, shown in Table 4, served as guidelines for programming alarm set points on selected channels. The analysis indicated al possible failure modes, the means of detection and the appropriate corrective action.

Table 4

Failure Sensing and Interlock Reaction

Failure Mode	Signal to Sensor	Reaction
Tube rupture	Decreased tube pressure Increased flow	Shut down electrical power and fuel pump and initiate 3 minute N_2 purge
Clogged tube	Increased tube pressure Decreased flow	Shut down electrical power and fuel pump and initiate 3 minute N_2 purge
Electrical overpower	Increased amperage	Shut down electrical power and fuel pump and initiate 3 minute N_2 purge
Valve sticking	Loss of response to flow changes	Shut down electrical power and fuel pump and initiate 3 minute N_2 purge
Low supply flows	Decreased tube pressure Decreased flow	Shut down electrical power and fuel pump and initiate 3 minute N_2 purge
Wall temperature above maximum limit	High thermocouple indication	Shut down electrical power and fuel pump and initiate 3 minute N_2 purge

Shakedown tests were performed to simulate each failure mode and to verify the effectiveness of the corrective actions. All variables were continuously scanned and compared with the programmed set points. Results indicated that safe unattended operation was assured.

EXPERIMENTAL PROCEDURES

Separate operating procedures were used in the various aspects of the investigation which included the determination of phase boundaries (bubble points, dew points, and critical point), throttle performance, heat transfer during deposit formation, and heating-cleaning cycles.

Phase Boundaries

Determination of the fuel phase boundaries was made by visual observation during the transition from a single phase (liquid or vapor) to two-phase flow. A single light source (backlighting) and a video monitoring system provided the operator a clear indication of all phenomena occurring in the viewing section. The fuel flowrate was fixed at a value that resulted in a negligible pressure drop across the throttling orifice. Upon reaching a prescribed fuel pressure in the liquid phase, the fuel temperature was increased slowly until the appearance of a two-phase region at the orifice discharge signaled a bubble point. The pressure and temperature were recorded and subsequently, the fuel temperature was further increased until the two phase region disappeared and the vapor phase was reached. The fuel temperature was then slowly decreased until again the appearance of a two-phase region in the viewing section signaled a dew point. This procedure was repeated at fuel pressures ranging from 10 to 30 atm and fuel temperatures ranging from 600 to 800 K until the dew point and bubble point boundaries were obtained.

Extrapolation of the dew point and bubble point boundaries supplied a starting point for the determination of the critical pressure of the fuel. The fuel temperature was slowly increased at a constant pressure and flow rate until a color change was observed. If no color change was found, the fuel pressure was increased or decreased by approximately 0.1 atm and the procedure was repeated. Upon observation of a color change in the viewing section, photographs were taken to document the critical opalescence phenomenon.

Throttle Performance

The procedure for the throttle performance experiments consisted of establishing a prescribed fuel pressure downstream of the throttling orifice and adjusting the fuel flowrate to obtain a pressure drop across the orifice corresponding to that which would occur at engine operating conditions including SLTO, cruise and idle. The fuel temperature was then increased until a value representing engine operating conditions was reached. The viewing window was observed to document the presence or absence of a two-phase region and the temperatures and pressures were recorded at each condition.

System Stability

The determination of heat exchanger and throttle system stability was determined by establishing a prescribed condition (e.g., temperature, pressure and flowrate) and then perturbing either the pressure, flowrate or input power (temperature) for a short period of time (approximately 5-10 seconds). The perturbed setting was then returned to its original value and data were continuously recorded while the other heat exchanger conditions returned to original values. In the process, the time-history of the measured parameters was obtained.

Heat Transfer

The determination of deposit thermal resistance and deposit formation rate was preceded by a measurement of heat transfer rates in the clean tubes. The operating procedure used for each test (tube) was to first obtain tube wall temperature distributions at fuel flow rates of 14, 20 and 27 Kg/hr and at a prescribed value of fuel exit pressure and temperature. Input power, pressures, wall temperatures, and fuel bulk temperatures were recorded at each flow rate upon reaching steady state conditions. Subsequently, the flow rate was adjusted to the prescribed values for long term testing. All instrumentation was continuously monitored and automatically recorded in 30 minute intervals. Appropriate limits were set on tube wall temperatures, power input, fuel pressures and fuel flowrates; if limits were exceeded, the run was terminated by an automatic shutoff of power and fuel flow and startup of a 3 minute nitrogen purge. Termination of each test occurred at the end of 36 hours or sooner if a limit of wall temperature or tube pressure drop was reached. Tests were performed at fuel flow rates of 14, 20, and 27 kg/hr, fuel pressures of 23.8 and 30.6 atmospheres and fuel exit temperatures of 700 and 780 K.

After each test, the tube was divided into several sections for post-test analysis. The mass of the deposit was determined in twelve of the sections by passing hot air at approximately 900 K through the inside of the tube section(7.6 cm length) while continuously recording the CO_2 of the effluent gas stream. The apparatus used for the deposit burnoff tests is shown schematically in Fig. 7. Knowledge of the air flowrate and percentage of CO_2 in the effluent yields the total mass of carbon in the test section. The carbon evolved during the process was considered to represent the mass of the deposit.

Tube Cleaning

Tube cleaning tests consisted of cycles which were divided into two portions. The deposit formation portion was run at a flowrate of 14 kg/hr, a fuel exit temperature of 730 K and a fuel pressure of 30.6 atm for a period of 5 hours. The cleaning portion was run for 10 minutes using air at temperatures ranging from 710 K to 810 K. Tube wall temperatures were recorded every 30 minutes during heating and every 2 minutes during cleaning.

EXPERIMENTAL RESULTS

The experimental program was run with three fuels: Jet-A, ERBS, and premium diesel. The program was divided into three categories as follows:

1. Throttle performance which included a determination of the transient stability of the heat exchanger-throttle system and examination of the flow at the throttle exit for single-phase purity. It was also convenient in this portion of the program to measure critical temperature and pressure and to define the region encompassing the two-phase dome.

2. Deposit formation which consisted of the determination of the heat transfer rate in clean tubes and during operation with deposit forming conditions. During this portion of the program, post test analysis was performed including morphology using a scanning electron microscope, deposit composition using a scanning electron microprobe and measurement of deposit mass.

3. Deposit cleaning which consisted of cyclic tests as follows: fuel heating periods of 5 hours were followed by hot air cleaning periods of 10 minutes.

Throttle Performance

The throttle was a drilled hole with a 0.10 cm diameter in a plate which was 0.094 cm thick. Although the fuel pressure was above the critical pressure at the throttle entrance, the temperature was high enough to considerably reduce the fuel density; as a result, the flow was semi-compressible. The pressure loss was calculated as a function of assumed flow coefficient and the results were compared with the measured pressure loss as shown in Fig. 8. The results indicated that the throttle flow coefficient was approximately 0.73.

Initial testing indicated that an instability was present in the flow system. It was manifested by the inability to change the input power and thus vary the fuel exit temperature without an accompanying change in flow rate and pressure as shown in Fig. 9. An orifice of fixed size was added at the tube inlet and the problem was solved. The orifice had a pressure drop of approximately 7 atm at the minimum rig flow and 22 atm at the maximum flow.

Following the installation of the tube inlet orifice, a series of tests was run to investigate the stability of the flow system. The first test was run by rapidly increasing the flow rate of the fuel while the power (heat flux) was held constant, then decreasing the flow rate to its initial value. The temperature and pressure each responded to the initial increase and subsequent restoration of flow rate as shown in Fig. 10. The next test was run by first decreasing, then increasing the fuel pressure. Flow rate and temperature excursions were minimal as shown in Fig. 11. The final test involved a power (exit fuel temperature) change. Flow rate and pressure responded to the initial increase and subsequent restoration of power as shown in Fig. 12. The results of the stability tests indicated that a vaporization system consisting of a single heated tube and orifice has satisfactory stability characteristics.

Critical temperature and pressure were measured by noting a color change at the throttle exit. As shown in Figs. 4 and 5, a reservoir containing a viewing window was located immediately downstream of the throttling orifice. With proper lighting, the presence of liquid, vapor, or a two-phase mixture could be distinguished in the reservoir. In the liquid state, the outline of the jet leaving the orifice was easily seen, but in the vapor state, the jet was not clearly visible. The two-phase mixture was characterized by the presence of density gradients which caused a portion of the stream to become opaque. When the critical point (temperature and pressure) was reached, the color seen throughout the window changed from shades of grey to a distinct yellow-red as seen in Fig. 13. The color was fairly uniform; however, the hue at the periphery of the window was sometimes different from the hue at the center.

The temperatures and pressures at which the critical opalescence was observed are contained in Table 5. These values are based on conditions upstream of the throttling orifice.

Table 5

Critical Temperatures and Pressures

	Temperature, K	Pressure, atm
Jet-A	683	23.3
ERBS	717	23.3
Premium Diesel	728	21.6

The yellow-red color persisted over a temperature range of approximately 6 K and a pressure range which was small enough to be negligible. The throttle pressure drop was maintained at approximately 0.3 atm and the throttle temperature drop was approximately 6 K.

The two-phase region is enclosed by the boiling point (bubble point) line on the liquid side, the dew point line on the vapor side; the critical point connects the two lines. Bubble points and dew points were measured by setting a single phase condition, then varying the pressure and/or temperature while viewing the reservoir window in a video monitor and noting the appearance of the second phase. Bubble points and dew points were measured for the three fuels and the results are shown in Fig. 14. A sharper delineation was noted between the liquid and the two-phase region than between the vapor and the two-phase region. As a result, the bubble point data contain less scatter than the dew point data.

It was shown in Table 1 that at the SLTO design point, the heat exchanger was designed to deliver fuel at its critical temeprature. The fuel pressure, which is equivalent to the sum of the burner pressure and the injector pressure drop, is considerably higher than the critical pressure of the fuel; the fuel has properties which are similar to those of a liquid. The burner pressure at SLTO is also above the critical pressure of the fuel. Since there is no change in the phase conditions of the fuel from the heat exchanger to the burner, the throttle is essentially wide-open. At off-design conditions such as cruise, approach, and idle, the pressure and temperature at the heat exchanger outlet are higher than the critical pressure and temperature and there is no change of phase in the heat exchanger. The pressure and temperature at the throttle outlet were chosen to establish a single phase at that location. To check these premises, tests were run in which conditions simulating SLTO, cruise, and idle were fixed at the throttle entrance and exit. It was found that the two-phase region was successfully avoided as shown in Fig. 15.

Heat Transfer and Deposit Formation

Heat transfer and deposit formation data were obtained for three fuels over a range of time, flow rate, pressure, and exit fuel temperature. A total of 13 tubes were tested; a summary of the test conditions for all of the tubes is contained in Table 6. The test matrix included 4 tubes (tests) with Jet-A, 5 with ERBS, and 4 with premium diesel fuel. The planned test matrix called for an uninterrupted test duration of 36 hours in nearly all tests. Intermediate shutdowns resulted from problems in the test apparatus or in the data logging system.

There were three reasons for test terminations: completion of planned duration, pressure drop increasing in a manner indicative of large internal area reduction, or a maximum limit of wall temperature (1030 K). Excluding test no. 2 which was shut down because of inadvertent plugging, 3 of the tests were run to full duration, 4 were shut down for excessive pressure drop, and 5 were shut down for excessive wall temperatures. The average test duration for each fuel was as follows: Jet-A (excluding Test 2) was 27.8 hours, ERBS was 20.6 hours, and premium diesel was 7.4 hours. The relatively better ranking of Jet-A over ERBS cannot be explained by the measured properties contained in Table 2, Analysis of Test Fuels.

The variation of initial pressure drop with fuel flow closely followed the square law; pressure drop increased with the square of fuel flow. Pressure drop also increased with exit fuel temperature because of the strong dependence of density on temperature at values near to and above the critical temperature.

Heat Transfer Measurements

Heat transfer coefficients were obtained from measurements of input electrical power, wall temperature, and fuel bulk temperature. Wall temperature was measured at twenty (20) axial locations; local bulk temperature was measured at the inlet, exit and three intermediate locations. The following equation was used to derive heat transfer coefficients for the fuel from the initial measurements obtained with clean tubes.

$$H = \frac{Q}{A(T_W - T_F)} \qquad (1)$$

Table 6

Summary of Test Conditions

Test No.	1	2	3	4	5	6	7	8	9	10	11	12	13
Fuel	Jet-A	Jet-A	Jet-A	Jet-A	ERBS	ERBS	ERBS	ERBS	ERBS	Diesel	Diesel	Diesel	Diesel
Flow Rate Kg/hr	13.6	13.6	13.6	20.4	13.6	13.6	20.4	27.2	13.6	27.2	20.4	13.6	27.2
Inlet Reynolds No. x 10^{-3}	1.5	1.5	1.5	2.2	1.5	1.5	2.2	3.0	1.5	3.0	2.2	1.5	3.0
Inlet Pressure atm	24.8	31.3	31.3	31.3	24.8	31.3	31.3	31.3	24.8	31.3	31.3	31.3	31.3
Exit Temperature K	700	780	780	780	700	780	780	780	700	780	780	780	780
Run Time hrs	36	12	36	12	36	21	10	9	27	9	5.5	10	5
Shutdown Reason	Time	*	Time	Wall Temp.	Time	Pressure Drop	Wall Temp	Wall Temp	Pressure Drop	Pressure Drop	Wall Temp	Pressure Drop	Wall Temp
Initial Max. Wall Temp. K	745	815	845	835	745	845	845	835	765	835	835	835	840
Final Max. Wall Temp. K	995	955	980	1030	910	975	1030	1040	860	1015	1050	1015	1030
Initial Pressure Drop atm	0.34	0.68	0.68	1.5	0.27	0.61	1.3	2.4	0.20	2.2	1.2	0.68	2.2
Final Pressure Drop atm	1.1	*	3.4	2.1	2.2	3.7	2.3	3.6	6.0	5.6	2.4	5.0	4.3
No. of Intermediate Shutdowns	1	1	2	3	5	None	None	1	None	1	1	None	None

* Inadvertent use of copper sleeve in fitting at downstream end of tube resulted in premature plugging.

This equation assumes that the measured outer wall temperature is equal to the inner wall temperature and that external heat loss is negligible. Both assumptions were checked analytically and appeared to be valid. The measurements indicated that near the tube entrance, wall temperature did not increase monotonically as shown in Fig. 16. The behavior at the tube entrance appeared to be representative of an entrance effect which was more pronounced at low Reynolds Number.

The initial clean tube maximum wall temperature occurred at the downstream end of the tube and it was not appreciably affected by flow rate. This means that the flow in the downstream portion of the tube was turbulent and that the fuel heat transfer coefficient at that location was approximately proportional to the fuel flow. Heat transfer coefficients in the turbulent region which depend in part on the viscosity and specific heat of the fuel, were considerably affected by the fuel temperature because of the dependence of fuel properties on temperature. The ratio of heat transfer coefficient to mass flow rate, $h/\dot{w}$, for all of the tubes is shown for the three fuels as a function of fuel temperature in Figs. 17-19. Because the wall temperature increases with the fuel bulk temperature in the turbulent portion of the tube (Fig. 16), the effect of wall temperature cannot be distinguished in the correlation. Although there is scatter in the data shown in Figs. 17-19, the dependence of heat transfer coefficient on fuel temperature is evident.

The presence of fuel deposits resulted in an increase in tube wall temperature in the turbulent region of the tube as shown in the example in Fig. 20; however, in the laminar entrance region, the wall temperature was often reduced as in the first 0.5 m of length in Fig. 20. Post test appearance of the tubes occasionally indicated the presence of two dark bands near the tube entrance and it was suspected that there were two regions of elevated wall temperature in some tubes. The exact axial position of the dark bands was not reproduced among the tubes; however, the thermocouple placement in one of the tubes revealed a double peak in the axial wall temperature pattern near the tube entrance as shown in Fig. 21. It was also found with this tube that the wall temperature in the vicinity of the upstream peak increased slightly with time and near the second peak, the wall temperature decreased with time. After 7 hours, the second peak had essentially disappeared.

Scanning electron photomicrographs which will be shown in a separate section of this report indicated that deposit roughness was usually greater than the roughness of a clean wall. The deposit roughness resulted in a change in the boundary layer and an increase in the heat transfer coefficient; however, this effect was too small in the turbulent region to overcome the added thermal resistance due to the deposit and the net result was an increase in wall temperature. In the laminar region, increased roughness resulted in an earlier transition to turbulent flow; the effect of the transition on the heat transfer coefficient was greater than the effect of deposit resistance, resulting in a decrease in wall temperature (Figs. 20 and 21). At higher Reynolds numbers where the apparent entrance region was less significant, there was less tendency for a decrease of wall temperature with time as indicated by a comparison of Figs. 20 and 22.

Time histories of wall temperature and pressure drop measured during tests which were terminated for each of three reasons, completion of planned duration, excessive pressure drop, and maximum wall temperature, are shown in Figs. 23-28. The tube wall thermocouples indicated that as deposits formed, the wall temperature gradually increased with time (unless the run was interrupted by an intermediate shutdown) as shown in Fig. 23 which represents a full-duration run. After the shutdowns which occurred near the 6th and 11th hours, the wall temperatures decreased; some of the thermocouples indicated temperature decreases of over 100 K. Frequently the wall temperature reached a constant level as in Figs. 23 and 25. In some cases, the wall temperature continued to increase throughout the run until it reached the maximum limit as shown in Fig. 25. Fig. 27 typifies a run which was terminated when the pressure drop became excessive. The location of the area reduction region is not apparent from the wall temperature readings from the same run as shown in Fig. 24 because there may have been no thermocouple at the position representing the greatest deposit. Although wall temperature at a particular location often reached a constant value, pressure drop always increased with time (Figs. 26-28).

The increase in wall temperature can be related to the thermal resistance of the deposit, t/k, if it is assumed that the fuel heat transfer coefficient remains constant with time. The following equations are used:

$$Q/A = U\,(T_W - T_F) \qquad (2)$$

$$\frac{1}{U} = \frac{1}{h} + \frac{1}{t/k} \qquad (3)$$

As expected from the variation found in the increase of the wall temperature along the tube length shown in Figs. 20 and 22, the thermal resistance of the deposit did not vary monotonically with temperature. Composite plots of data obtained with Jet-A and ERBS during tests of long duration (over 20 hours) are shown in Figs. 29 and 30. It can be seen that deposit resistance is a non-monatonic function of temperature. The peak value for both fuels is approximately 1×10^{-3} m^2 K/watt. This value is approximately 3 times as high as the peak value of 3.5×10^{-4} m^2K/watt assumed for Jet-A in the external fuel vaporization conceptual design study. Reaction rates are generally believed to increase with temperature and this factor can be used to explain the slope of the left side of the curve. The slope of the right side may be due to a change in the reaction mechanism. It may also be due to depletion of reactive species such as dissolved oxygen; in heated tube tests, the greatest deposit formation usually occurs considerably upstream of the exit end of the tube even though the greatest clean-tube temperature occurs at the exit end. The peculiar shapes of the curves in Fig. 29 and 30 has been reported by other investigators (Refs. 9-11).

The relation between wall temperature and time shown in Figs. 23-25 indicates that increase in deposit thermal resistance with time is not linear. A composite plot of peak deposit thermal resistance which includes three values for each of the tests at three times indicates that thermal resistance increased more rapidly at short times than at longer times as shown in Fig. 31. The short-time increase with Jet-A was greater than with ERBS but the long-time increase with ERBS was greater. The rate of increase of thermal resistance with premium diesel was greater than with the other two fuels.

Post-Test Deposit Analysis

Analysis of the tubes after testing included burning of the deposit to determine the quantity of carbon, visual examination of the deposits, determination of deposit morphology, and measurement of the chemical constituents of the deposit. It was felt that the primary constituent of the deposits was carbon, and a determination of the carbon mass gave a reasonable approximation of the mass of the deposit.

Twelve sections of each tube were chosen for analysis and the initial (clean wall) temperature at the center of each section was noted. The carbon mass was determined by flowing air through an individual section of the tube while it was immersed in an oven which was held at a temperature of 900 K. The quantity of CO_2 in the effluent was continuously recorded and after the carbon was completely burned, the recorded data were integrated to determine the total mass of carbon removed from the tube section. The carbon mass was plotted for each tube as a function of initial wall temperature.

The section of the tube containing the greatest deposit was usually located near the center of the tube rather than at the entrance or exit. The location of the peak did not exactly coincide with the location of the maximum thermal resistance, but the two peaks were close together as shown in Fig. 32. It can also be seen in Fig. 32 that considerable deposit was found near the entrance of the tube where the wall temperatures were found to decrease with time. However, the level of deposit formation at the entrance did not correspond to the level found at an equivalent wall temperature near the center of the tube.

Composite plots of rate of deposit formation for Jet-A and ERBS are shown in Figs. 33 and 34. The curves were found to be non-monatonic with a peak at a temperature of 650 - 750 K. This temperature range corresponds to the temperatures associated with the peak values of deposit thermal resistance in Figs. 29 and 30. The peak value of deposit formation rate with Jet-A was four times as high as the value assumed in the conceptual design study. An attempt was made to relate the peak values of deposit formation rate with run time and the results are shown in Fig. 35. The data are too scattered to depict the nature of this relationship.

Visual examination showed that the deposit had a dark color except in rare instances when the color had a slight hue of either red or grey. It was evident from visual examination that the surface formed by the deposit was usually rougher than the unused tube surface, and that the roughness varied in magnitude. In the limit, protrusions in the form of dendrites appeared to grow from the surface. The dendrites were usually found near the center of the tube where the greatest thermal resistance developed during the heating period. An attempt was made to mount and polish tube specimens in order that the deposit could be viewed in crossection. However, the deposit was too soft to withstand the preparation process. Scanning electron micrographs were made of an unused tube and of a number of deposits; the results are shown in Fig. 36. The varied roughness of the deposit can be seen by comparing the relatively smooth deposit with the rough or dendritic variety.

To determine the major constituents of the deposits, samples were scraped from the tubes and analyzed using a scanning electron microprobe. All deposits were found to have carbon as the chief ingredient as indicated by the high density of white dots in Fig. 36. In addition, Jet-A deposits contained copper and sulfur and premium diesel deposits contained sulfur; ERBS deposits had negligible quantities of either constituent as shown in Fig. 37. A search for additional constituents was made and it was found that deposits obtained with ERBS and premium diesel contained oxygen and nitrogen as shown in Fig. 38. The presence of oxygen, sulfur, nitrogen, and copper all increase the tendency for deposit formation (Ref. 12); therefore, their presence in the deposits was not surprising. Red and grey deposits contained various metals such as lead, silicon, and copper which may have diffused from brazed joints.

Deposit Cleaning Tests

Deposit cleaning tests were run by alternating 5 hour heating periods during which fuel was flowed through the tube with 10 minute cleaning periods during which heated air was substituted for the fuel. A total of five tests were run as shown in Table 7.

Table 7

Cleaning Test Matrix

Test No.	Fuel	Nominal Cleaning Temp.	No. Cycles
1	Diesel	815	5
2	Diesel	760	5
3	Jet-A	775	5
4	Jet-A	715	5
5	Jet-A	715	9

The nominal cleaning temperature refers to the wall temperature at the center of the tube. Wall temperature along the tube was not uniform; it varied approximately 30 K at low cleaning air temperature and 100 K at high cleaning air temperature. The process of burning resulted in a temporary increase in wall temperature of approximately 20 K during cleaning.

It was found that the cleaning process was effective in all tubes tested. After each cleaning period, the tube wall temperature returned to the value initially measured at the beginning of the first cycle as shown in Fig. 39 for Test 1 and Fig. 40 for Test 3. The first cycle of Test 1 was run with a lower fuel flow and only the 2nd-4th cycles are shown. The upper set of curves contains measurements in turbulent flow where wall temperature increased with time and the lower portion contains measurements in the transition region where wall temperature decreased with time. The curves are generally reproduced after each cycle showing the effectiveness of the cleaning process. All of the tubes were sectioned and examined with a scanning electron microprobe for the presence of carbon sulfur, nitrogen, and copper and no evidence of residual deposit was found.

IMPACT OF RESULTS ON VAPORIZATION SYSTEM

Many of the measured data which are significant in defining the external fuel vaporization system compare favorably with the key parameters used in the conceptual design study but in some cases considerable differences were noted. A summary of data comparisons is contained in Table 8.

Table 8

Comparison of Measured and Assumed Parameters

	JET-A		ERBS	
	Assumed	Measured	Assumed	Measured
Critical Temperature, K	684	684	700	717
Critical Pressure, atm	23.3	23.3	22.8	23.3
Max. Deposit Thickness, cm	0.020	0.055*	0.033	0.055*
Time to Reach Max. Thickness, hrs	100	36	100	28
Single Phase at Throttle Exit	Yes	Yes	Yes	Yes
Stable Flow	Yes	After Orifice Addition	Yes	After Orifice Addition
Deposit Removal With Hot Air	Yes	Yes	Yes	Yes

* Derived from deposit thermal resistance for comparison

With Jet-A, a favorable comparison of critical temperature and pressure, the stable performance, and deposit removal was demonstrated. Stable flow was obtained with a simple orifice at the heat exchanger inlet which imposed a relatively small pressure loss and pumping penalty on the fuel delivery system. The measured deposit thermal resistance was 2.7 times the anticipated value and it occurred in 36 hours instead of 100 hours as anticipated. With ERBS, the critical temperature was 17 K higher than anticipated. The deposit thermal resistance with ERBS was 1.7 times the anticipated value, occurring in 28 hours. The use of premium diesel resulted in severe deposit problems in 5-10 hours and it cannot be considered for use in an external fuel vaporization system.

The difference between the measured and assumed heat transfer resistance of the Jet-A deposit can be offset by increasing the compressor bleed flow at SLTO from 2.85 percent to 3.74 percent. Since the bleed flow used in cooling the turbines of high pressure ratio engines such as E^3 is considerably greater than 3.74 percent, there is no engine performance penalty associated with this increase. A relatively minor impact will result in the form of a larger auxiliary burner and larger pipes and manifolds for handling the air. The difference between measured and anticipated critical temperature with ERBS will require a further increase in bleed flow to 4.8 percent.

A serious compromise results from finding that deposit thickness as derived from measured deposit thermal resistance and deposit formation rate measurements reached the values shown in Table 8 (0.055 cm) in very short time periods. Cleaning would be required more frequently than anticipated: 36 hours instead of 100 hours with Jet-A and 28 hours instead of 61 hours with ERBS.

CONCLUSION

The fundamental fuel property data required in support of the study of external fuel vaporization was successfully acquired by the experimental program. The concept of flash vaporization which delivers single phase fuel requiring no further heat addition for vaporization in the engine combustor was demonstrated and the two-phase region was avoided in the process. A flow instability which was noted in the beginning of the experimental program was eliminated by adding an orifice upstream of the heat exchanger. Removal of deposits was achieved using air at reasonable temperature. However, severe deposit formation was encountered which requires considerably greater cleaning frequency than previously expected. Although cleaning of the deposits with heated air appears to be feasible, the problem of maintenance would be severe.

REFERENCES

1. Saunders, N. T.: Advanced Component Technologies for Energy Efficient Turbofan Engines. AIAA Paper 80-1086, July 1980.

2. Szetela, E. J. and L. Chiappetta: External Fuel Vaporization Study, Phase I Report. NASA CR 159850. June, 1980.

3. Lay, J. E.: Thermodynamics. C. E. Merrill Publishing Co., 1963.

4. Technical Data Book -- Petroleum Refining, Second Edition. American Petroleum Institute. 1970.

5. Cohen, S.: Private Communication. October, 1980.

6. Bahlke, R. and Kay, W. B.: Physical and Thermal Properties of Petroleum Distillates. Ind. Eng. Chem. 24, 291. 1932.

7. Roess, L.: Determination of Critical Temperature and Pressure of Petroleum Fractions by a Flow Method. Journal of Institution of Petroleum Technologists. V. 22, 1936.

8. Smith, R. L. and Watson, K. M.: Boiling Points and Critical Properties of Hydrocarbon Mixtures. Ind. Eng. Chem. 29, 12, 1937.

9. Taylor, W. F., and Frankenfeld, J. W.: Development of High Stability Fuel. Exxon Report GRV. 12 GAHF.75. January, 1975.

10. Hazlett, R. N. Progress Report on Advanced Hydrocarbon Fuel Development. Naval Research Laboratory. March, 1975.

11. Spadaccini, L. and Szetela, E. J.: Approaches to the Prevaporized-Premixed Combustor Concept for Gas Turbines. ASME 75-GT-85. 1975.

12. Szetela, E. J.: Deposits from Heated Gas Turbine Fuels. ASME 76-GT-9. 1976.

NOMENCLATURE

A	Surface Area	m^2
h	Heat Transfer Coefficient	watts/m^2K
k	Thermal Conductivity	watts/mK
P	Pressure	atm
Q	Heat Flux	watts/m^2
t	Thickness	m
T	Temperature	K
U	Overall Heat Transfer Coefficient	watts/m^2K
$\dot{w}$	Mass Flow Rate	Kg/hr

Subscripts

C	Critical
F	Fuel
W	Wall

EXTERNAL VAPORIZER — FUEL SYSTEM DIAGRAM

SCHEME 1 — FLASH VAPORIZATION

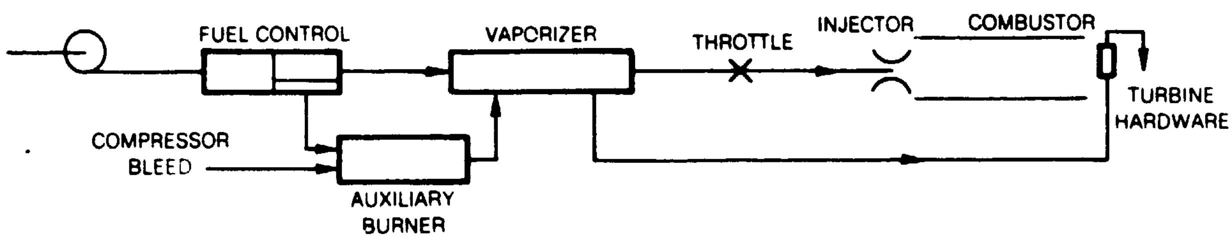

	SLTO	CRUISE	APPROACH	IDLE	ALTITUDE RELIGHT
COMPRESSOR DISCHARGE					
PRESSURE ATM	31 1	13 8	11 7	4 4	0 38
TEMP K	810	754	621	473	220
VAPORIZER INLET					
AIR TEMP K	1185	1145	1000	865	1255
FUEL TEMP K	311	311	311	311	311
THROTTLE INLET					
MINIMUM PRESSURE ATM	34 6	21 8	21 1	20 7	13 6
SELECTED PRESSURE ATM	34 6	21 8	21 8	21 8	21 8
MINIMUM TEMP K	683	683	678	636	585
CALCULATED TEMP K	683	683	750	780	585
THROTTLE EXIT					
PRESSURE ATM	34 6	16 0	12 6	4 7	0 38
TEMP K	683	660	750	780	495
DEW POINT K	683	660	644	594	495
INJECTOR ΔP %	10	10	7	4	8

FIG. 2

FUEL VAPORIZATION PROCESS

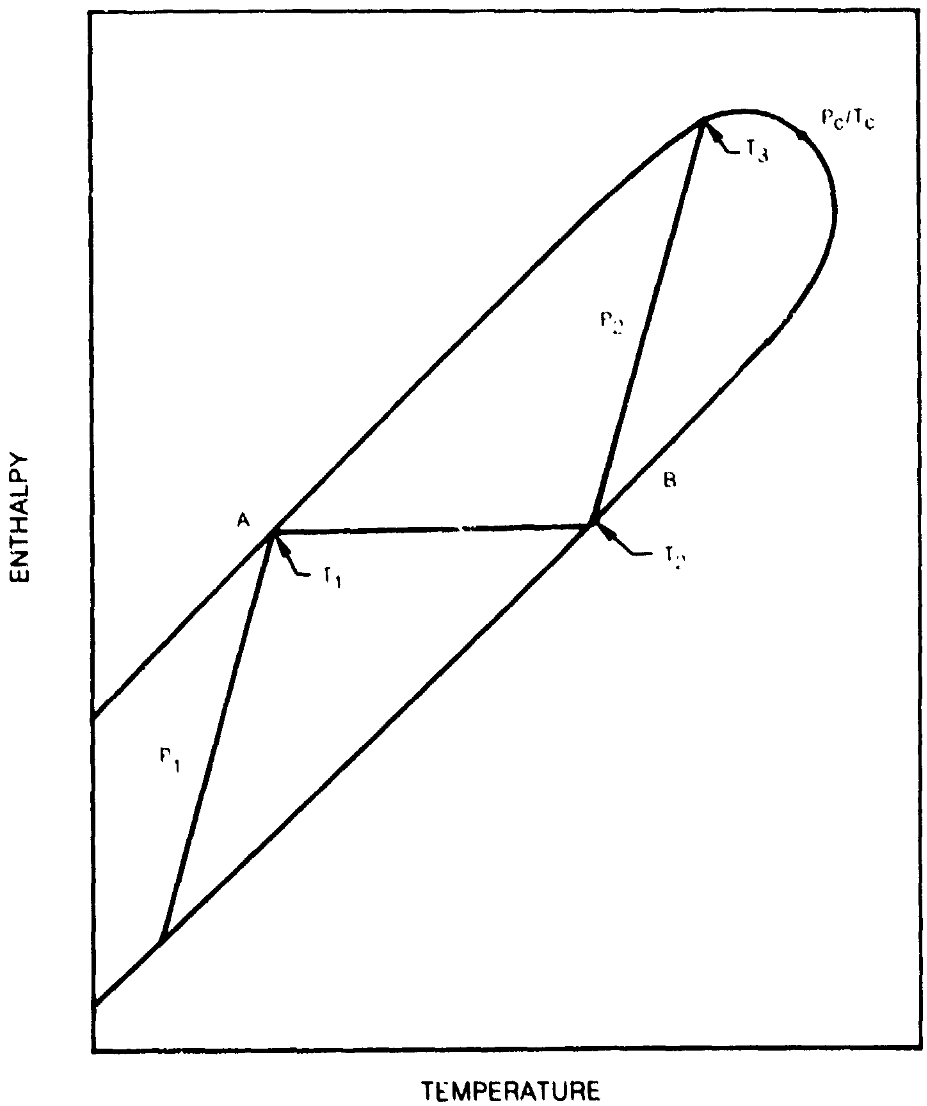

VAPORIZER-THROTTLE VALVE SIMULATOR TEST APPARATUS

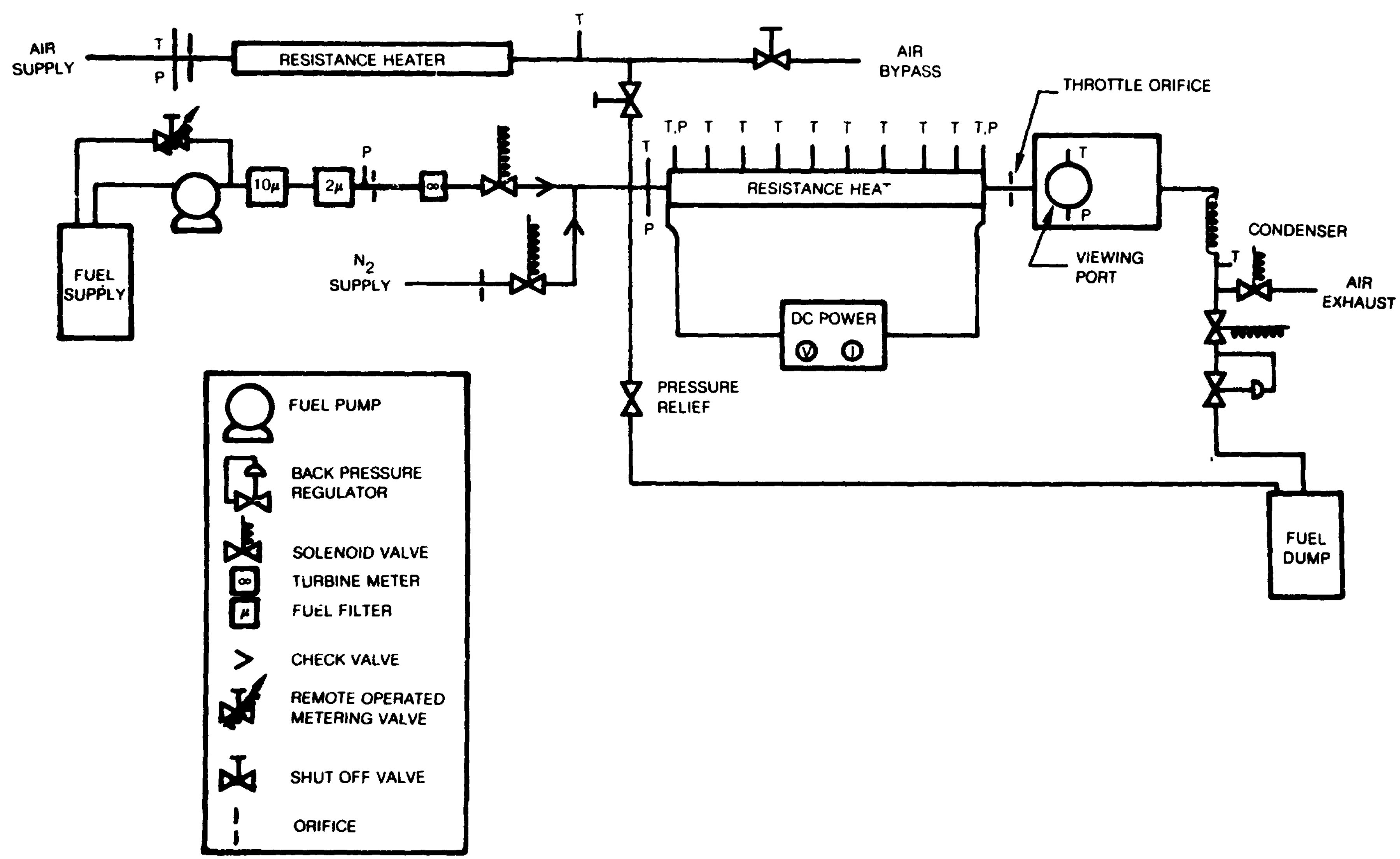

FIG. 3

81-8-44-2

FIG. 4

THROTTLE ORIFICE AND VIEWING SECTION

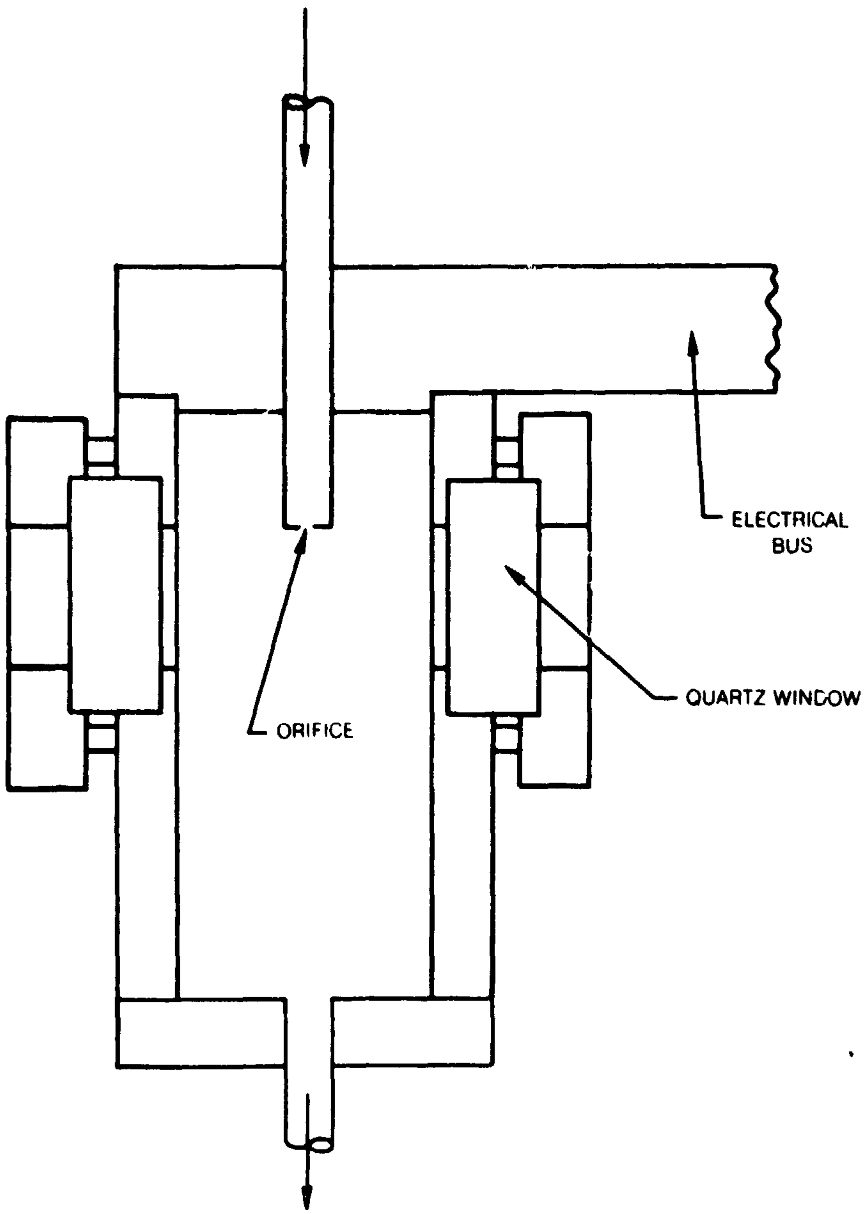

81-8-44-12

FIG. 5

VIEWING SECTION INSTALLATION

FIG. 6

TEST ASSEMBLY INSTRUMENTATION

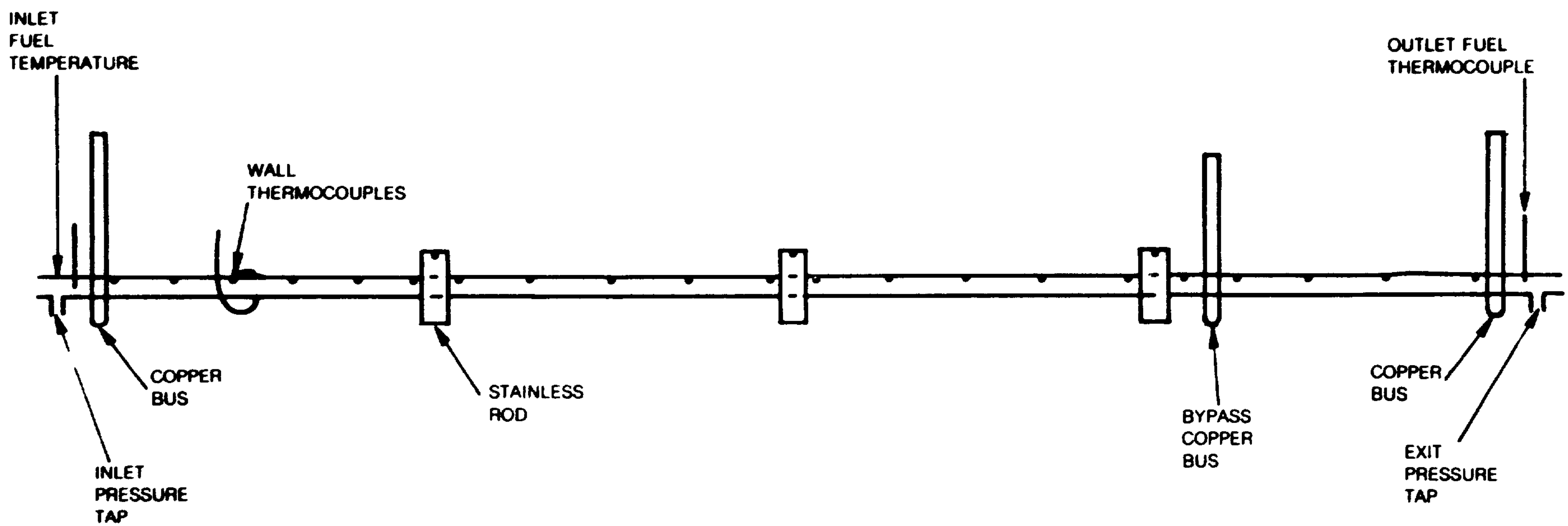

81-9-97-2

FIG. 7

DEPOSIT BURNOFF APPARATUS

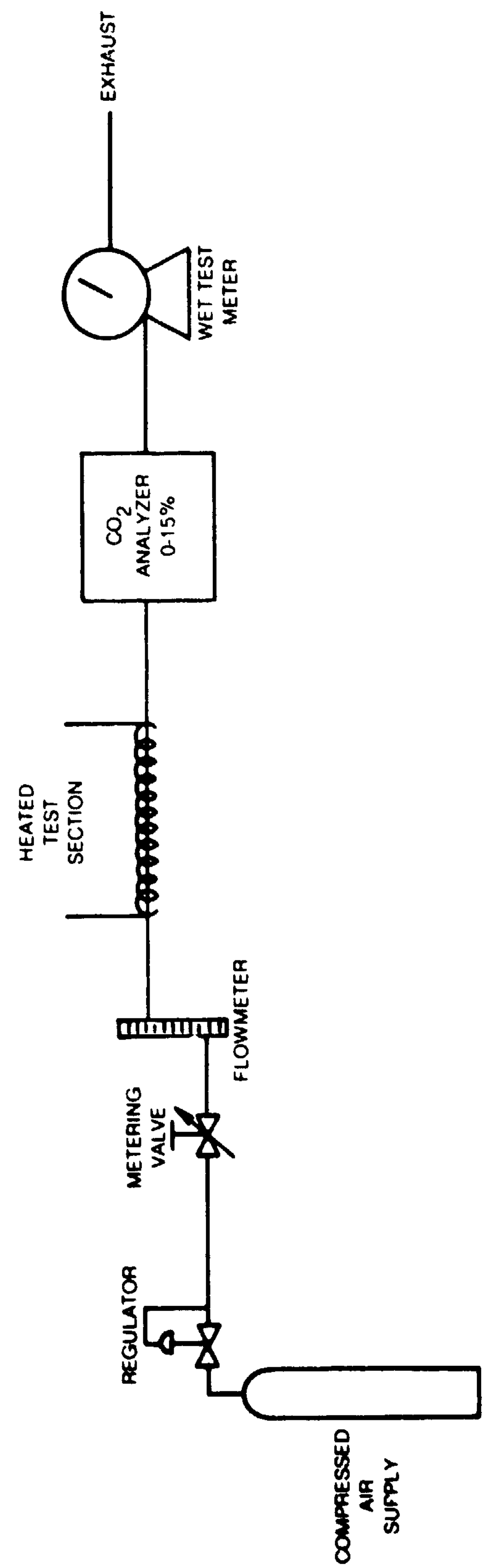

81-0-97-3

THROTTLE FLOW COEFFICIENT

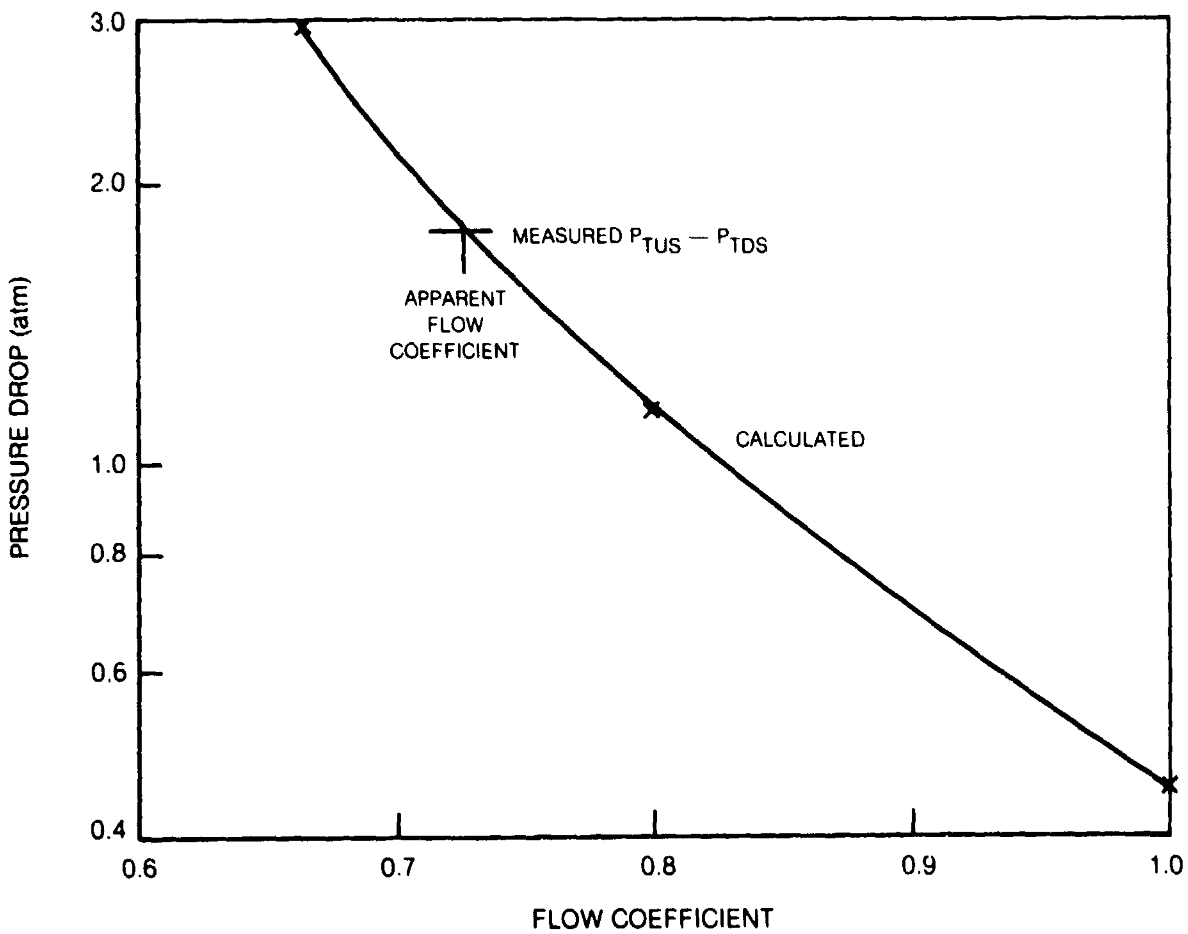

FIG. 9

CONTROLLABILITY OF TEMPERATURE AND FLOW WITH ORIFICE

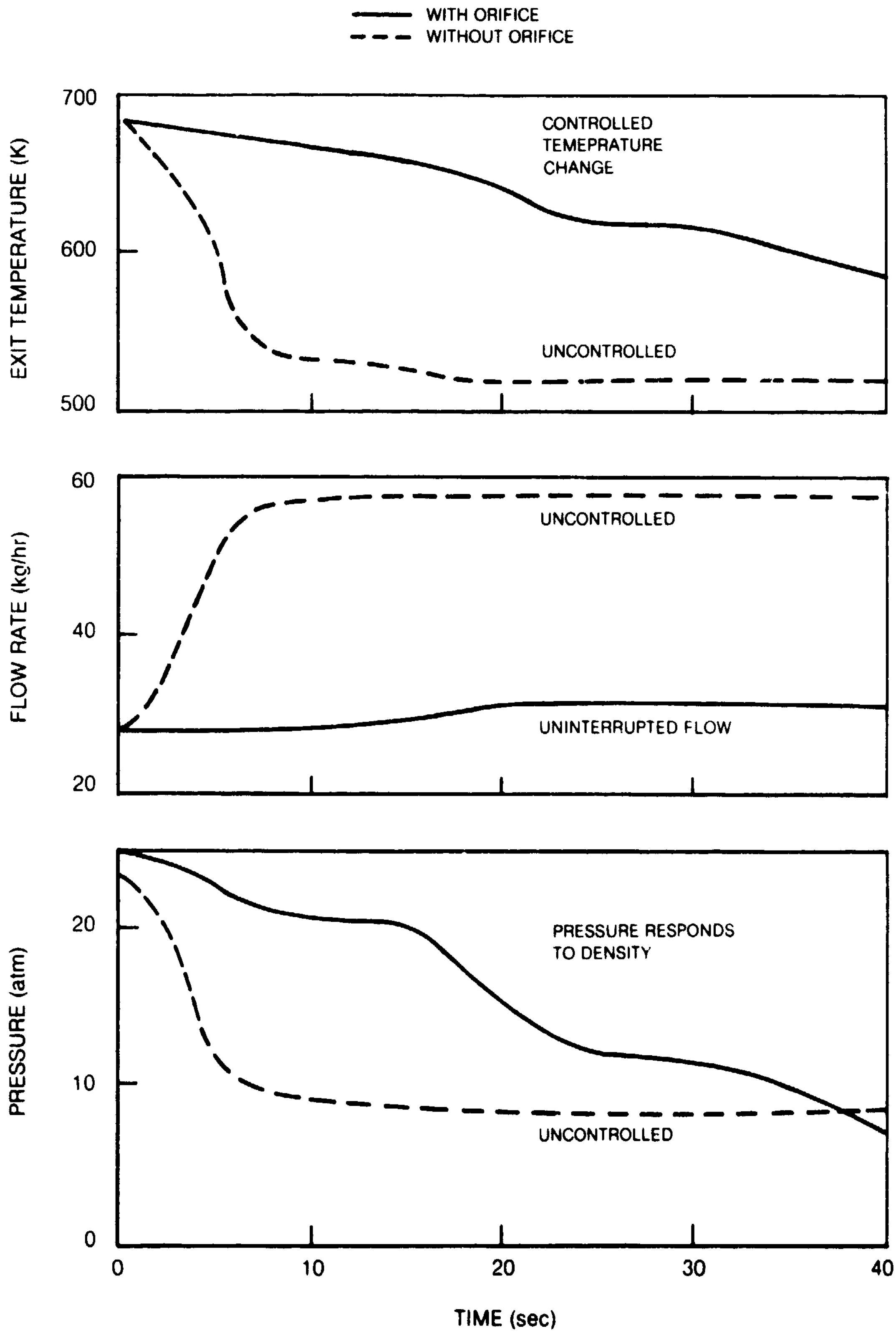

81-9-41-8

FIG. 10

RECOVERY OF OPERATING CONDITIONS AFTER FLOW EXCURSION

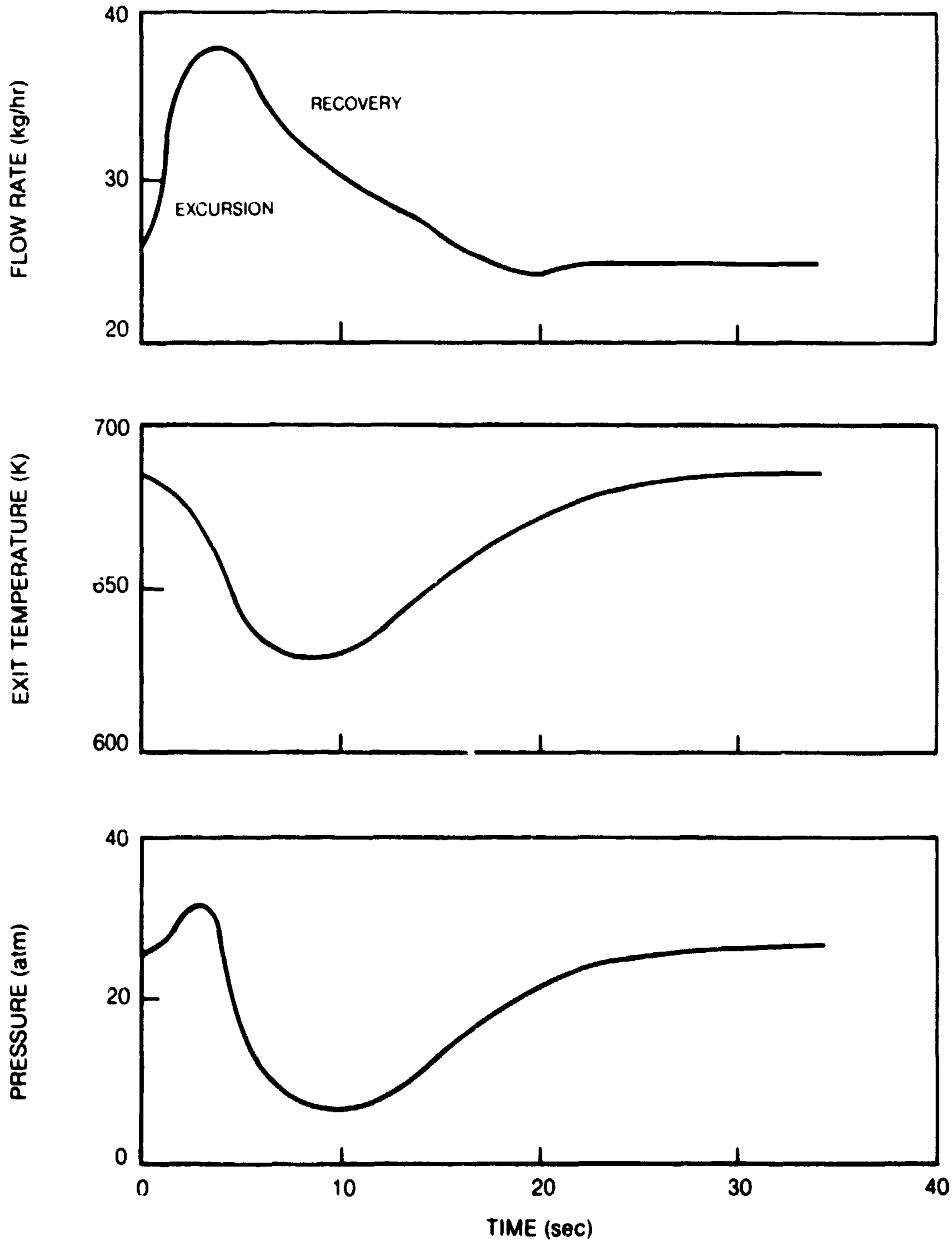

FIG. 11

RECOVERY OF OPERATING CONDITIONS AFTER PRESSURE EXCURSION

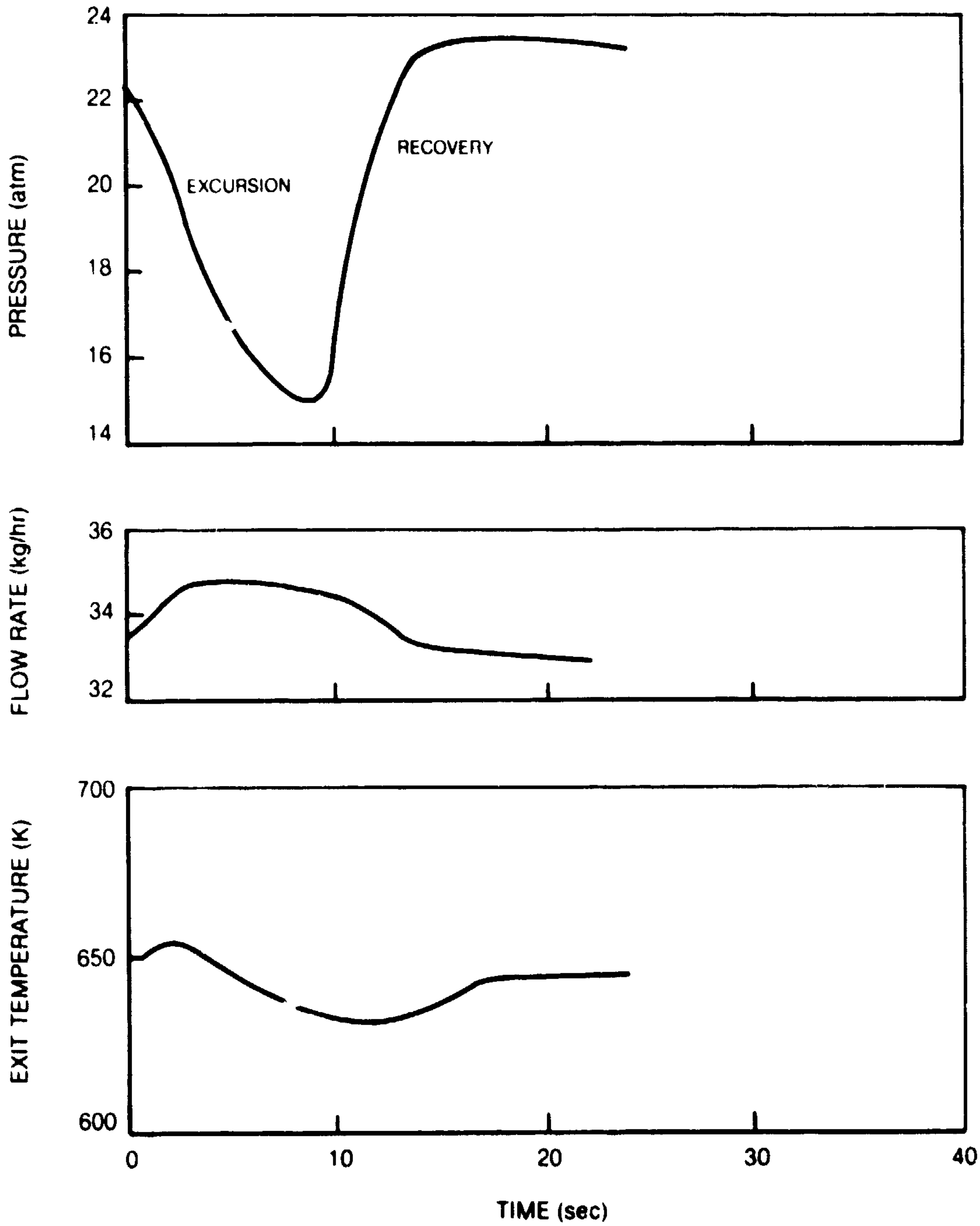

81-9-41-10

FIG. 12

RECOVERY OF OPERATING CONDITIONS AFTER TEMP EXCURSION

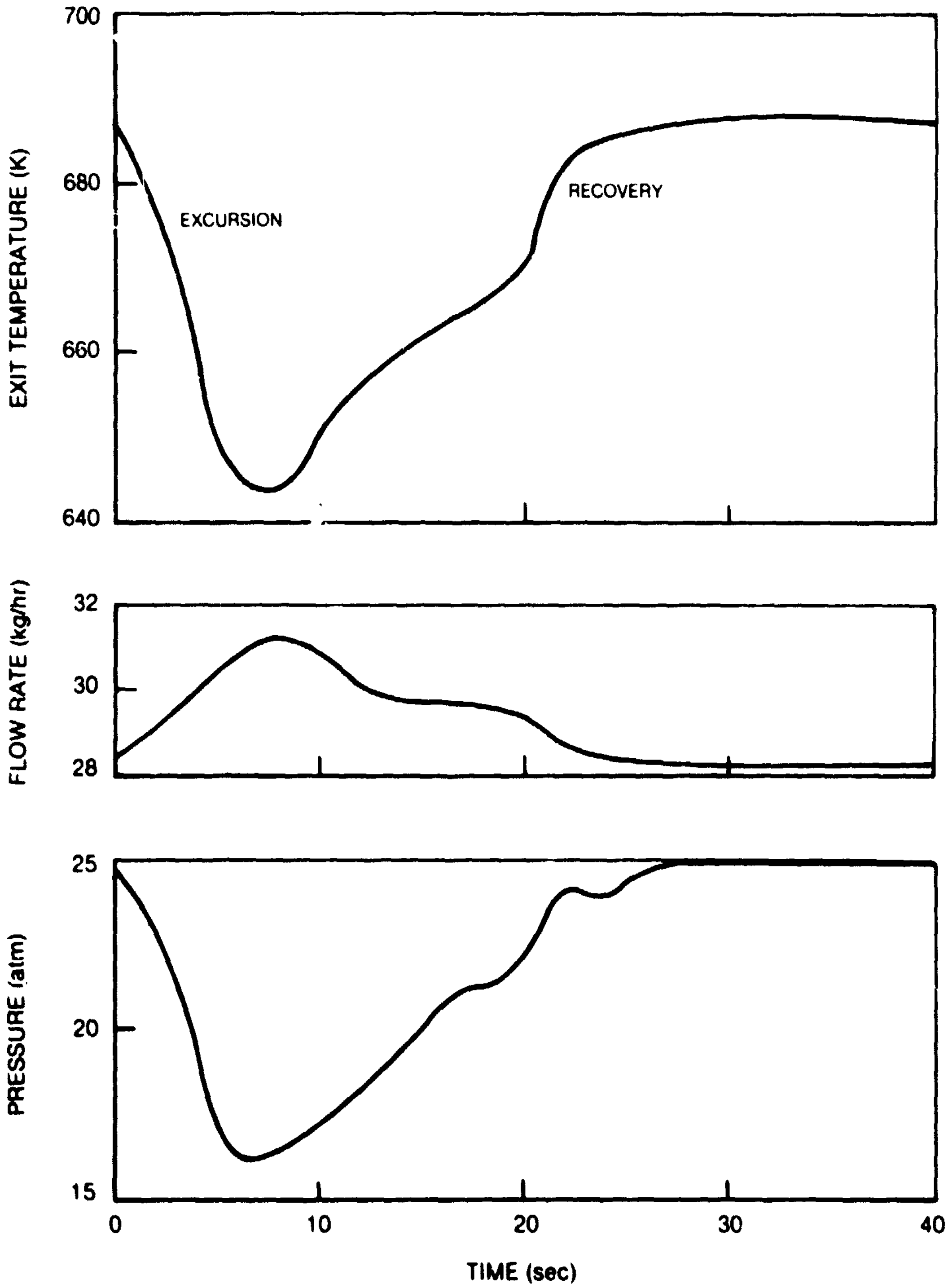

ORIGINAL PAGE
COLOR PHOTOGRAPH

FIG 13

OBSERVED OPALESCENCE AT CRITICAL POINT

JET-A

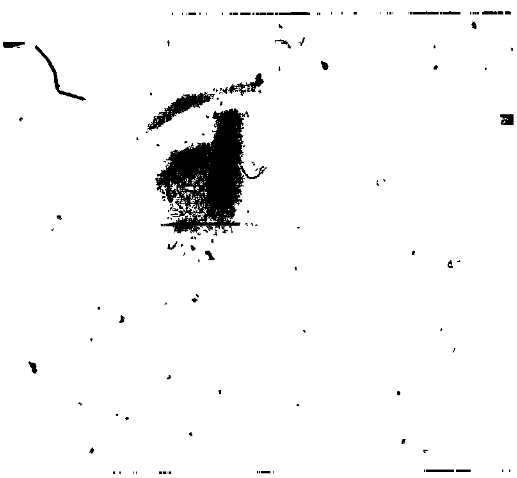

NEAR CRITICAL TEMP

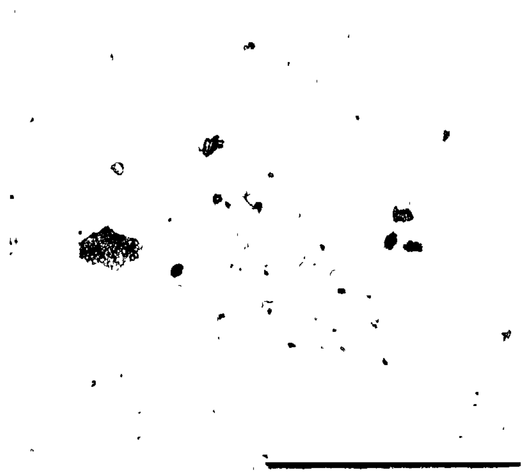

AT CRITICAL TEMP

ERBS

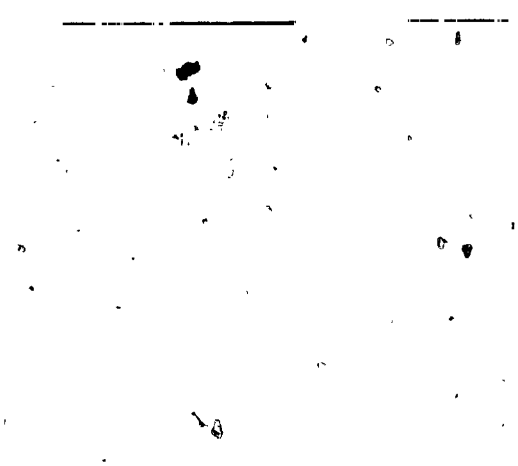

NEAR CRITICAL TEMP

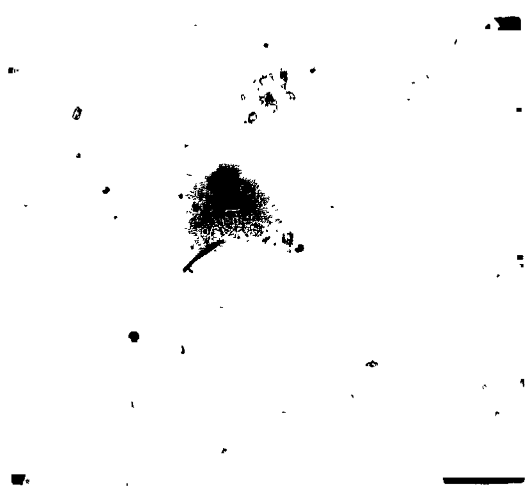

AT CRITICAL TEMP

8 9 41 25

FIG. 14

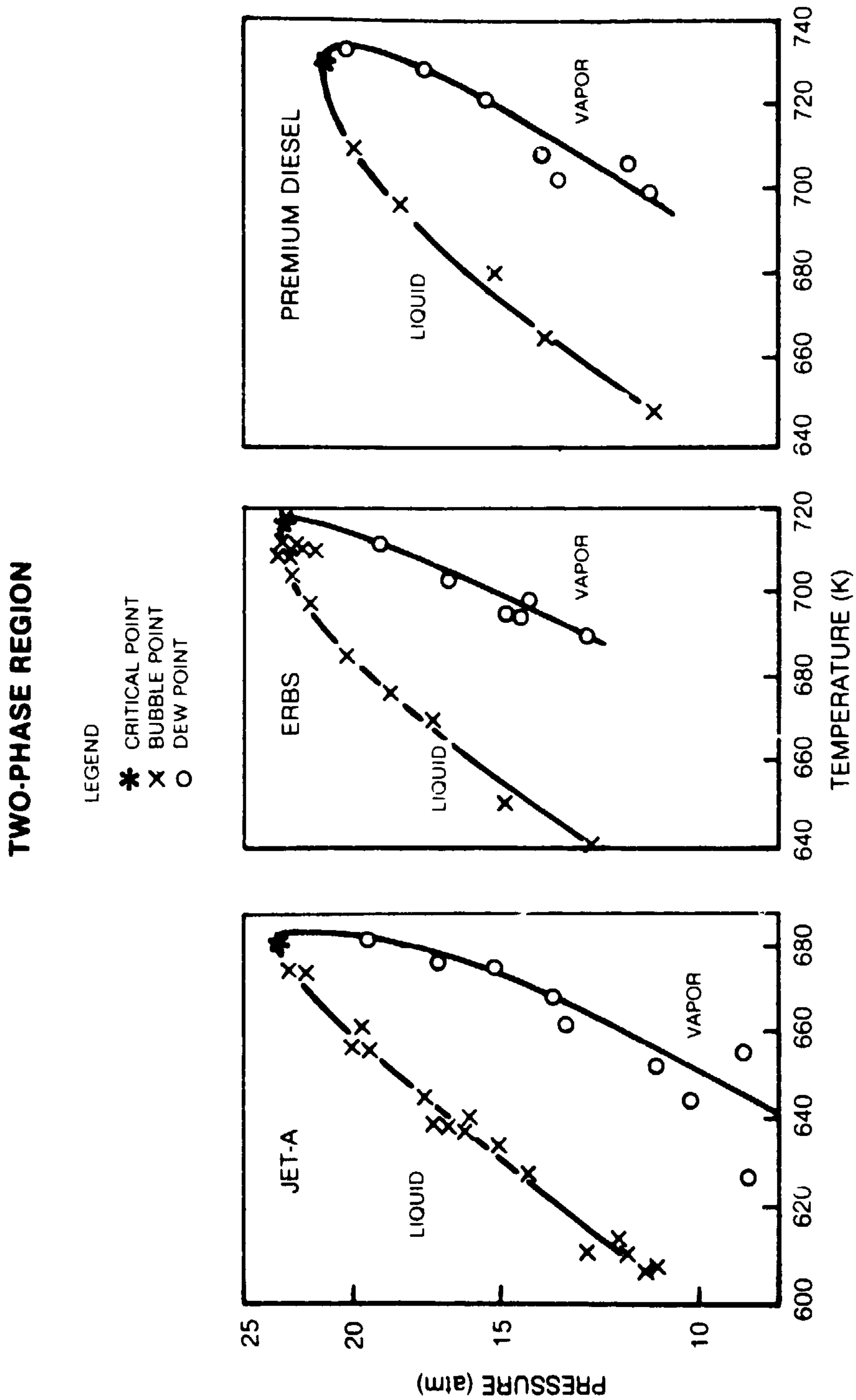

81-8-44-3

THROTTLE OPERATION TESTS WITH JET-A

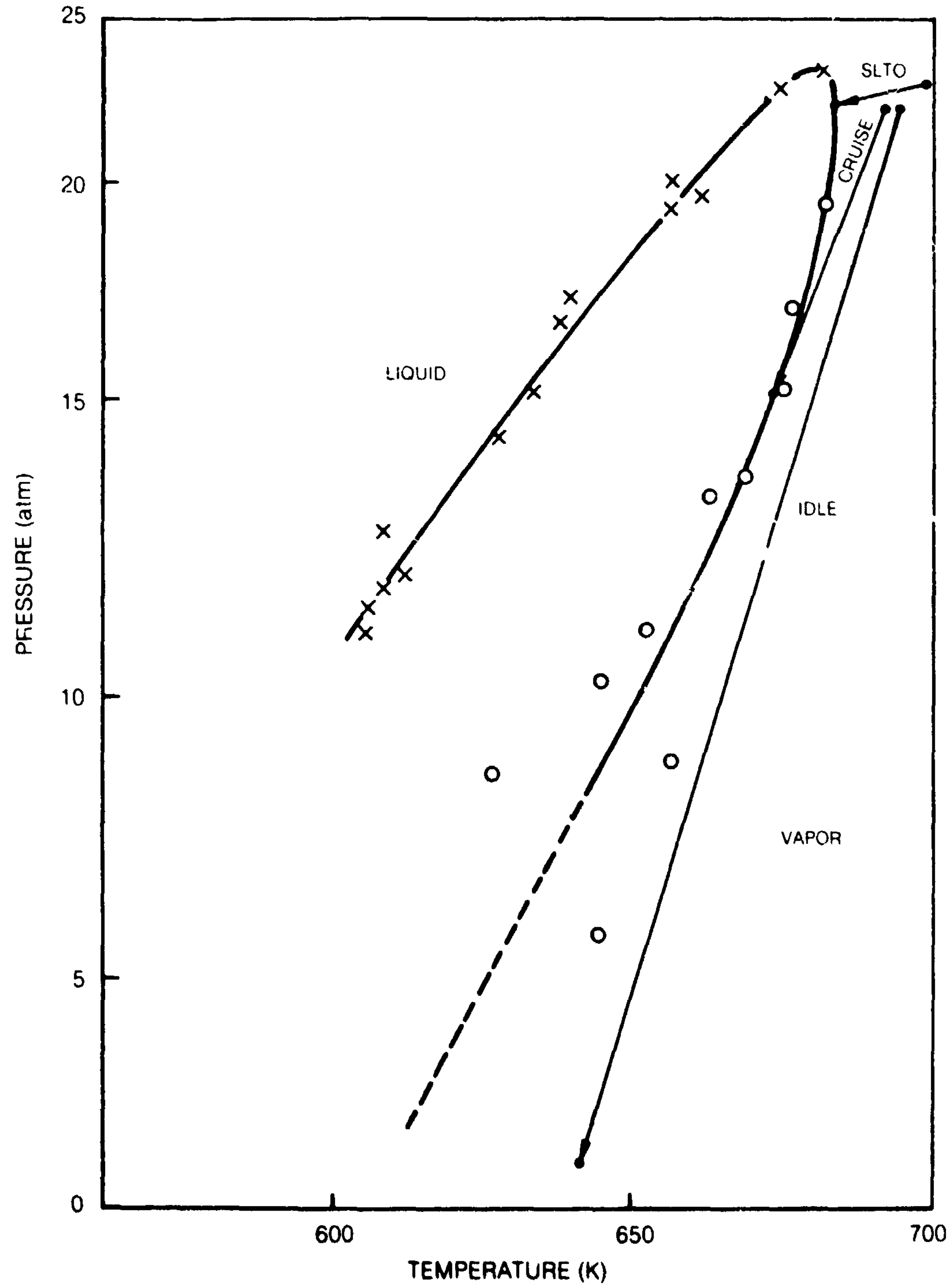

81-8-44-4

HEAT TRANSFER MEASUREMENTS IN CLEAN TUBE

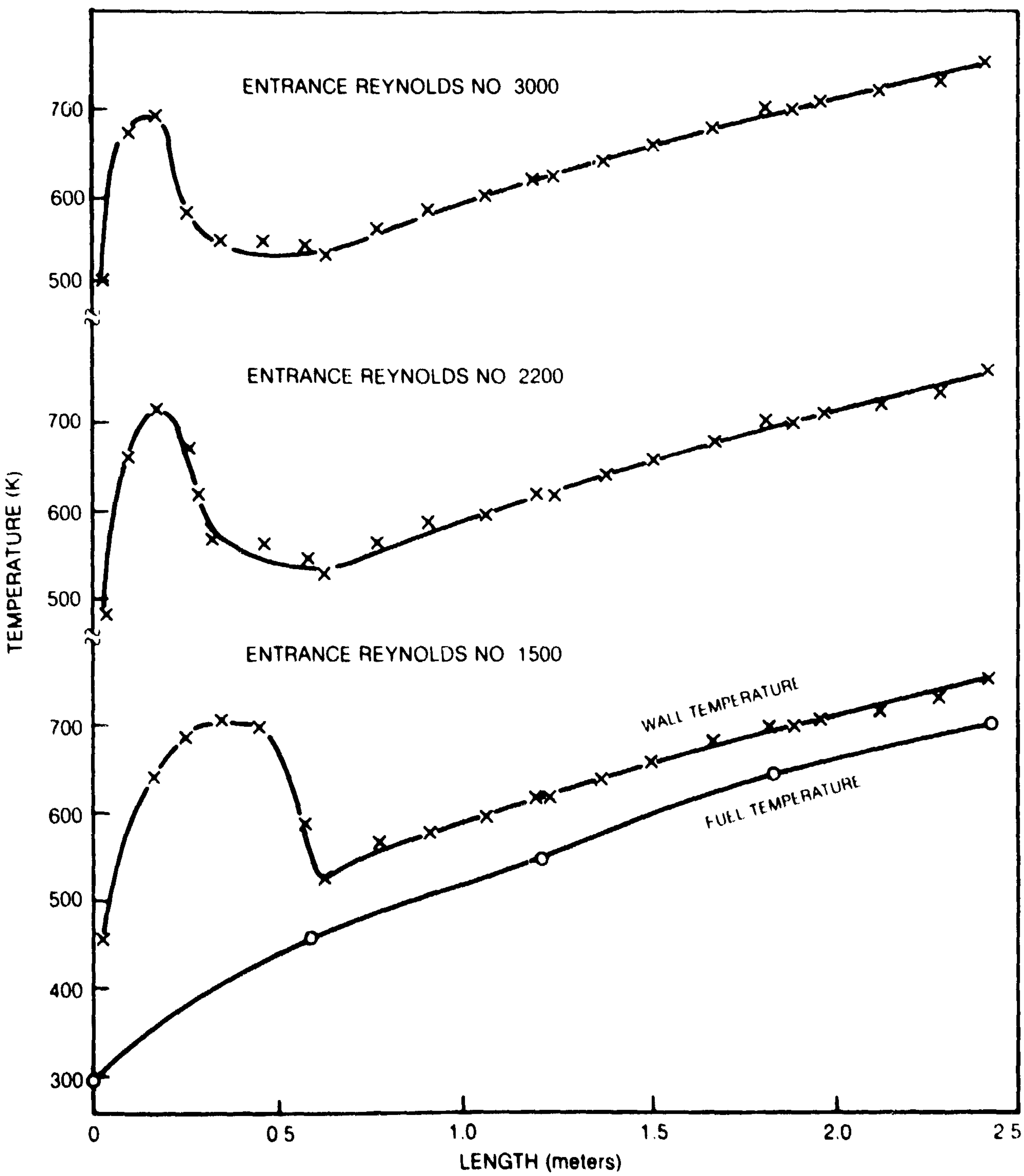

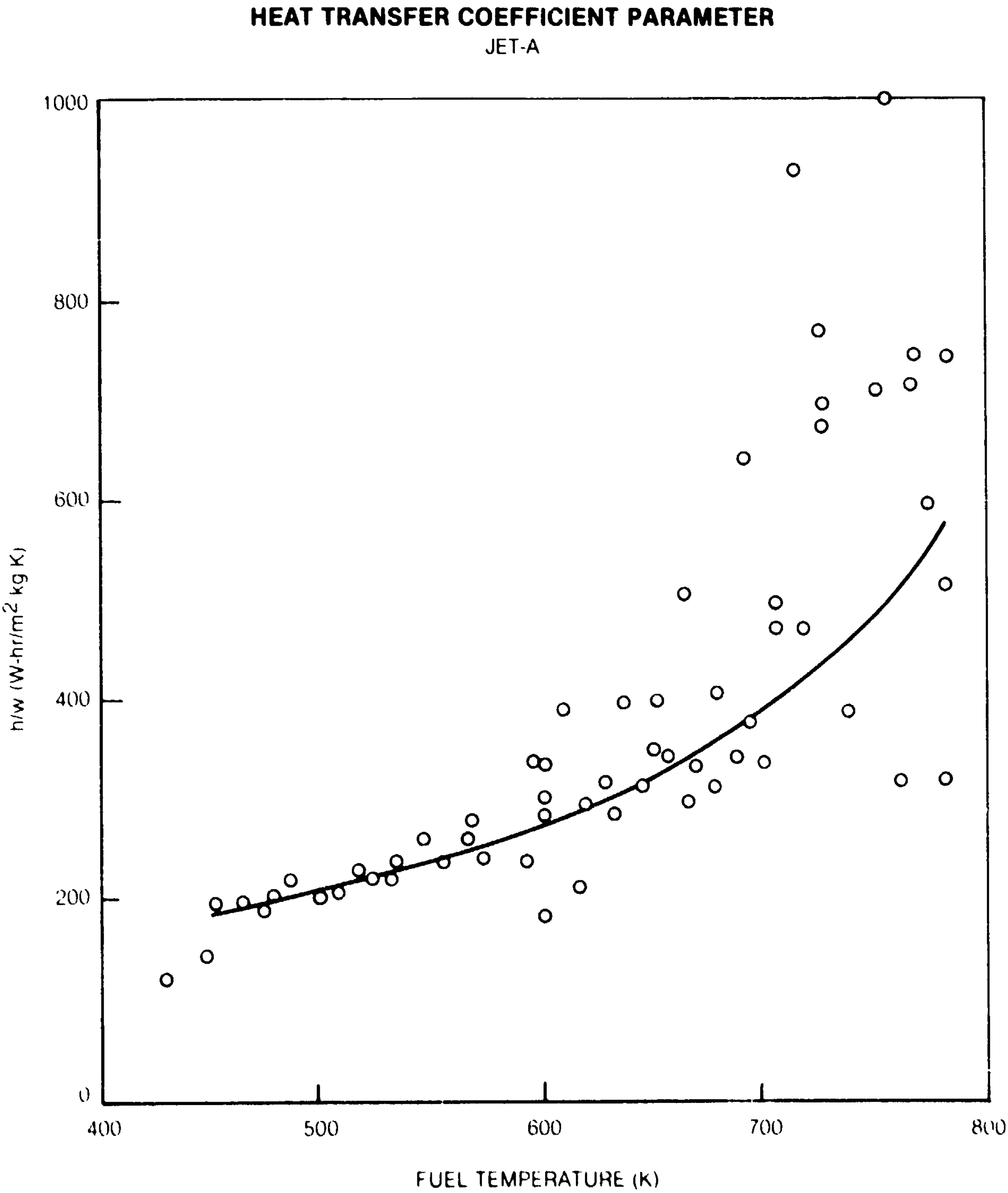
HEAT TRANSFER COEFFICIENT PARAMETER
JET-A
1000
800
600
400
200
0
h/w (W-hr/m2 kg K)
400
500
600
700
800
FUEL TEMPERATURE (K)

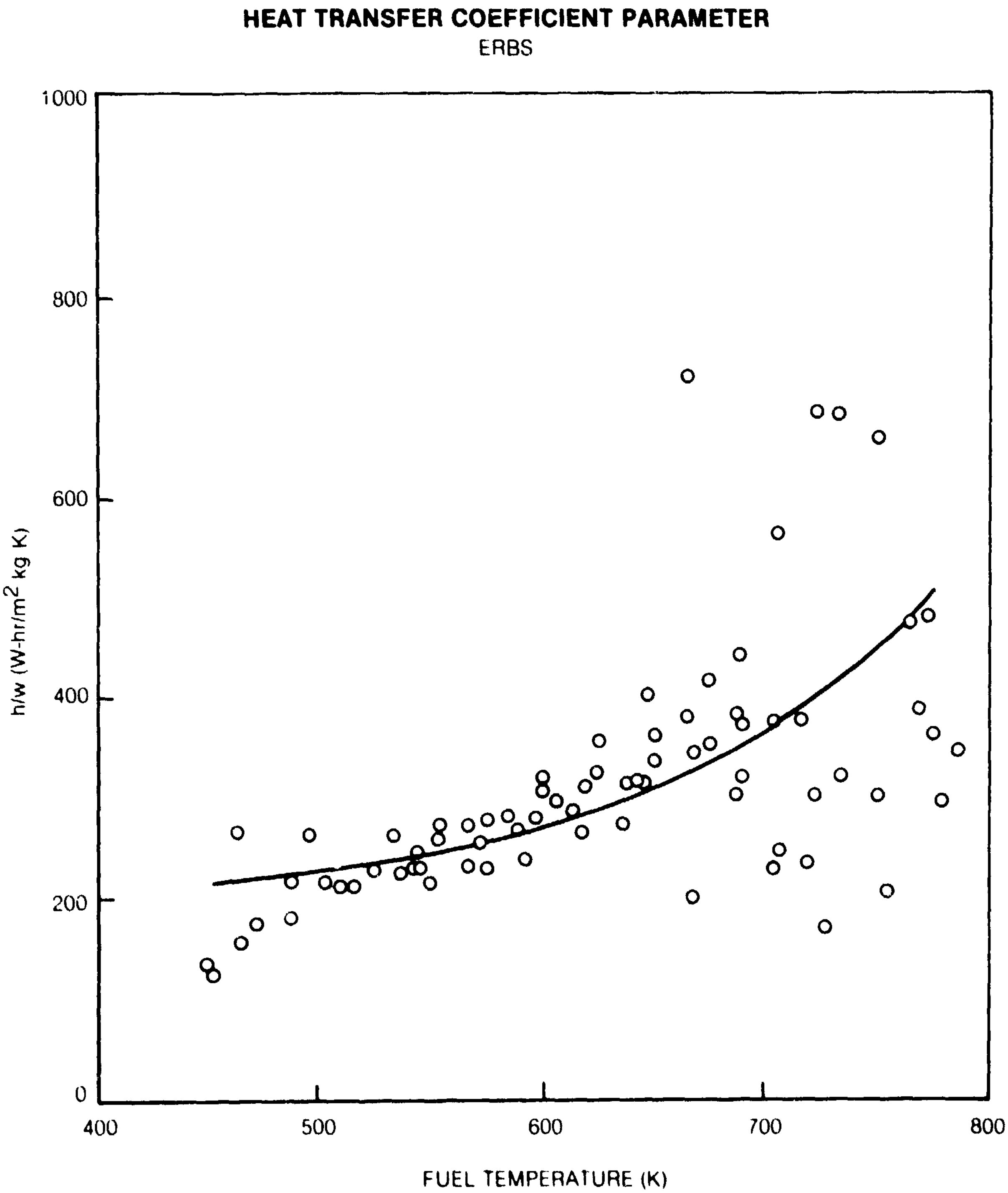
HEAT TRANSFER COEFFICIENT PARAMETER
ERBS
h/w (W-hr/m2 kg K)
1000
800
600
400
200
0
400
500
600
700
800
FUEL TEMPERATURE (K)

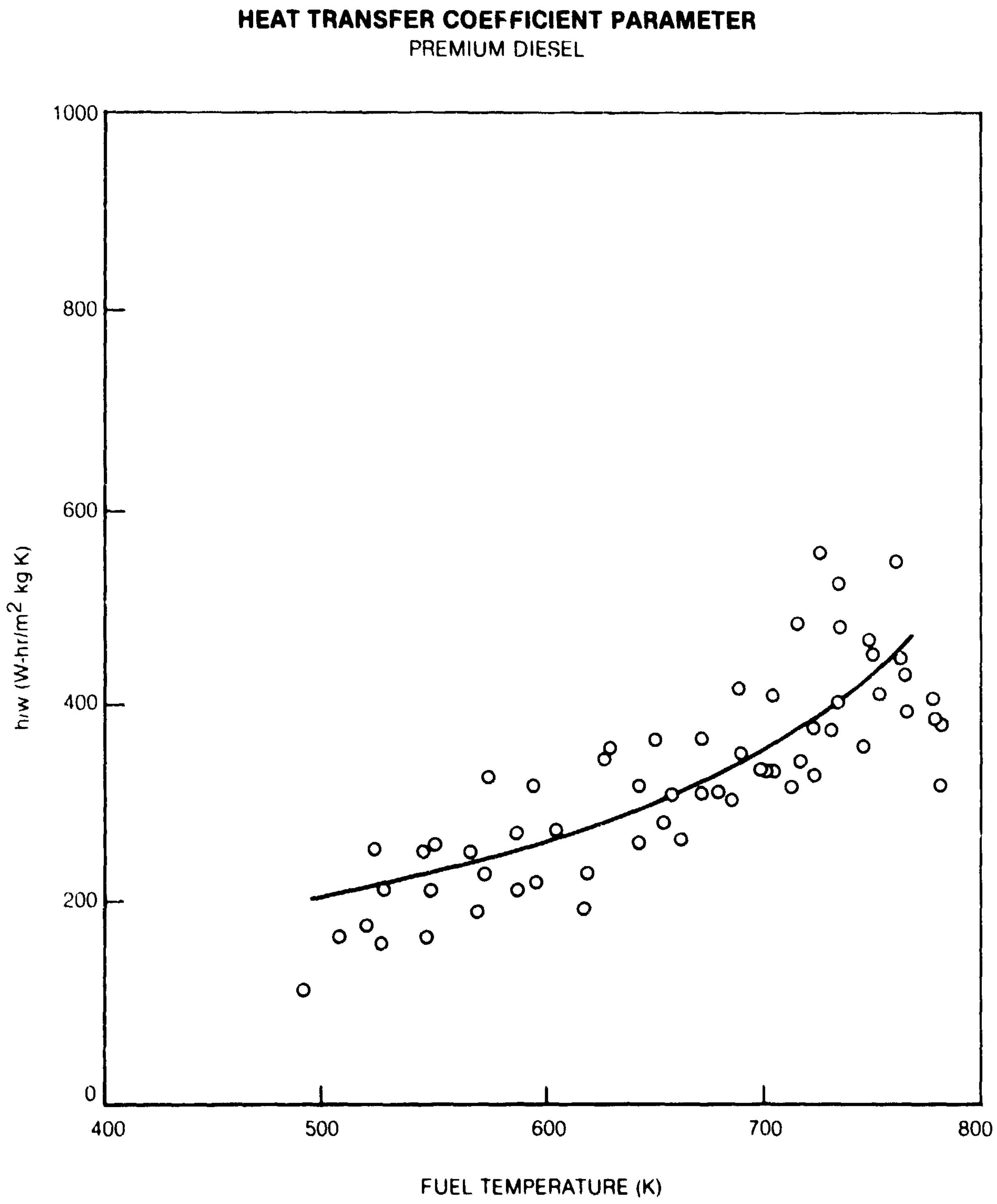
HEAT TRANSFER COEFFICIENT PARAMETER
PREMIUM DIESEL
h/w (W-hr/m2 kg K)
1000
800
600
400
200
0
400
500
600
700
800
FUEL TEMPERATURE (K)

TUBE WALL TEMPERATURE WITH DEPOSITS AT LOW VELOCITY

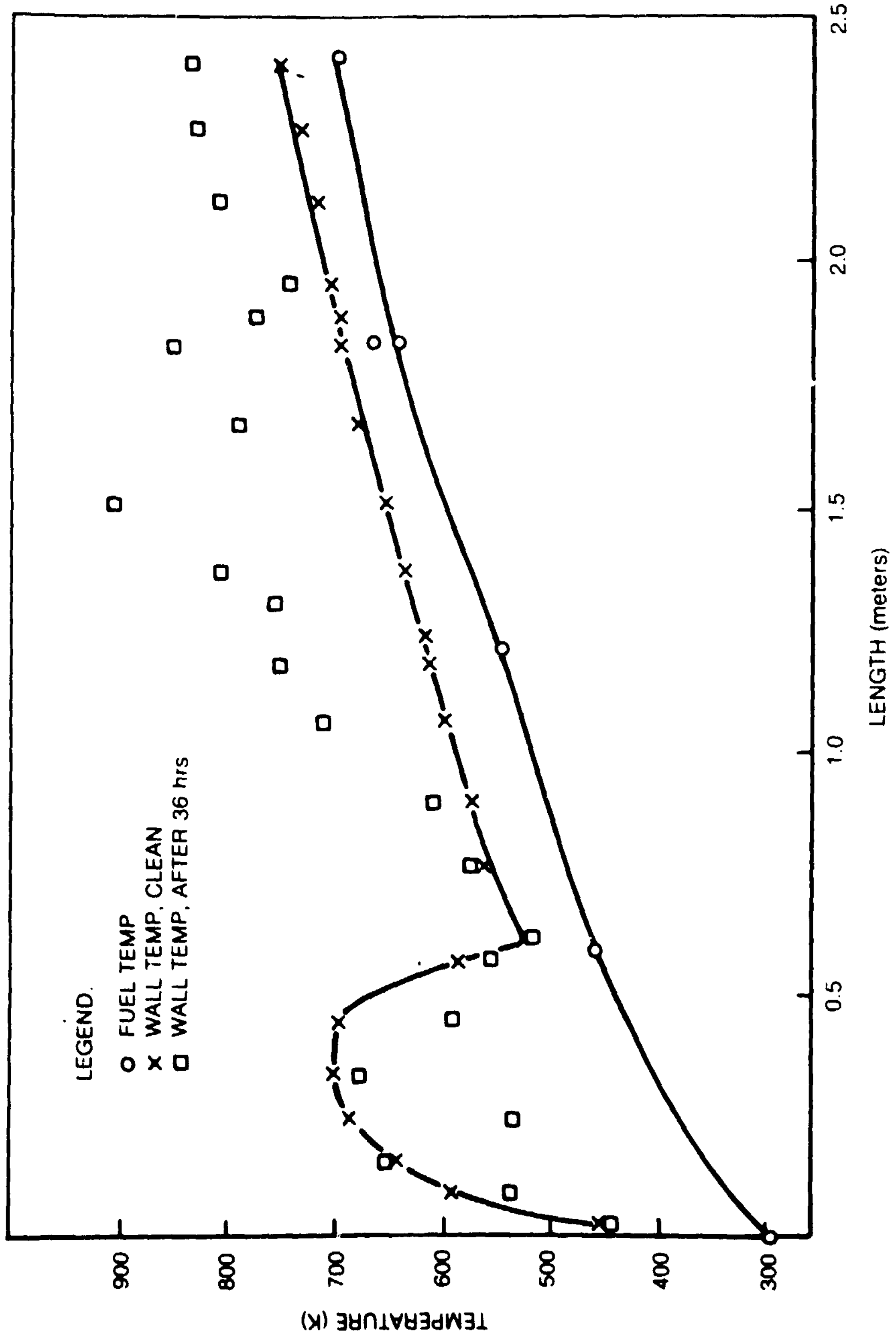

81-8-44-7

TUBE WALL TEMPERATURE NEAR ENTRANCE

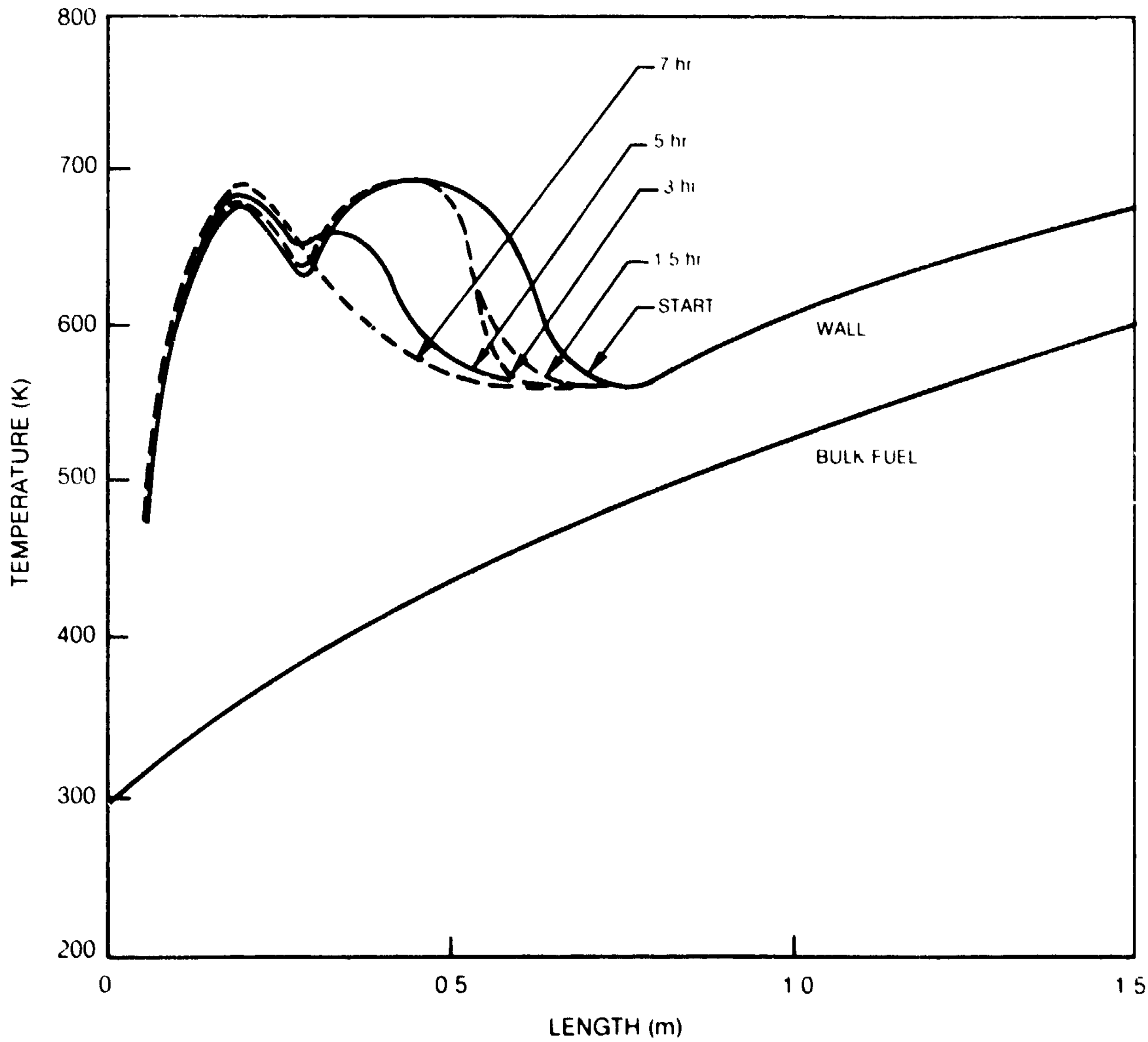

FIG 22

TUBE WALL TEMPERATURE WITH DEPOSITS AT HIGH VELOCITY

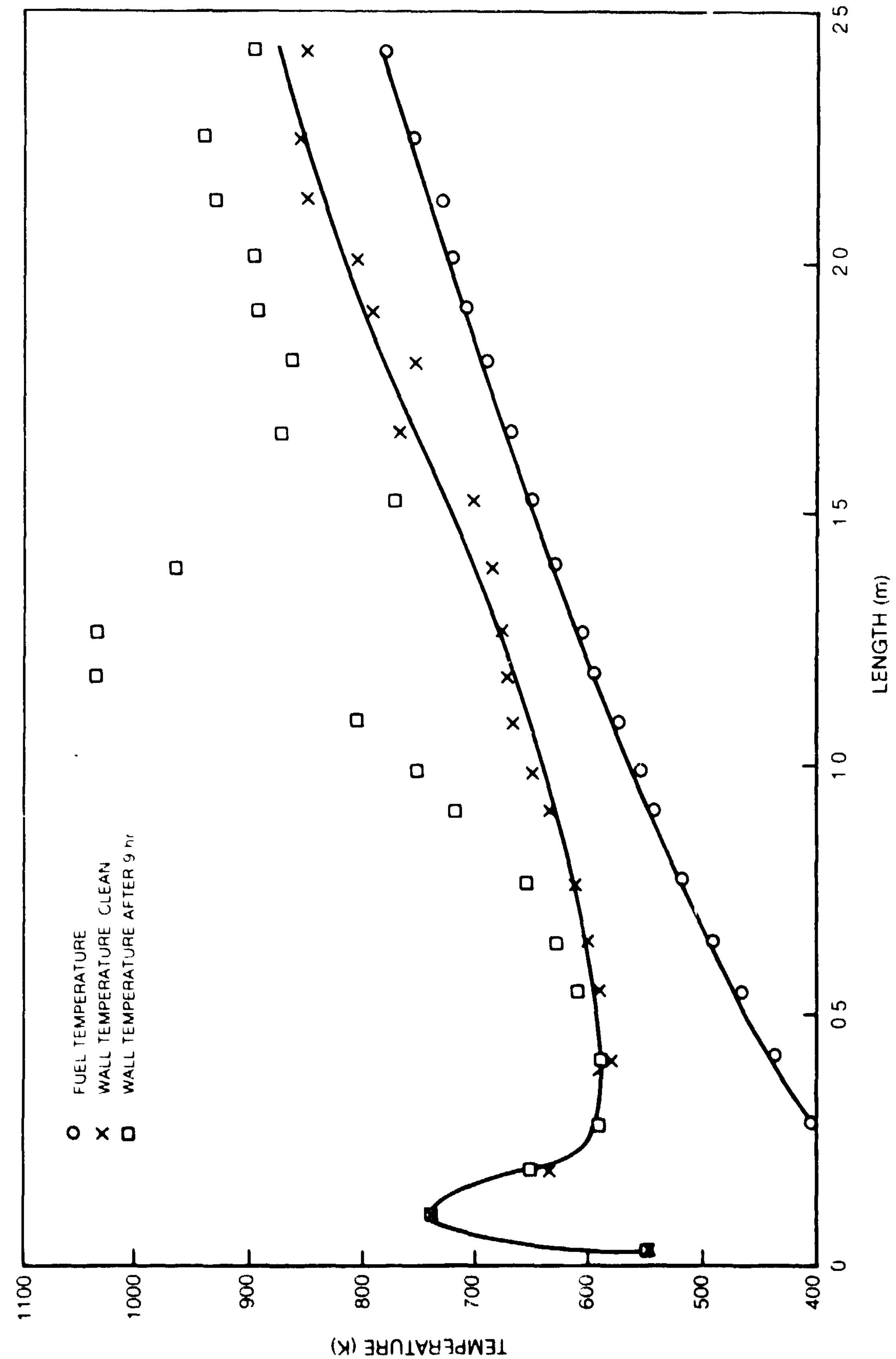

81-9-41-17

WALL TEMPERATURE DURING FULL DURATION RUN

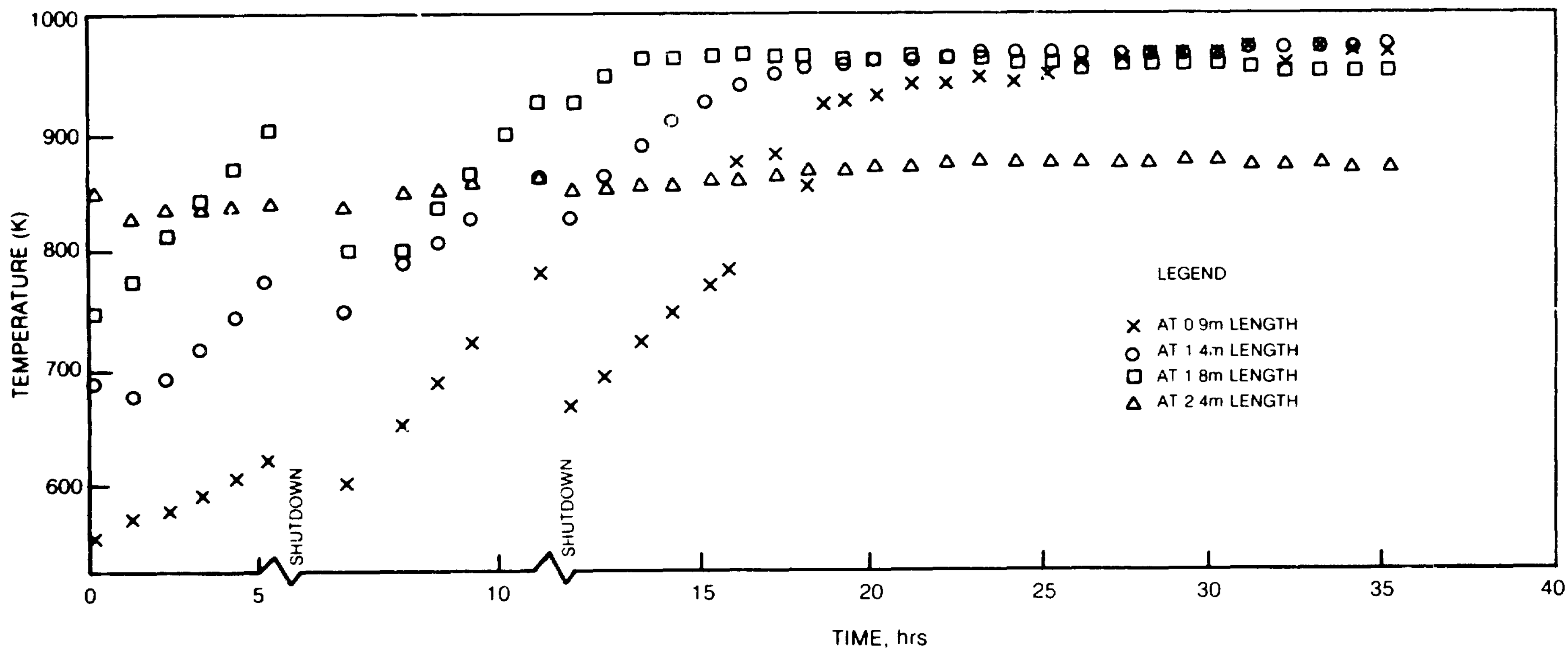

FIG. 23

81-9-41-26

WALL TEMPERATURE WITH MAXIMUM WALL TEMPERATURE SHUTDOWN

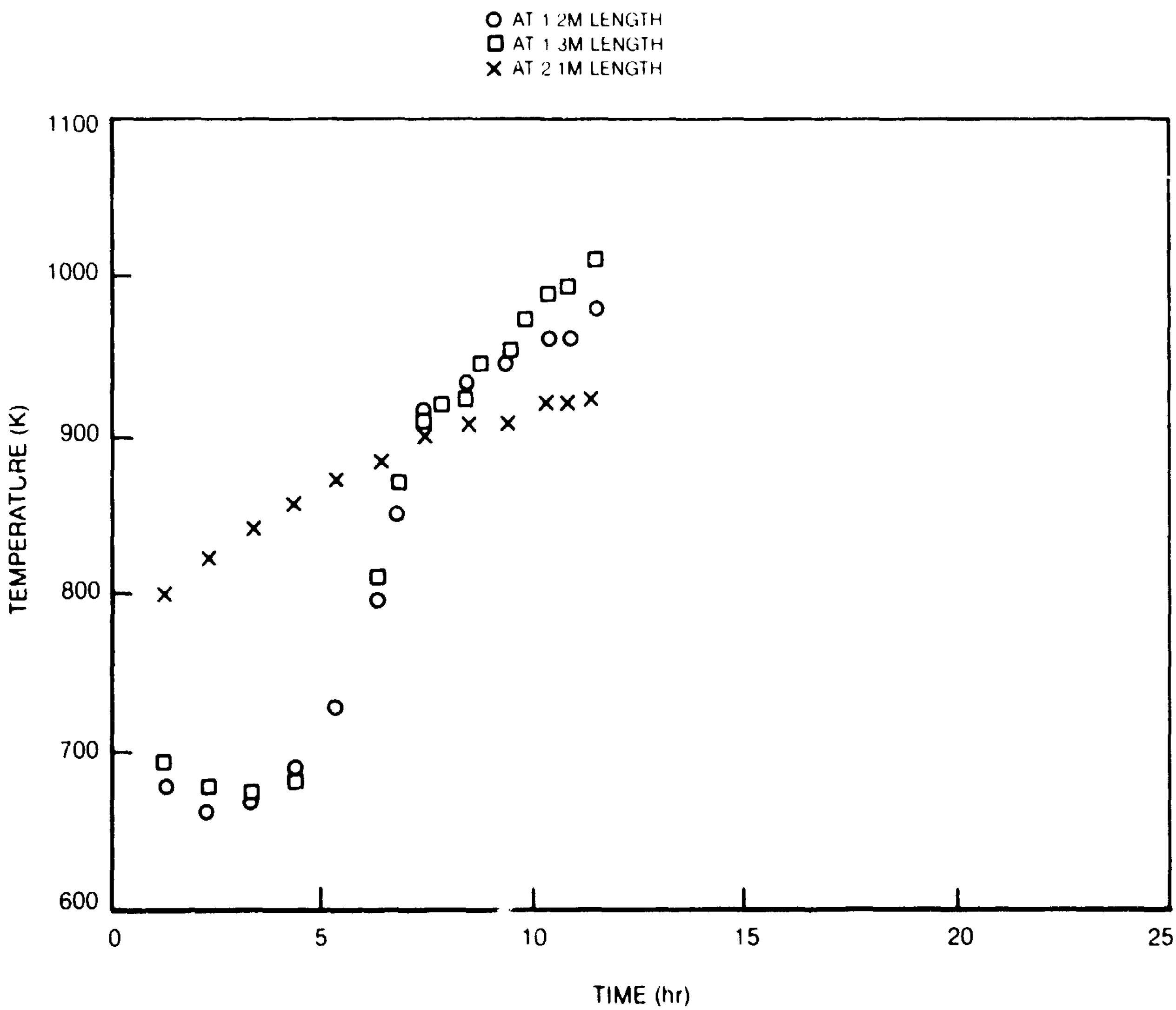

81-9-41-20

WALL TEMPERATURE WITH HIGH ΔP SHUTDOWN

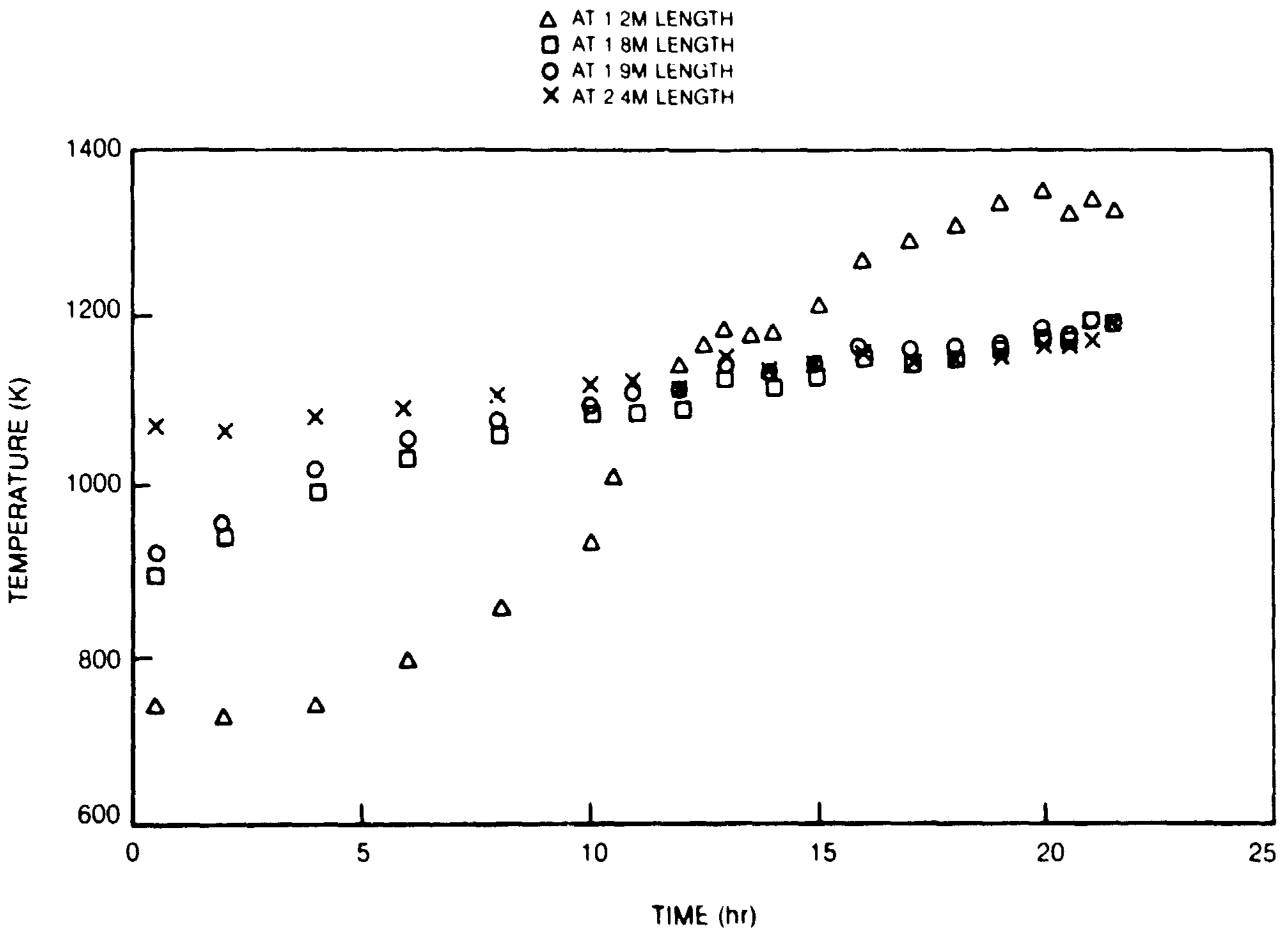

FIG. 26

PRESSURE DROP DURING FULL DURATION RUN

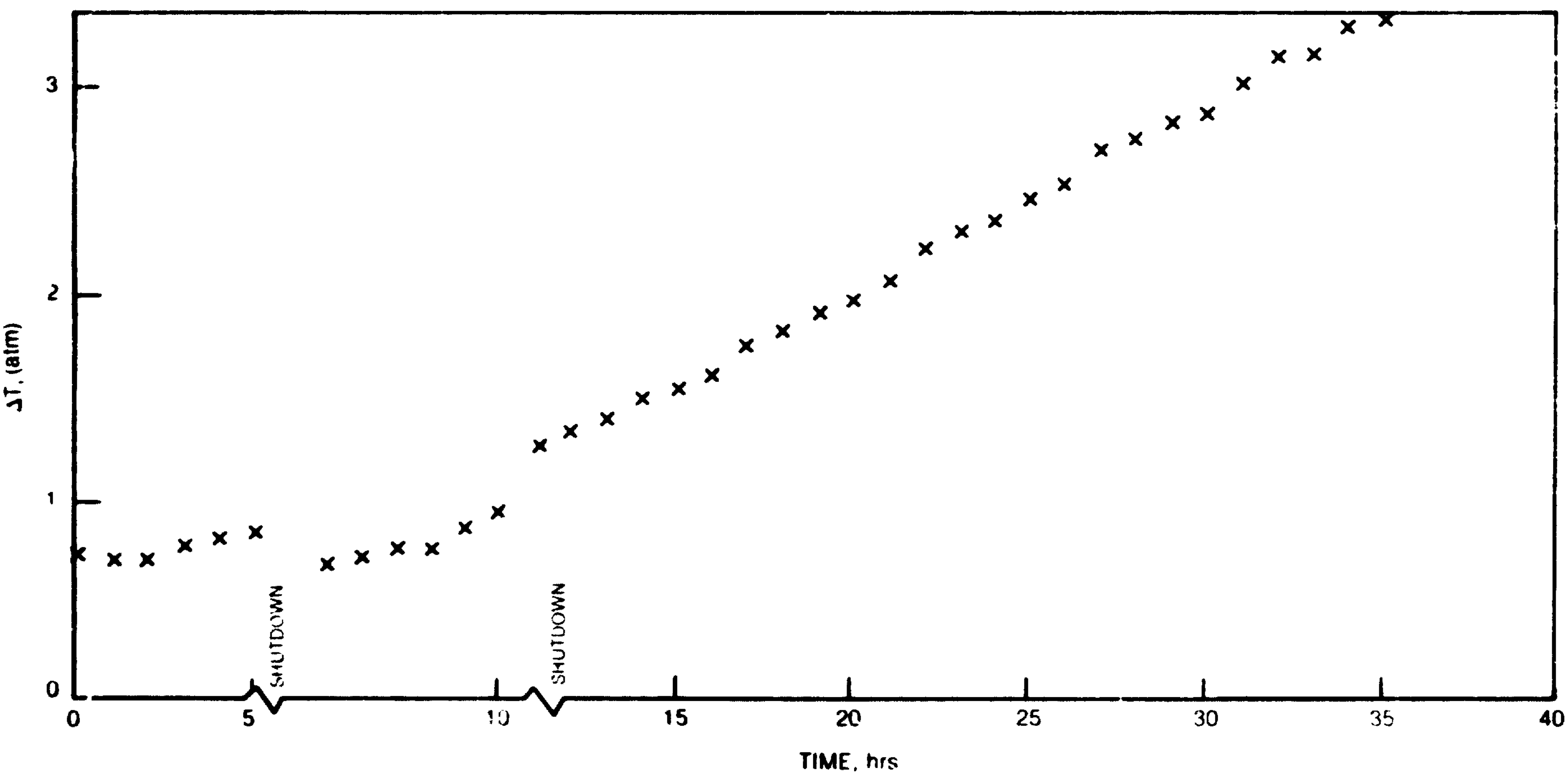

81-9 41-27

PRESSURE DROP WITH HIGH ΔP SHUTDOWN

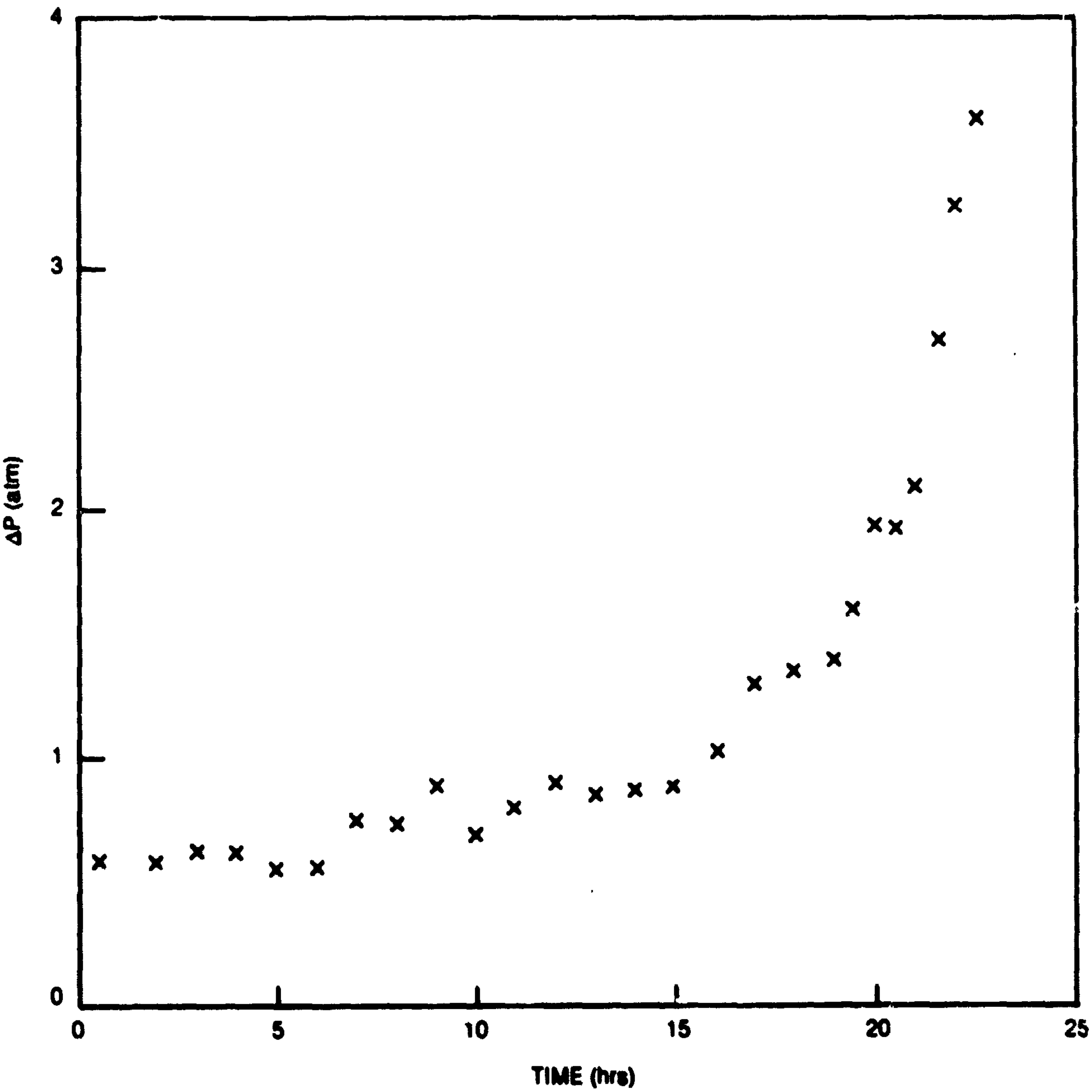

81-9-41-1

PRESSURE DROP WITH MAX WALL TEMP SHUTDOWN

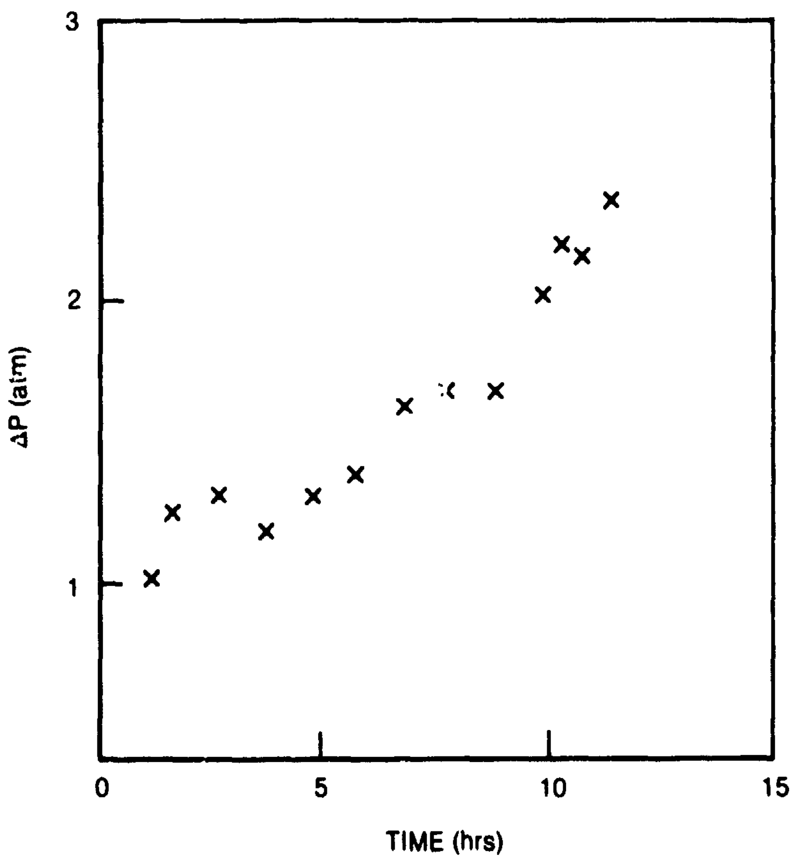

FIG. 29

DEPOSIT THERMAL RESISTANCE FOR JET-A

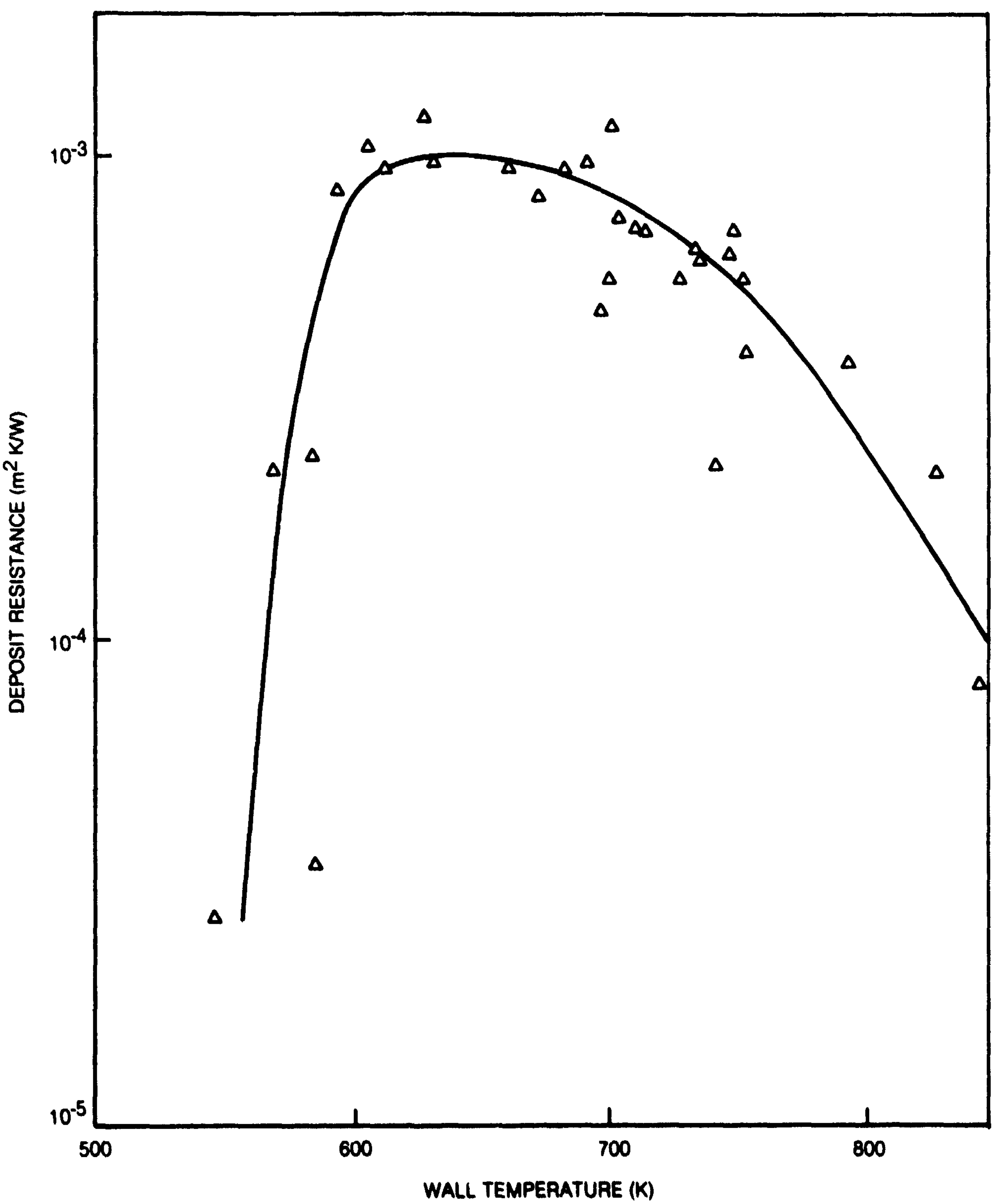

81-9-41-23

DEPOSIT THERMAL RESISTANCE FOR ERBS

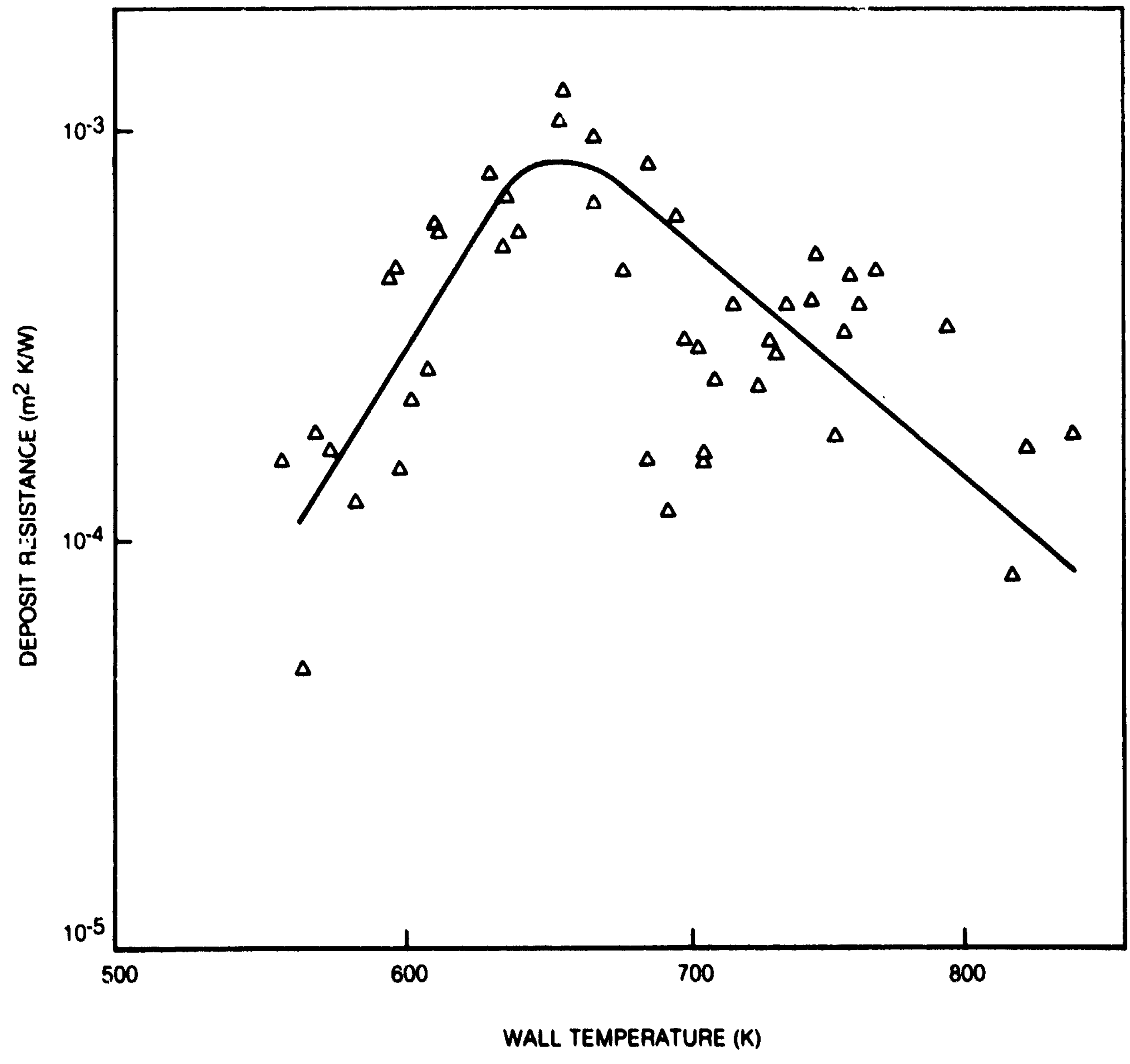

81-6-41-24

COMPOSITE PLOT OF MAXIMUM DEPOSIT RESISTANCE

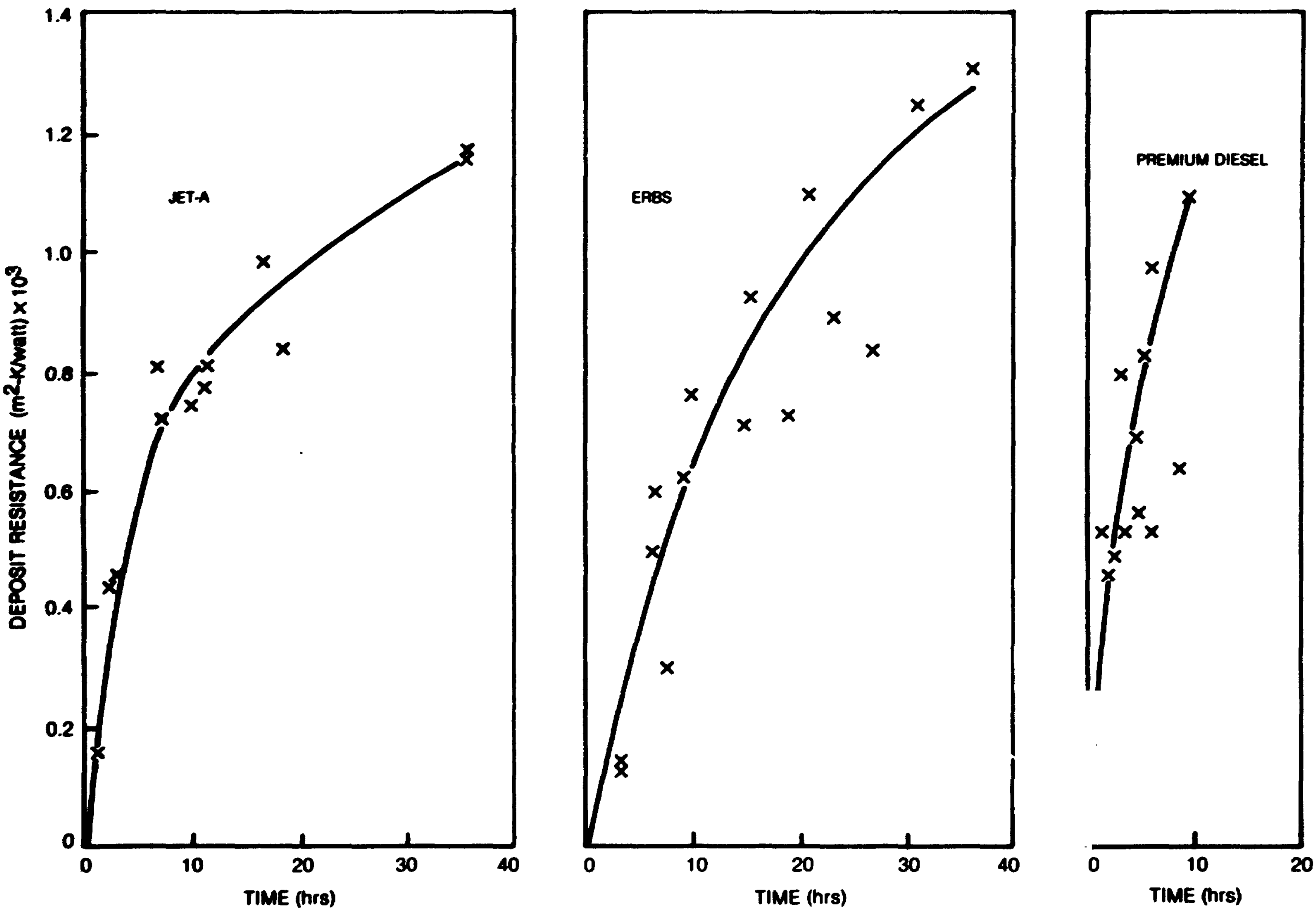

FIG. 31

81-8-44-8

WALL TEMPERATURE AND DEPOSIT MASS

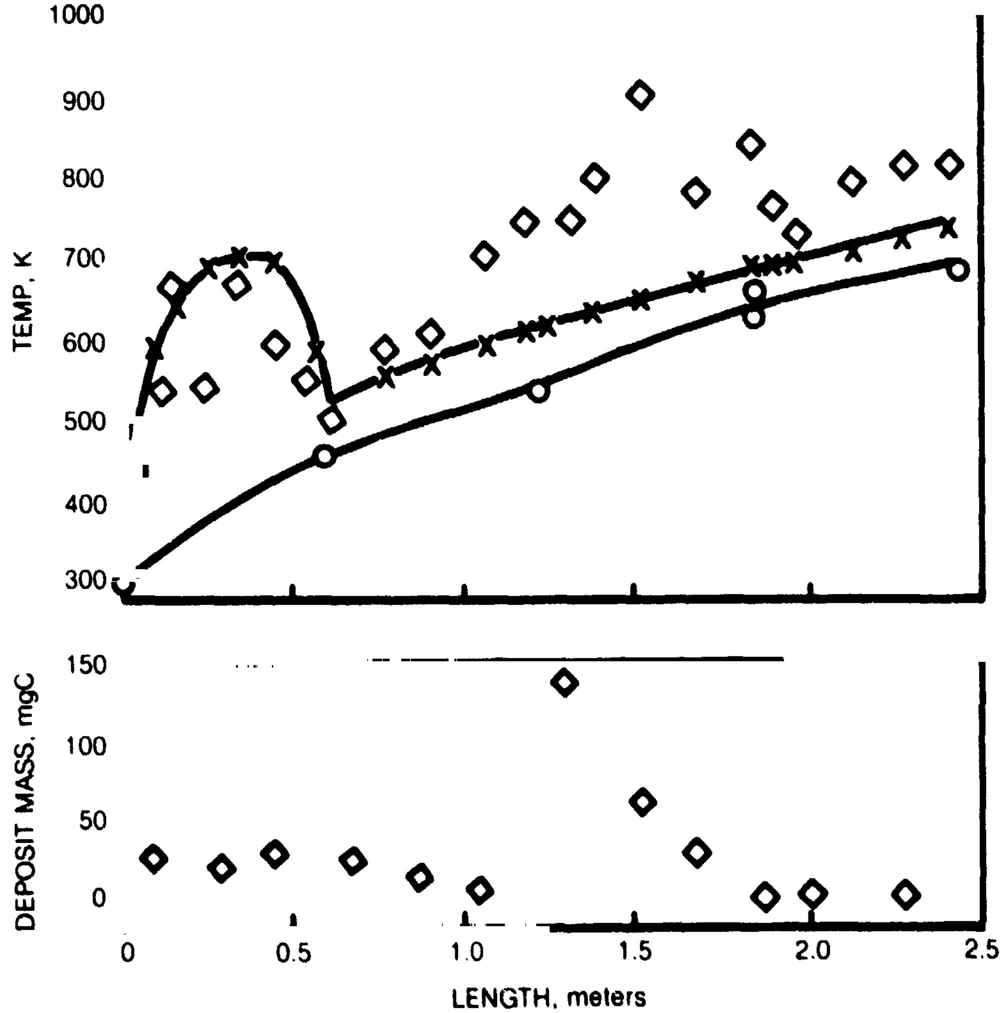

FIG. 33

DEPOSIT FORMATION RATE WITH JET-A

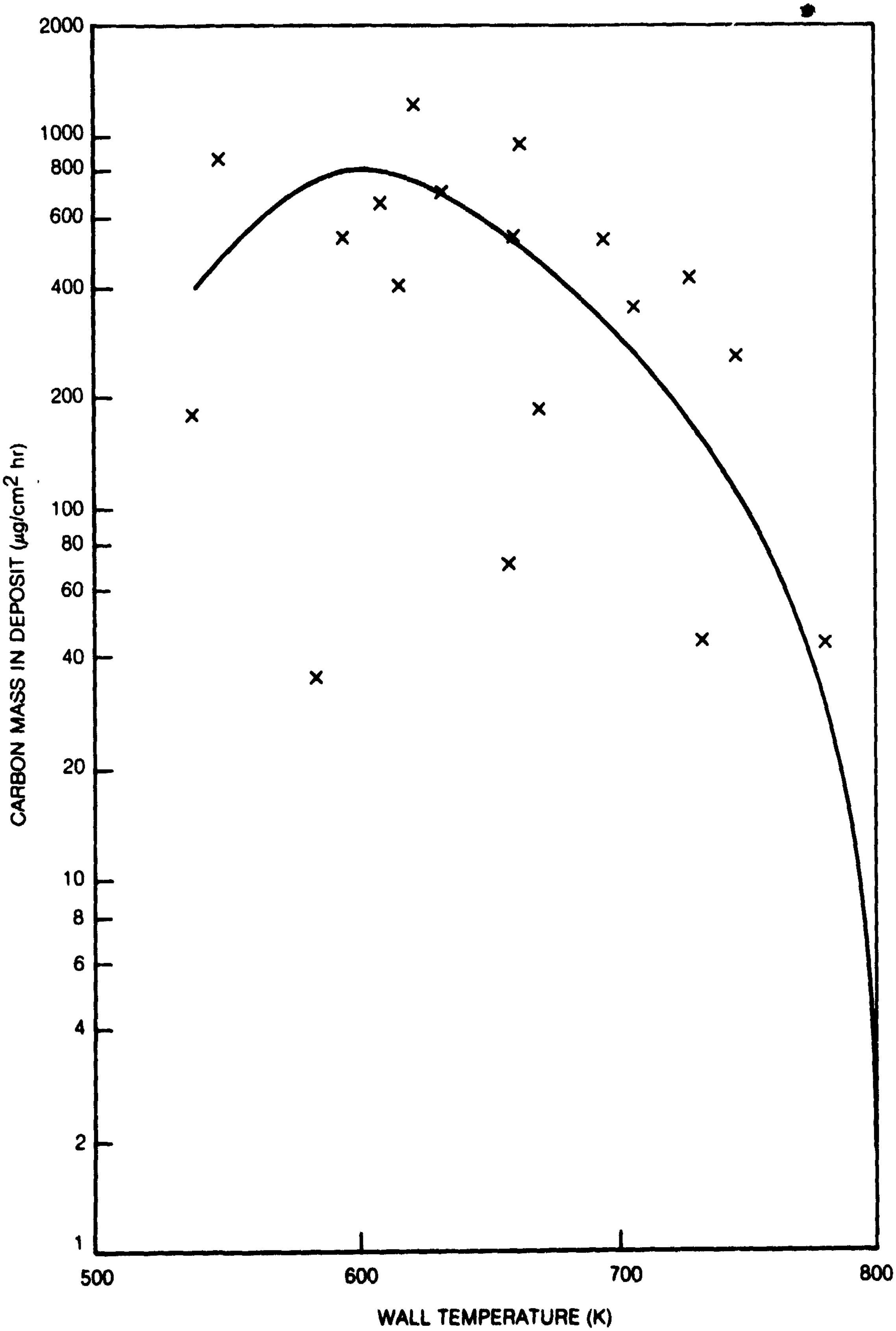

81-9-41-22

FIG. 34

DEPOSIT FORMATION RATE WITH ERBS

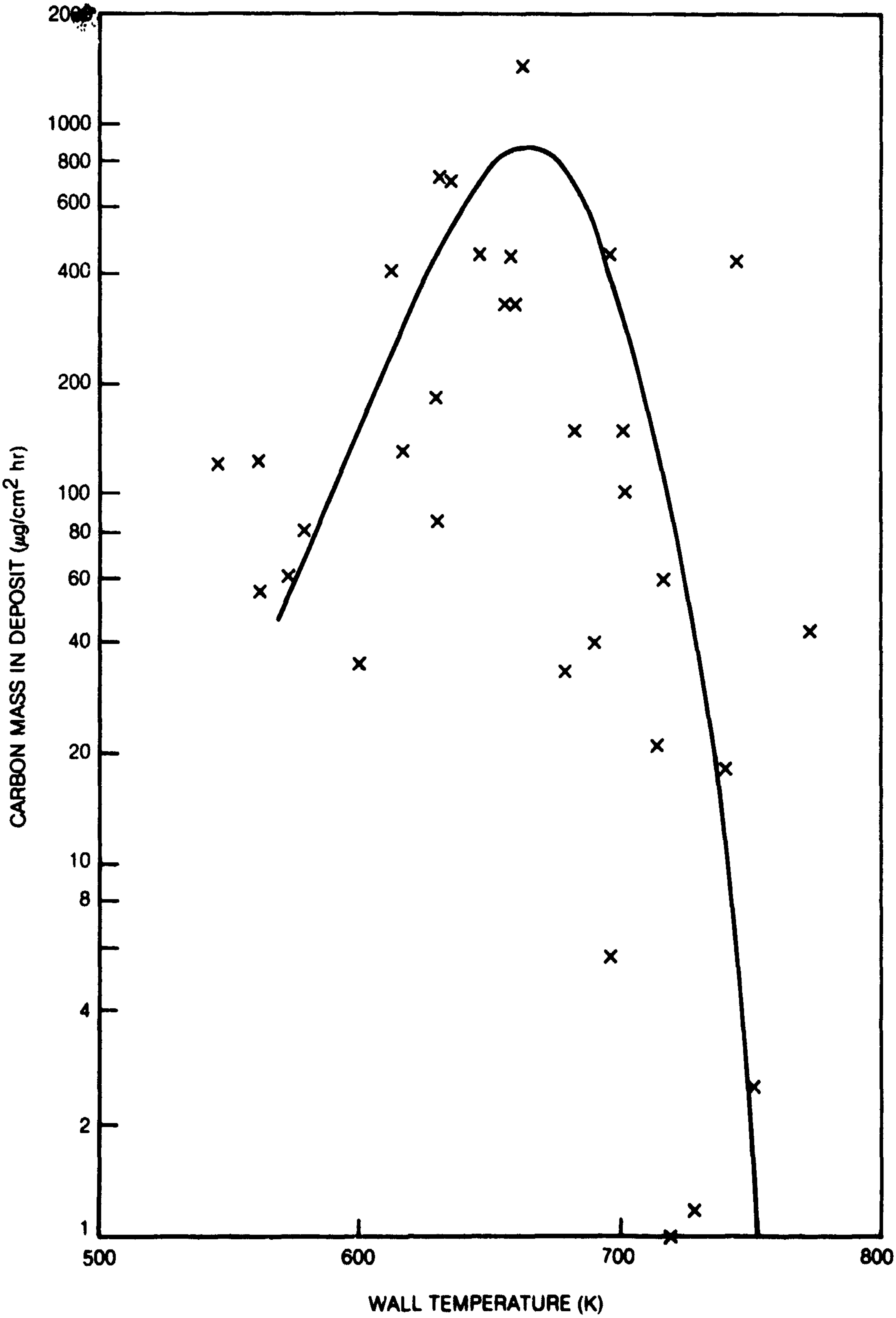

81-9-41-21

MAXIMUM DEPOSIT FORMATION

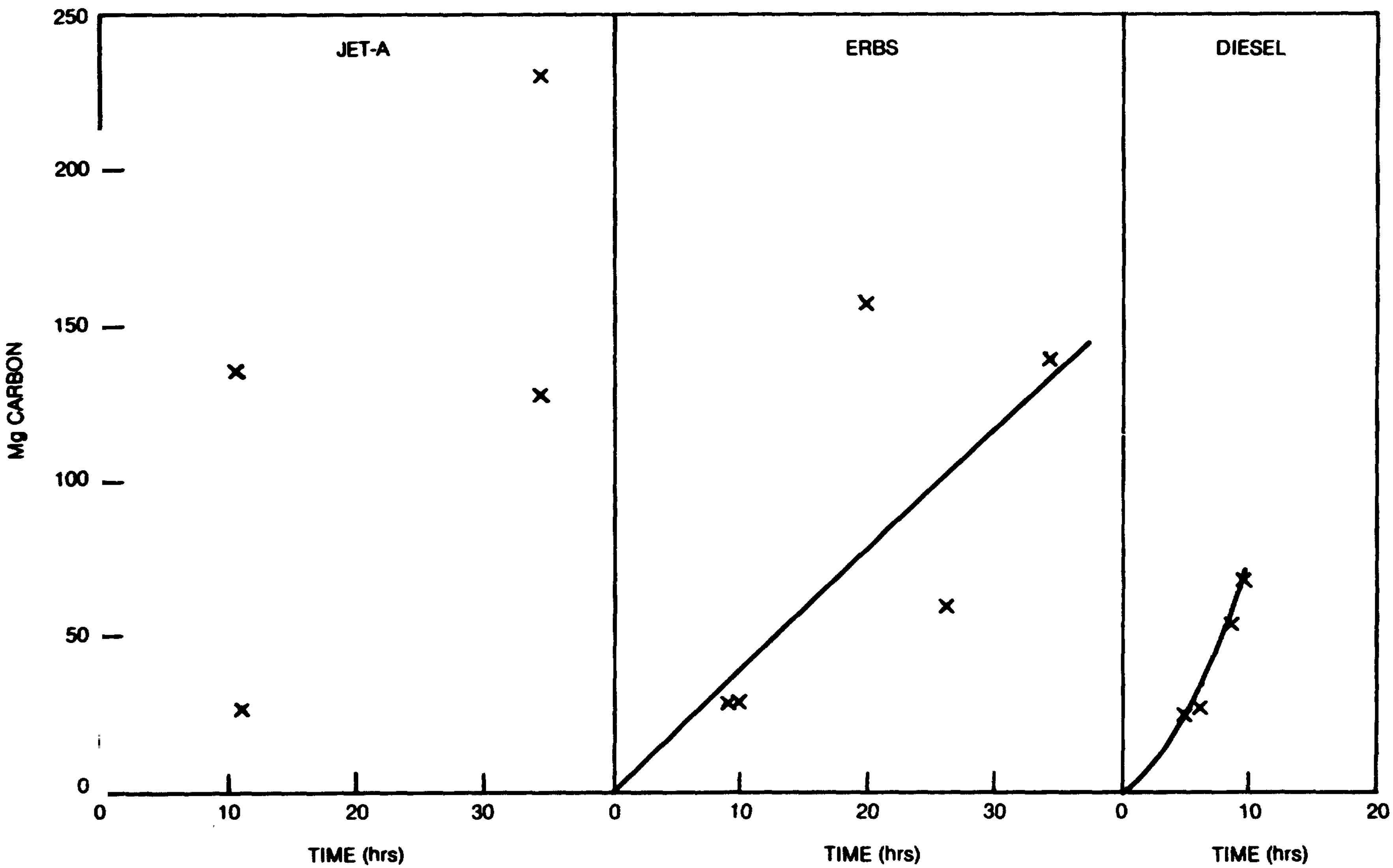

FIG. 35

81-9-41-3

ORIGINAL PAGE IS
OF POOR QUALITY

FIG. 36

SCANNING ELECTRON MICROGRAPHS

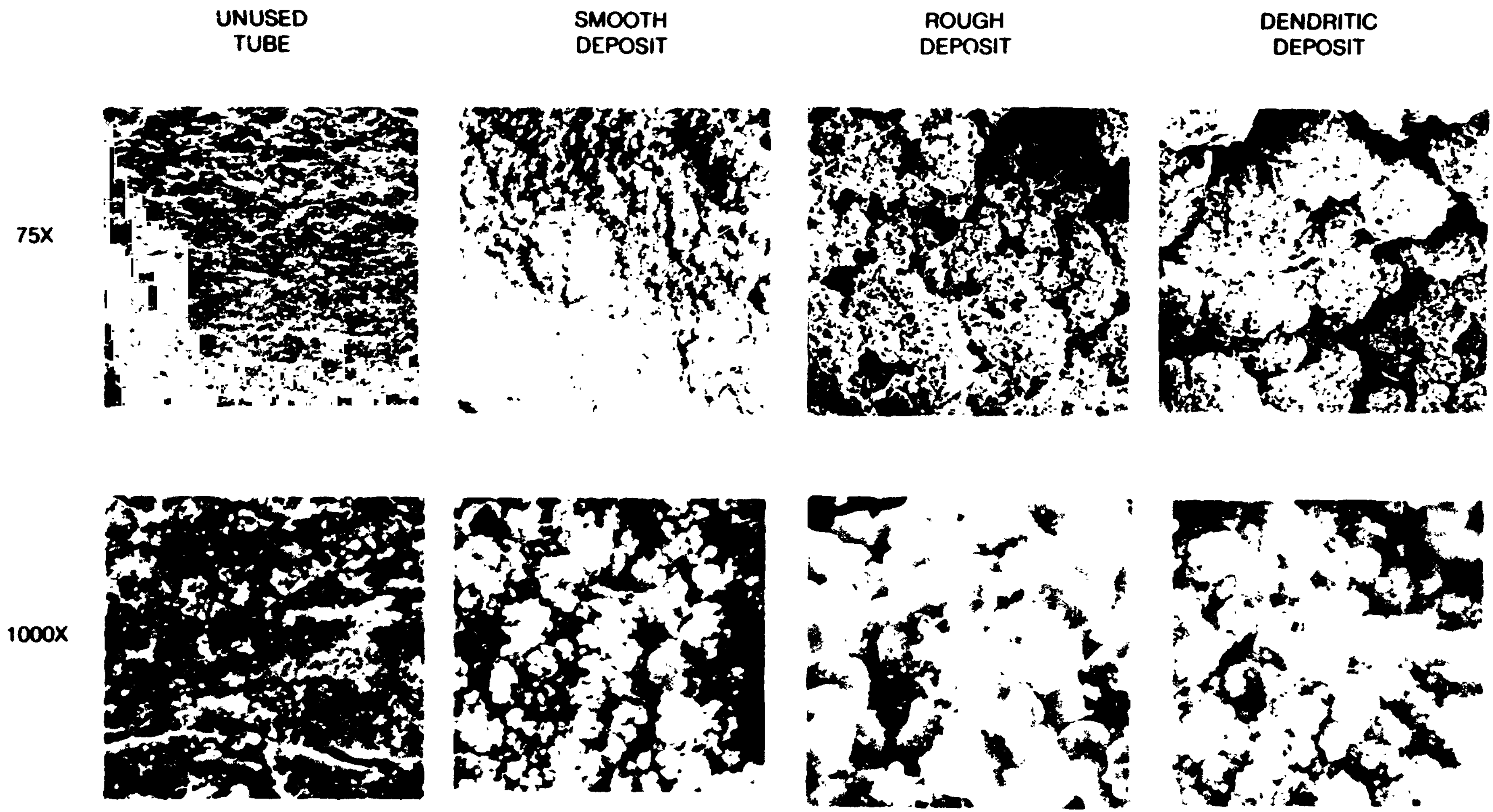

81–9–41–6

ORIGINAL PAGE IS
OF POOR QUALITY

FIG. 37

SCANNING ELECTRON MICROPROBE ANALYSIS

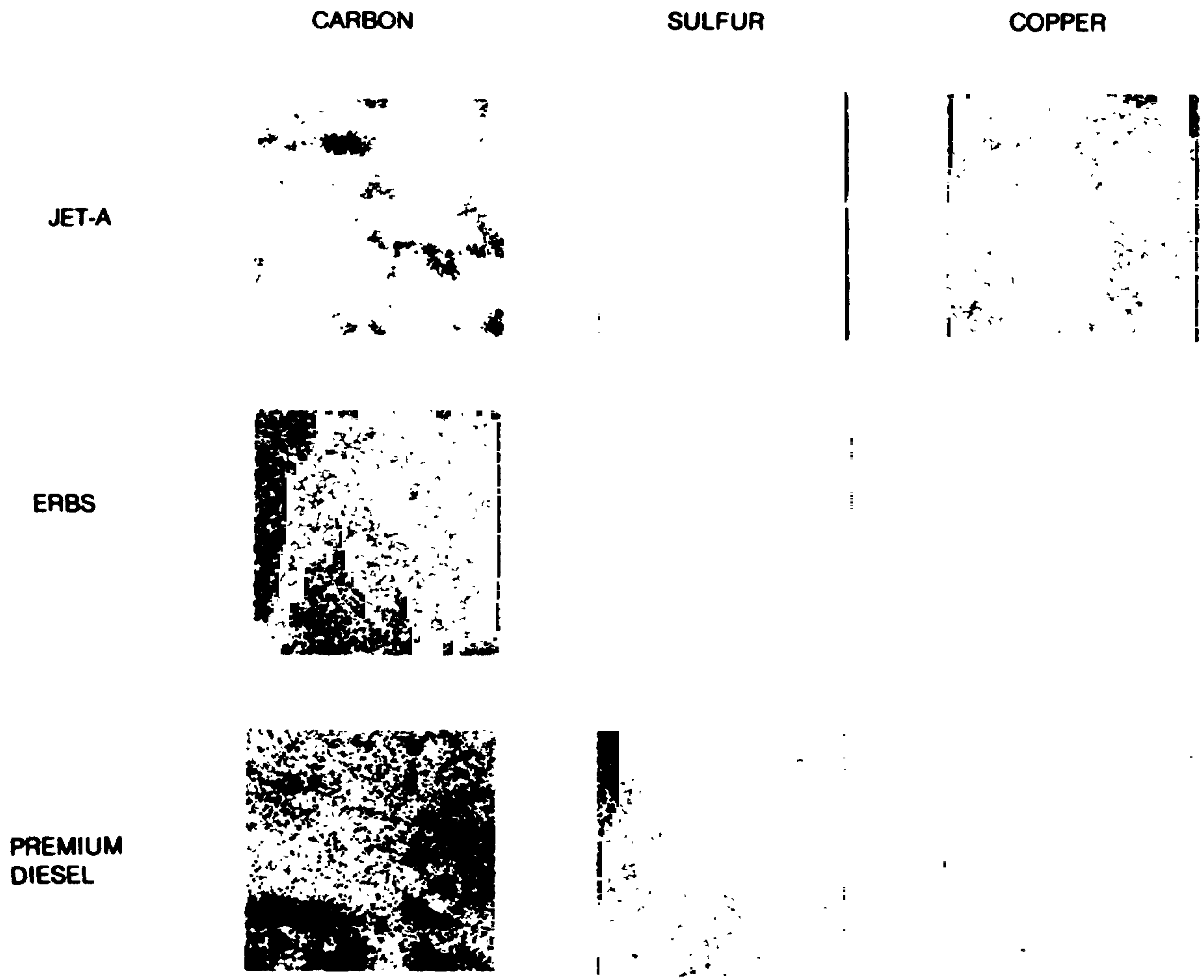

81-9-41-6

EXPANDED MICROPROBE ANALYSIS

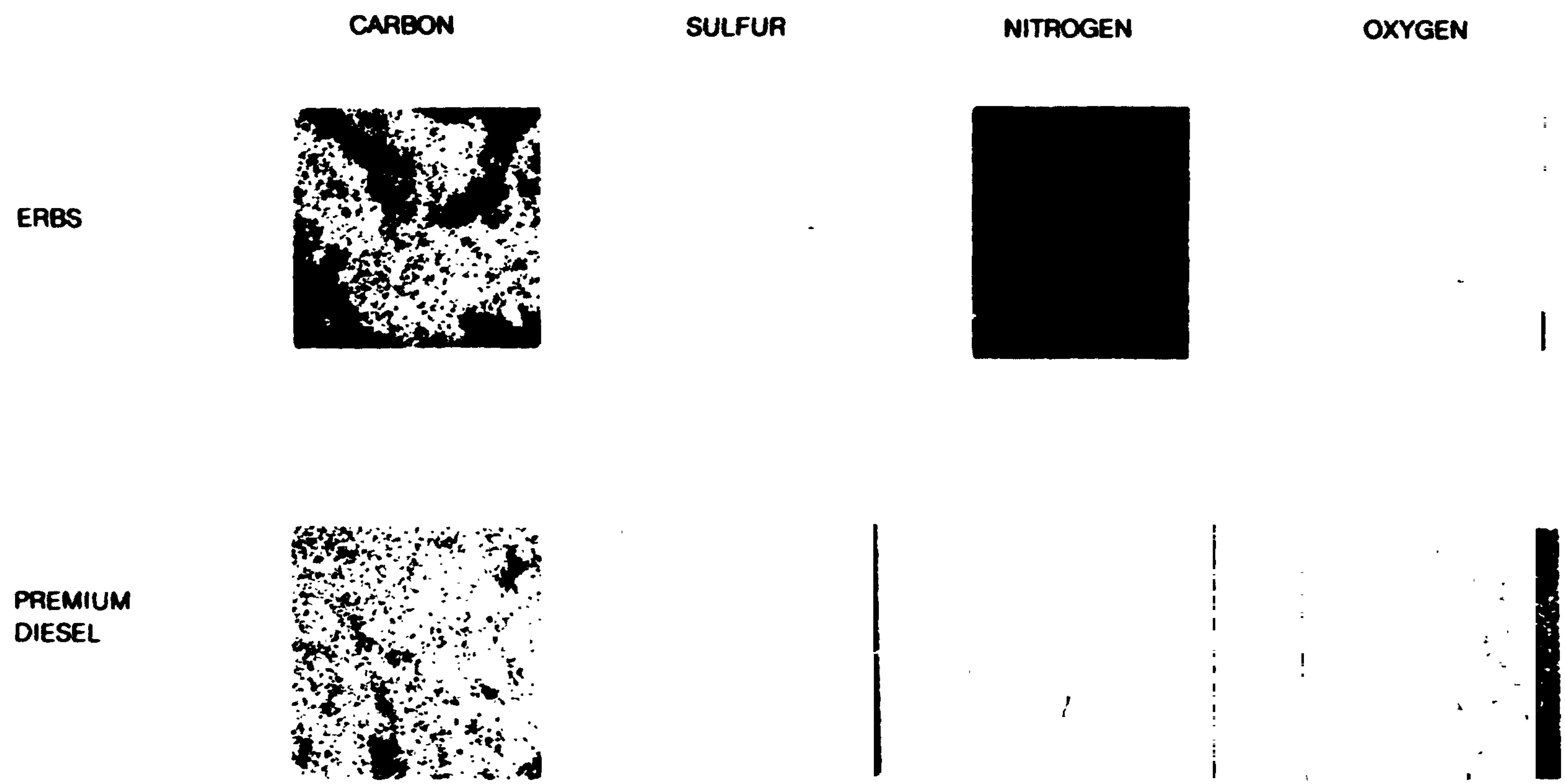

ORIGINAL PAGE IS OF POOR QUALITY

FIG. 38

81-9-41-7

FIG. 39

HEATING — CLEANING CYCLES WITH 815 K AIR

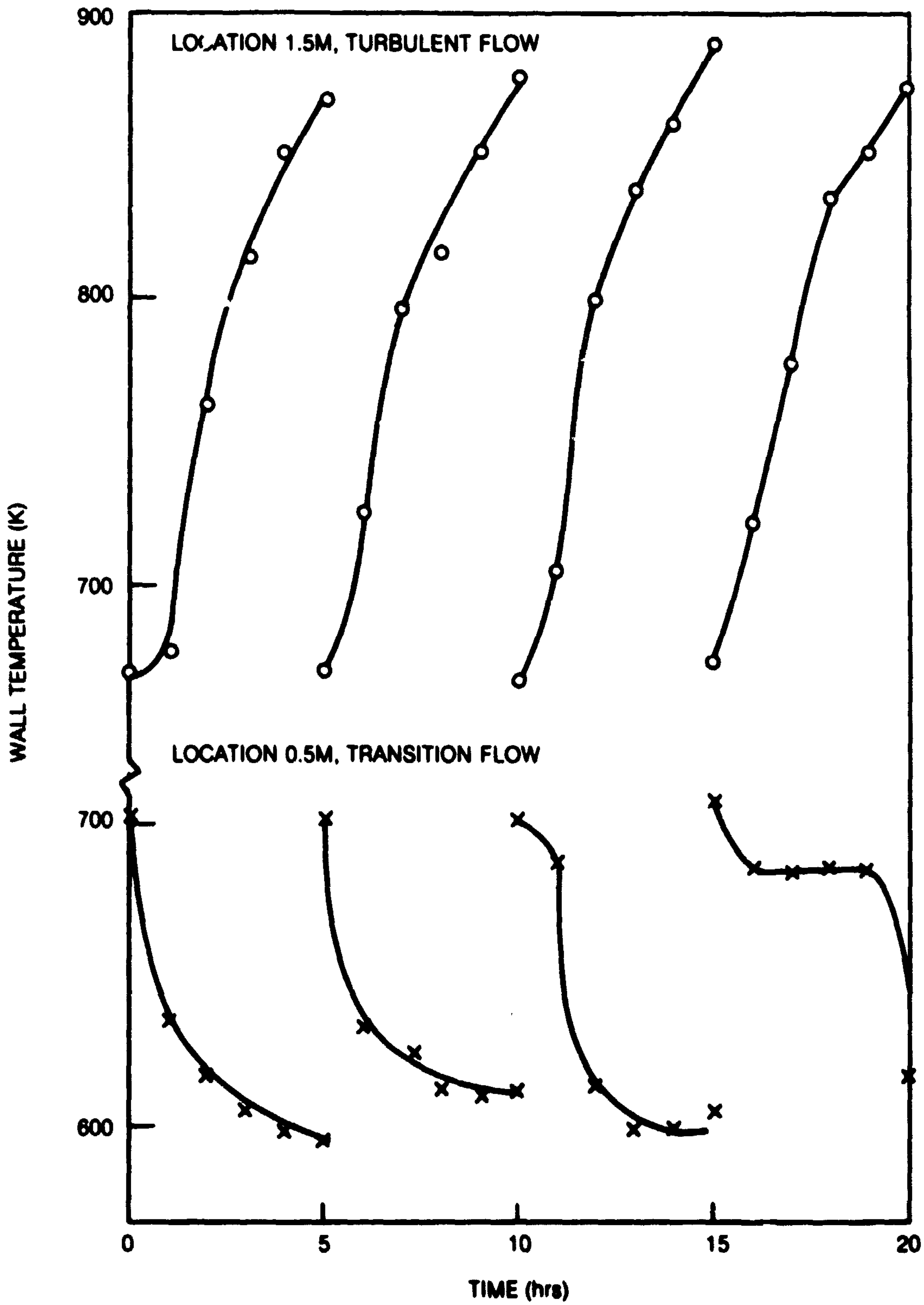

81-9-41-4

HEATING — CLEANING CYCLES WITH 775 K AIR

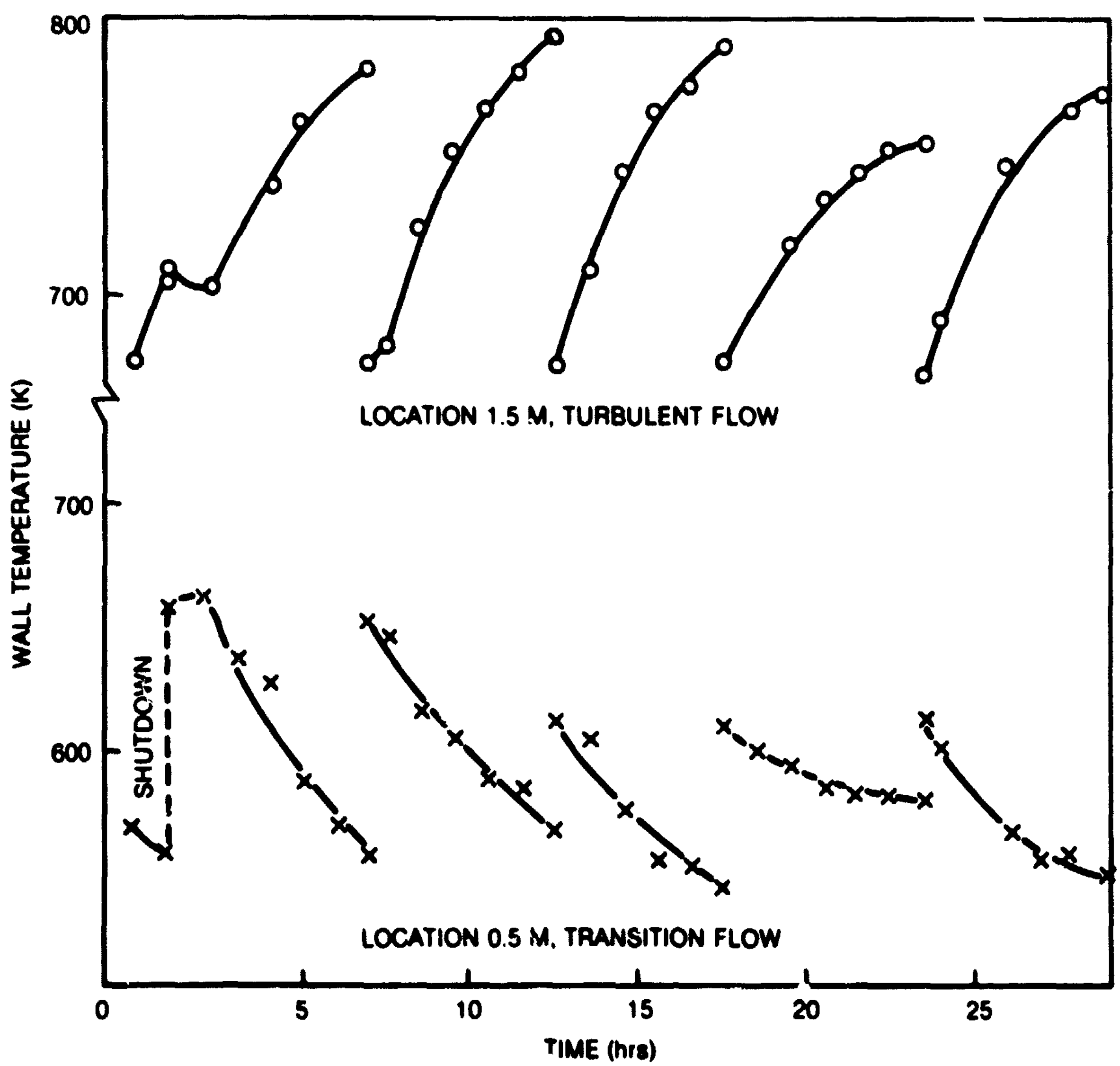

81-8-44-11

APPENDIX

Analytical Evaluation of Effect of Fuel Properties on the Design of the External Fuel Vaporization System

INTRODUCTION

During Phase II of the External Fuel Vaporization Study, the analytical work begun in Phase I was extended to determine the effect of using fuels of a quality poorer than that of current commercial aviation fuel. The results of the analytical evaluation are described in this Appendix. It covers the design and operation of the external fuel vaporization system with fuel properties that represent possible future changes in aviation fuel.

DEFINITION OF FUEL PROPERTIES

Approach

Discussions were held with several individuals concerning the probable properties of future aviation fuels. Included were R. Lohmann, A. Marsh, and F. Haviland of P&WA/CPD, S. Mosier of P&WA/GPD, C. Baker and G. Reck of NASA LeRC, W. Taylor of Exxon, and A. Vranos of UTRC. Publications dealing with future fuels that may be available in the United States which were reviewed included the papers of P. Cambell of United Airlines and A. Momenthy of Boeing published in Ref. A-1, A. Churchill, C. Delaney and H. Lander of AFAPL (Ref. A-2) and W. Dukek and J. Longwell of Exxon (Ref. A-3). Not surprisingly, there is disagreement among the various interested parties. In most instances, the users feel that the present quality of Jet A can be maintained; the suppliers feel that in order to match jet fuel demands with refinery economics in the future, present fuel quality cannot be maintained. It has been noted that recent literature from communist countries contains discussions of improved quality jet fuels (Refs. A-4 and A-5).

In view of the unsettled status of future fuels, it was deemed desirable to investigate fuels with lower quality than present-day Jet A in the present program. The fuel properties which are of specific interest are enthalpy, critical pressure and temperature, viscosity, and thermal conductivity; these properties can be estimated from specific gravity and distillation range data. Also required are data on the deposit formation rate at elevated temperatures (the deposit formation rate is a function of the type of compounds in the fuel and the type and quantity of impurities). It is believed that thermal stability of the fuel is the most important fuel property from the standpoint of heat exchanger design. For the heat exchangers designed in Phase I (Ref. A-6) the thermal resistance of the fuel deposit resulted in a surface area increase of 20 percent in the heat exchanger regions where deposit thickness reached 0.005 cm and 100 percent where the deposit thickness reached 0.020 cm. During cleaning, the heat liberated by the oxidation of a 0.020-cm thick deposit can increase the cleaning air temperature 50 K per cm of length; although some heat release is desirable to overcome loss of heat in the cleaning air to the environment, a rapid air temperature rise can damage the heat exchanger.

Only limited amounts of deposit formation data are available for various fuels. A comparison between deposit thickness after 100 hours for JP-5 (Ref. A-7), Jet A (Ref. A-1) and No. 2 oil (Ref. A-1) is shown in Fig. 1. Linear extrapolation of deposit formation data with time was assumed in the development of the figure. (The validity of such an extrapolation is questionable. According to Ref. A-8, a tube with an inner diameter of 0.46 cm had a deposit from No. 2 oil 0.025 cm thick after 50 hours but the tube was plugged in 120 hours.) Because of severe deposits that would be encountered, fuel with the properties of No. 2 oil should not be considered in this program. The limiting properties that should be considered are essentially those for Experimental Referee Broad Specification (ERBS) fuel as documented in Ref. A-9.

Fuel Property Selection

The fuel properties that were considered in this program include thermal stability, critical temperature and pressure, specific heat and volatility, viscosity and thermal conductivity.

In reviewing the influence of these properties on heat exchanger performance it was found that critical temperature significantly effects the size requirements of the heat exchanger while critical pressure has minimal affects on heat exchanger performance. Specific heat is the slope of the enthalpy temperature curve, and hence changes in enthalpy are directly related to changes in specific heat. Thermal conductivity is not appreciably affected by fuel type while viscosity is appreciably affected.

As stated previously, it is felt that the limiting fuel deposit properties that should be considered are those of Experimental Referee Broad Specification (ERBS) fuel. However, only a single deposit data point is available for ERBS and it is derived from the assumption that the deposit thickness for ERBS and Jet A are the same at their respective JFTOT breakpoint temperatures. The breakpoint temperature for ERBS, obtained from Ref. A-9 is shown in the deposit curve in Fig. A-2. Additional points for the ERBS deposit curve were obtained by assuming that ERBS deposit rates are midway between those of No. 2 heating oil and Jet A. Data for No. 2 oil were obtained from Refs. A-1 and A-10.

The variation in critical temperature, enthalpy and volatility was defined by comparing Jet A with hypothetical fuels having the properties shown in Table 1. Fuel critical temperature and enthalpy can be calculated (Ref. A-11), from specific gravity and the distillation curve; gravity and distillation range of the hypothetical fuels were chosen to obtain an increase in critical temperature and enthalpy.

Table A-1

Properties of Selected Fuels

	Jet-A	Hypothetical Fuels		
		1	2	3
Gravity (API)	43	33.5	53.5	43
Distillation Range (K)				
10%	464	492	372	492
90%	520	520	575	520
Critical Temperature (K)	683	715	683	694
Enthalpy at Tcrit (KCal/Kg)	319	319	346	341

Hypothetical Fuel No. 1 has the specific gravity and 10 percent distillation point of No. 2 heating oil, the 90 percent distillation point of Jet A, a critical temperature higher than that of Jet A but the same enthalpy at the critical temperature. Hypothetical Fuel No. 2 has the specific gravity and 10 percent distillation point of JP-4, the 90 percent distillation poinc of No. 2 heating oil, critical temperature the same as that of Jet A, and a higher enthalpy at the critical temperature. Hypothetical Fuel No. 3 is the same as Jet A except that it has the 10 percent distillation point of No. 2 heating oil and a higher critical temperature and enthalpy than those of Jet A.

To obtain the effect of changes in fuel viscosity, data were obtained (Ref. A-12) for a premium diesel fuel which has a viscosity that is 50 percent higher than that of Jet A at room temperature. It was assumed that the viscosity-temperature curve for the diesel fuel had the same shape as the Jet A curve.

REVISED CALCULATION PROCEDURE

Prior to starting detailed heat exchanger calculations using varying fuel properties, the calculation procedure was reviewed to determine if a previously observed computational problem could be corrected. The analysis failed when the iteration procedure did not result in a stable combination of wall temperature and deposit thickness for the selected fuel deposit curve such as that shown for Jet A in Fig. A-2. It was found that a change in the calculation procedure would stabilize the iteration and the procedure was modified.

In the original calculation procedure, steady state temperature and deposit thickness were assumed at every operating condition being considered and no information concerning the previous flight history was included in the calculation. It is presently felt that a more realistic approach is to assume that the allowable (limiting) deposit buildup of 0.02 cm occurs at the engine cruise condition and that the deposit thickness can be calculated from the wall temperature distribution in a clean heat exchanger. Therefore, a revised procedure has been established in which the analysis of a heat exchanger is made in three steps.

The first two steps in the revised calculation procedure are (1) determine the wall temperatures in a clean heat exchanger at cruise conditions and (2) use the wall temperatures to determine the deposit thickness distribution at 100 hours using the data for Jet A as shown in Fig. A-2. The results of these two calculations are stored in the program and recalled in the analysis of subsequent steady-state or transient operating conditions such as Sea-Level Takeoff (SLTO), altitude relight, and engine acceleration and deceleration.

The revised procedure was applied to the analysis reported in Ref. A-6 and revealed that additional heat exchanger design options are available; specifically, either the heat exchanger size or the inlet air temperature can be reduced as shown in Table A-2.

TABLE A-2

Comparison of Heat Exchanger Analyses

	Length (in direction of hot gas flow) cm	Air Inlet Temperature K	Max. Fuel Side Wall Temp. K
Original Procedure			
SLTO	66	1255	1120
Cruise	66	1145	1005
Revised Procedure-reduced size			
SLTO	48	1255	1010
Cruise	48	1145	880
Revised Procedure-reduced temperature			
SLTO	66	1185	930
Cruise	66	1145	825

With the revised procedure, the maximum fuel side wall temperature is lower than previously calculated. This is a significant design advantage since it was concluded in Ref. A-6 that corrosion-erosion considerations could limit the allowable wall temperature to a value on the order of 800 K.

The revised calculation procedure was also applied to the other operating conditions that were developed in Ref. A-6. Satisfactory steady-state operation at approach and idle are illustrated in Fig. A-3 where the heat exchanger exit fuel temperature is plotted against hot gas inlet temperature. The minimum required fuel temperature which is sufficient to obtain completely vaporized fuel downstream of the throttle can be easily attained. However, the corresponding hot gas inlet temperature and related auxiliary burner fuel-air ratio is too low for efficient combustion at the minimum temperature. A higher fuel-air ratio, approximately 0.010, and the corresponding fuel exit temperature, approximately 750 K, would probably be selected at approach and idle.

Acceleration and deceleration were also investigated using the revised operating procedure. It was found that the times required for the transients between idle and sea level takeoff (SLTO) were reduced by a factor of approximately two. As a result, the increase in transient time resulting from the presence of the heat exchanger is calculated to be 1-2 seconds as compared with 2-4 seconds for the original procedure.

EFFECT OF FUEL PROPERTIES

Increased fuel deposits affect the size of the heat exchanger because deposits add to the overall resistance to heat transfer. Increased deposits also aggravate the problem of deposit removal. Increased viscosity increases the overall resistance to heat transfer by increasing the fuel film resistance. Critical temperature, enthalpy and volatility (which affects critical temperature and enthalpy) of the fuel significantly affect the size requirements of the heat exchanger. An increase in either property increases the amount of heat that must be added to the fuel, and for a fixed hot gas flow rate, the temperature difference across the heat exchanger is also reduced. The effects of fuel critical temperature and enthalpy at the fuel critical temperature can be shown using the following simplified analysis. The heat required to raise the fuel temperature to a specified outlet temperature is:

$$\dot{Q} = (\dot{W}Cp)_F \, (T_{F_{OUT}} - T_{F_{IN}}) \tag{1}$$

This heat is supplied by the hot gas products of combustion:

$$\dot{Q} = (\dot{W}Cp)_A \, (T_{A_{IN}} - T_{A_{OUT}}) \tag{2}$$

The heat gained by the fuel (and lost by the hot gas) can also be expressed in terms of the overall heat transfer coefficient for the heat exchanger:

$$\dot{Q} = UA_W \, (\bar{T}_A - \bar{T}_F) \tag{3}$$

where

$$\bar{T}_A = \frac{1}{2} (T_{A_{IN}} + T_{A_{OUT}}) \tag{4}$$

and

$$\bar{T}_F = \frac{1}{2} (T_{F_{IN}} + T_{F_{OUT}}) \tag{5}$$

These equations may be combined to yield an expression for the product of overall heat transfer coefficient and surface area, a measure of the size of the heat exchanger:

$$UA_W = \frac{2(\dot{W}Cp_F)\,\Delta T_F}{D_I} \tag{6}$$

where

$$\Delta T_F = T_{F_{OUT}} - T_{F_{IN}} \tag{7}$$

and

$$D_I = 2(T_{A_{IN}} - T_{F_{IN}}) - \Delta T_F \left[1 + \frac{(\dot{W}Cp)_F}{(\dot{W}Cp)_A} \right] \tag{8}$$

As the critical temperature is increased while all other parameters are held constant, the required fuel outlet temperature is increased. The amount of heat that must be supplied to the fuel is increased (Eqn. 1). Differentiating Eqn. (6) with respect to ΔT_F yields

$$\frac{\partial(UA_W)}{\partial(\Delta T_F)} = \frac{4(\dot{W}Cp)_F (T_{A_{IN}} - T_{F_{IN}})}{D_I^2} > 0 \tag{9}$$

since necessarily $T_{AIN} > T_{FIN}$. Thus, as the fuel critical temperature is increased, the heat exchanger must become larger.

As the enthalpy of the fuel at the critical temperature is increased while the critical temperature is held constant, the average fuel specific heat is increased and therefore the product $(\dot{W}Cp)_F$, is increased. Thus, the amount of heat that must be supplied by the fuel is increased (Eqn. 1). Differentiating Eqn. (6) with respect to $(WCp)_F$ yields:

$$\frac{\partial(UA_W)}{\partial(\dot{W}Cp)_F} = \frac{2\Delta T_F}{D_I^2} \left[T_{A_{IN}} - T_{F_{IN}} + T_{A_{IN}} - T_{F_{OUT}} \right] > 0 \tag{10}$$

since $T_{AIN} > T_{FOUT} > T_{FIN}$. Thus, as the enthalpy at the fuel critical temperature is increased, the heat exchanger must become larger.

The effects of fuel critical temperature and enthalpy may also be examined in terms of the mean temperature difference across the heat exchanger. Defining

$$\Delta\bar{T} = \bar{T}_A - \bar{T}_F \tag{11}$$

then Eqns. (1) through (5) may be combined to obtain:

$$\Delta\bar{T} = \frac{T_{A_{IN}} - T_{F_{IN}}}{D_2} \tag{12}$$

where

$$D_2 = 1 + \frac{UA_W}{2}\left[\frac{1}{(\dot{W}Cp)_A} + \frac{1}{(\dot{W}Cp)_F}\right] \tag{13}$$

Upon differentiating (Eqn. 12) with respect to ΔT_F and using Eqn. (9) in the resulting expression, it can be shown that:

$$\frac{\partial(\Delta\bar{T})}{\partial(\Delta T_F)} < 0 \tag{14}$$

Upon differentiating (Eqn. 12) with respect to $(\dot{W}Cp)_F$ and using Eqns. (6) and (10), it can be shown that

$$\frac{\partial(\Delta\bar{T})}{\partial(\dot{W}Cp)_F} < 0 \tag{15}$$

Thus, an increase in either the fuel critical temperature (T_F) or critical enthalpy ($\dot{W}C_p$) results in a decrease in the mean temperature difference across the heat exchanger.

This simplified analysis is presented only for illustrative purposes. A more rigorous analysis is contained in the computer program that is used for heat exchanger performance analysis and design.

The vaporizer design approach that was used to evaluate the effect of fuel properties consisted of calculating the size and weight of the heat exchanger for each fuel described previously. The required computer program input and the target fuel temperature were identified for each fuel and the heat exchanger size was varied until the target temperature was obtained. Intermediate points were also included in order to present the results in graphical form.

Deposit Thickness

An increase in deposit formation because of the differences in properties between Jet A and ERBS would increase the weight of the heat exchanger by 22 kg as shown in Fig. 4. The maximum wall temperature would also be increased, but the amount (20 K) is not considered to be significant. However, a very significant difference between Jet A and ERBS is the deposit formation rate which would result in a maximum thickness of 0.033 cm with ERBS after 100 hours compared with 0.020 cm with Jet A. A maximum thickness of 0.020 cm is advisable from a cleaning standpoint; therefore, the operating time between cleaning for ERBS would be 61 hours compared with 100 hours with Jet A.

Critical Temperature

An increase in critical temperature would increase the weight of the heat exchanger as shown in Fig. A-5. The maximum wall temperature with hypothetical Fuel No. 1 would be 40 K lower than the wall temperature with Jet A. A tradeoff between weight and wall temperature is possible; therefore, the weight penalty of 40 kg can be slightly reduced in a more extensive design effort.

Enthalpy

An increase in fuel enthalpy could increase the weight of the heat exchanger by 40 kg as shown in Fig. A-6. Also required would be an increase in hot gas flow of 10 percent to supply the required energy to the fuel. The increased gas flow would be obtained by an increase in the compressor bleed flow. This would not seriously affect the engine cycle because only a portion of the bleed flow would be utilized in the vaporization system. However, an increased bleed flow of 10 percent slightly affects the auxiliary combustor size and the gas flow distribution system. The maximum wall temperature with hypothetical Fuel No. 2 would be 40 K lower than the wall temperature with Jet A.

Volatility

An increase in volatility exemplified by Hypothetical Fuel No. 3 was defined as an increase in the temperature corresponding to the distillation of 10 percent of the fuel. The critical temperature and the enthalpy at critical temperature of the fuel are also increased (Table A-3) which would result in an increase in the heat exchanger weight of 40 kg and the required gas flow rate by 7 percent. These effects are shown in Fig. A-7. The maximum wall temperature with hypothetical Fuel No. 3 would be 45 K lower than that with Jet A.

Viscosity

The effect of fuel viscosity on heat exchanger size was found to be negligible. The heat transfer resistance of the fuel film in the heat exchanger would be low compared with the resistance of the air film, and both would be lower than the maximum resistance of the deposit. Therefore, a change in the fuel film resistance resulting from an increased fuel viscosity would not noticeably affect the overall heat transfer rate or the weight of the heat exchanger.

Engine Transient Response and Altitude Relight

The effect of fuel properties on the transient times required between idle and SLTO during acceleration and deceleration was investigated for ERBS and hypothetical Fuels Nos. 1 and 2. Transient times for the three fuels would be approximately one second (slightly lower than for Jet A). Engine transient response would not be substantially affected by the fuel properties.

The effect of fuel properties on altitude relight was investigated for ERBS and hypothetical Fuels Nos. 1 to 3. Altitude relight with Jet A requires the fuel temperature in the heat exchanger be raised to 585 K in order to obtain a dew point of 495 K. The heat exchanger calculations indicated that the target temperature of Jet A can be reached with all of the other fuels with the heat exchanger size and airflow (compressor bleed flow) as specified by the sea level take off design requirements. However, the required fuel temperature of ERBS is estimated to be approximately 40 K higher than for Jet A. If the airflow were to be maintained at the level used with Jet A, the heat exchanger weight would be increased by 100 percent. This would correspond to an increase in vaporization system weight of 90 percent.

Hypothetical Fuels No. 1 and 3 (increased critical temperature and volatility) have the same 90 percent distillation point as Jet A; therefore, the required fuel temperature for these fuels should be close to that of Jet A. The use of Fuel No. 3 would require an increase in airflow and since compressor bleed flow will be difficult to obtain at altitude relight conditions, this fuel will cause relight problems. Hypothetical Fuel No. 2 (increased critical enthalpy) has a higher 90 percent distillation point than Jet A requiring an increase in heat exchanger size for altitude relight. Fuel No. 2 also would require an increase in airflow; therefore, relight problems will be encountered with this fuel.

Engine Performance

In Ref. 6 it was found that the fuel vaporization system would permit an improvement in engine performance because the cooled gas (vitiated air) leaving the heat exchanger can be used more effectively for turbine cooling than hot compressor bleed air at certain turbine locations. Performance improvement included specific fuel consumption, thrust, and thrust/weight ratio when the engine bypass ratio was varied and the engine core remained unchanged. The engine performance results were reviewed to determine if the effect of the external fuel vaporization system on engine weight can be estimated. The results indicated that the improvement in thrust/weight ratio of approximately 3 percent resulting from the use of heat exchanger exit air for turbine cooling can be applied to engine weight to estimate potential weight reduction in a re-designed engine. The projected E^3 engine weight is at present in the vicinity of 3000 Kg; therefore, the vaporization system with Jet-A has the potential of decreasing that weight by approximately 100 Kg.

Estimates of the effect of fuel properties indicate that use of any of the other fuels being considered in this program would result in a weight saving which is approximately the same as that with Jet-A. The use of any of the other fuels in conjunction with an external fuel vaporization system would produce the same reduction in specific fuel consumption as Jet-A (0.5 percent at cruise, based on an increase in turbine inlet temperature).

CONCLUSIONS

The assessment of the effect of fuel properties indicated that in comparison with Jet-A, future aircraft fuels will impose more stringent design requirements on the external fuel vaporization system. Maintenance of the engine will be more frequent; the allowable operating time between cleaning will be decreased with fuels having a greater tendency for deposit formation. Vaporization system weight will be increased by 20 to 40 percent (0.5 to one percent of engine weight). Although engine transient response and engine performance will not be appreciably affected, altitude relight will be considerably more difficult. The calculated gains in engine performance attributable to the use of Jet-A with an external fuel vaporization system are retained with lower quality fuels.

REFERENCES

A-1. Aircraft Research and Technology for Future Fuels. NASA Conf. Publ. 2146. 1980.

A-2. Churchill, A. V., C. L. Delaney, and H. R. Lander: Future Aviation Turbine Fuels. J. Aircraft, Vol. 15, No. 11, Nov. 1978.

A-3. Dukek, W. G. and J. P. Longwell: Alternative Hydrocarbon Fuels for Aviation. Exxon Air World. Vol. 29, No. 4, 1977.

A-4. Bekiesinski, K: Some Aspects of Aircraft Jet Engine Fuels (Translation). NASA TM 75395. 1979.

A-5. Veselyanskaya, V. M., E. D. Radchenko, B. A. Eglin, and A. A. Kiryanova: Effect of Naphthenoaromatic Hydrocarbons on the Oxidizability of Hydrotreated RT Jet Fuel (Translation). Chemistry and Technology of Fuels and Oils. June, 1980.

A-6. Szetela, E. J. and L. Chiappetta: External Fuel Vaporization Study, Phase I Report. NASA CR 159850. June 1980.

A-7. Taylor, W. F. and J. W. Frankenfeld: Development of High Stability Fuel. Final Report for Phase I. Exxon Report GRU.13GAHF.75. January 1975.

A-8. Szetela, E. J: Deposits from Heated Gas Turbine Fuels. ASME 76-67-9. 1976.

A-9. Prok, G. M. and G. T. Seng: Initial Characterization of an Experimental Referee Broadened-Specification (ERBS) Aviation Turbine Fuel. NASA TM 81440. January, 1980.

A-10. Spadaccini, L. J. and E. J. Szetela: Approaches to the Prevaporized-Premixed Combustor Concept for Gas Turbines. ASME GT-85-75. 1975.

A-11. Technical Data Book - Petroleum Refining. Second Edition. American Petroleum Institute. 1970.

A-12. Cohen, S.: Private Communication. October, 1980.

List of Symbols

A	Surface Area, m^2
Cp	Specific heat at constant pressure, cal/g-K
$\dot{Q}$	Heat transfer rate, cal/hr
T	Temperature, K
U	Overall heat transfer coefficient, cal/hr-m^2-K
$\dot{w}$	Weight flowrate, g/hr

Subscripts

A	Hot gas
F	Fuel
IN	Inflow condition
OUT	Outflow condition
w	Wall

DEPOSIT THICKNESS AFTER 100 HOURS

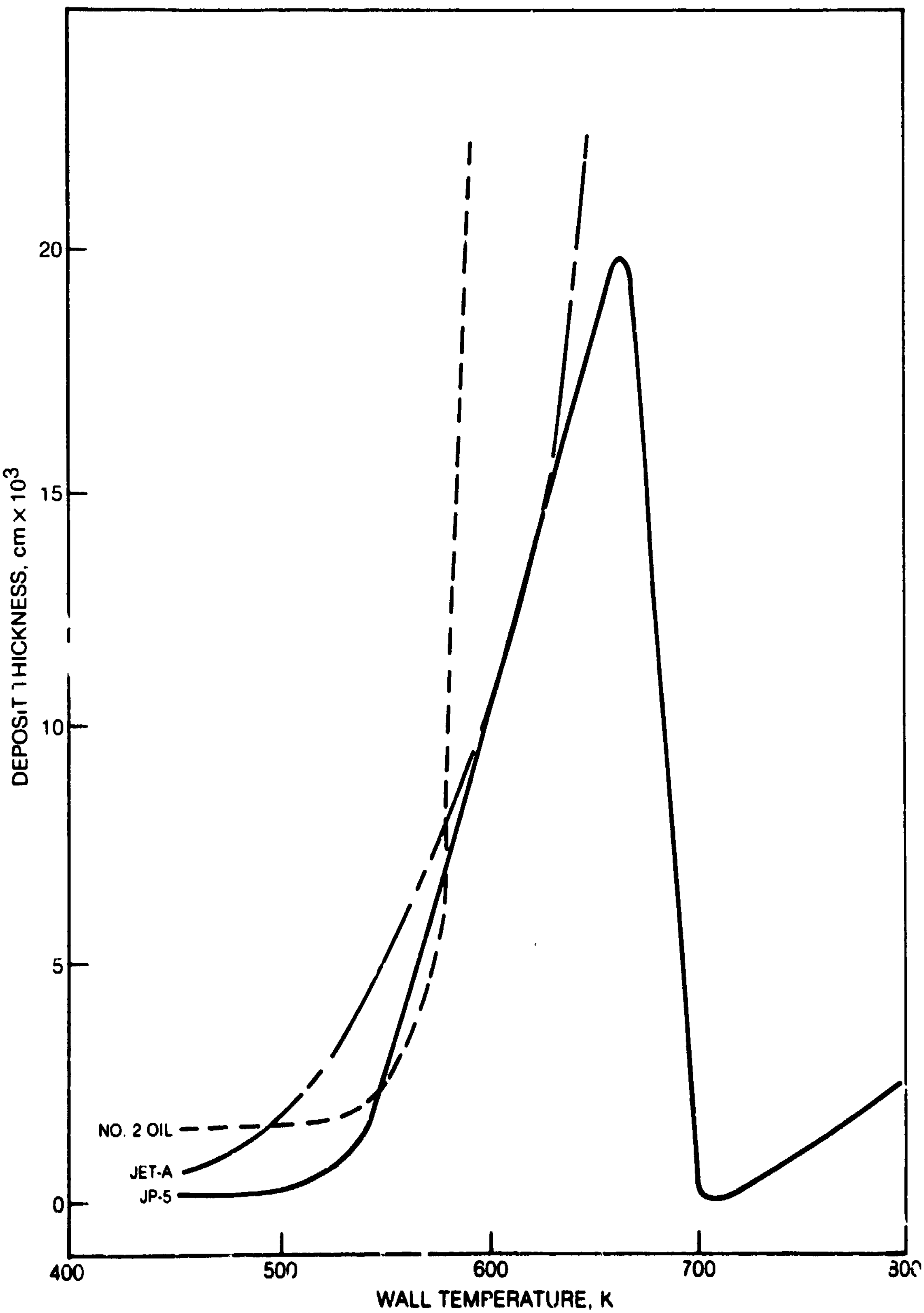

80-10-15-1

DEPOSIT FORMATION FOR JET-A AND ERBS

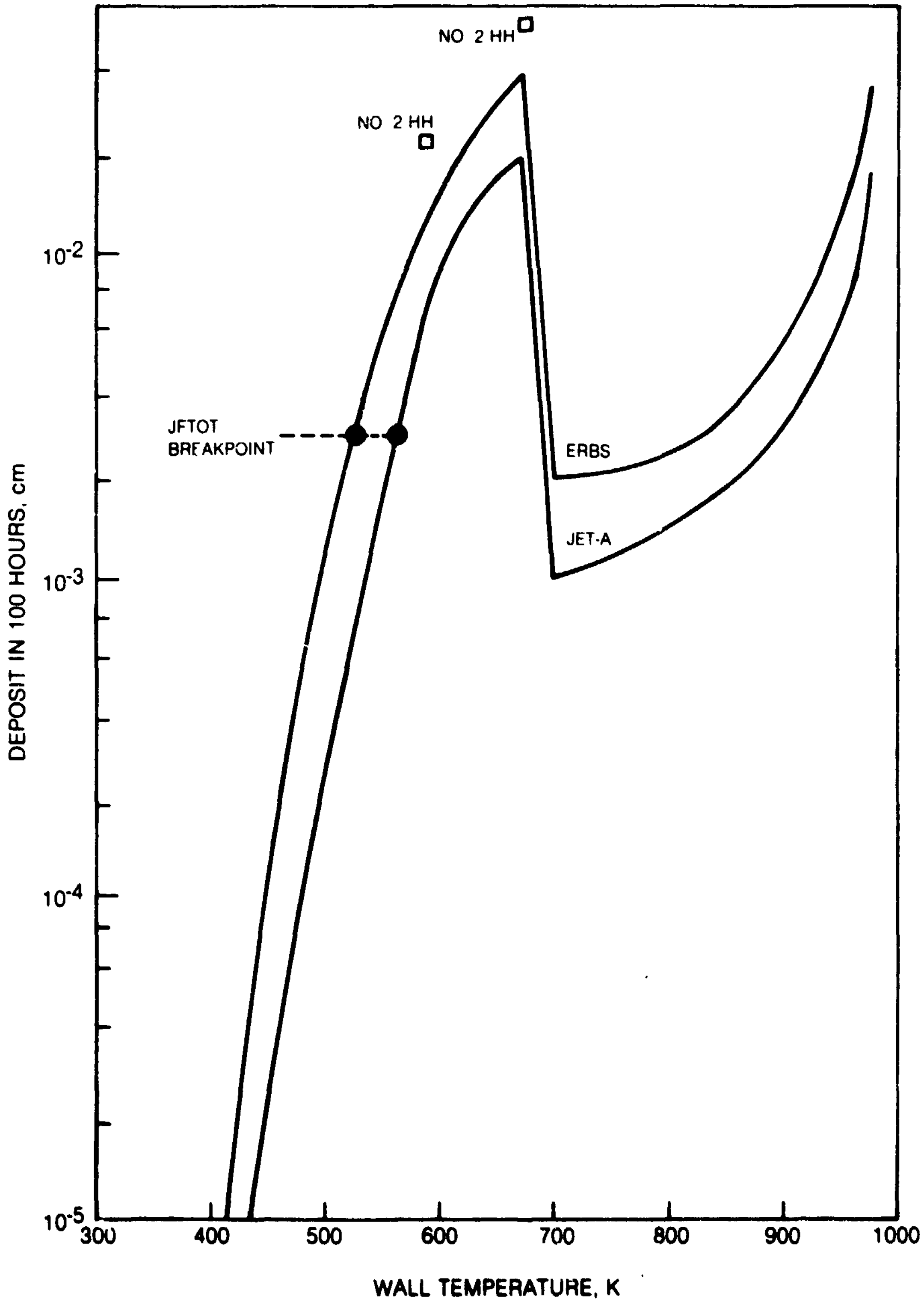

HEAT EXCHANGE PERFORMANCE AND AUXILARY BURNER REQUIREMENTS

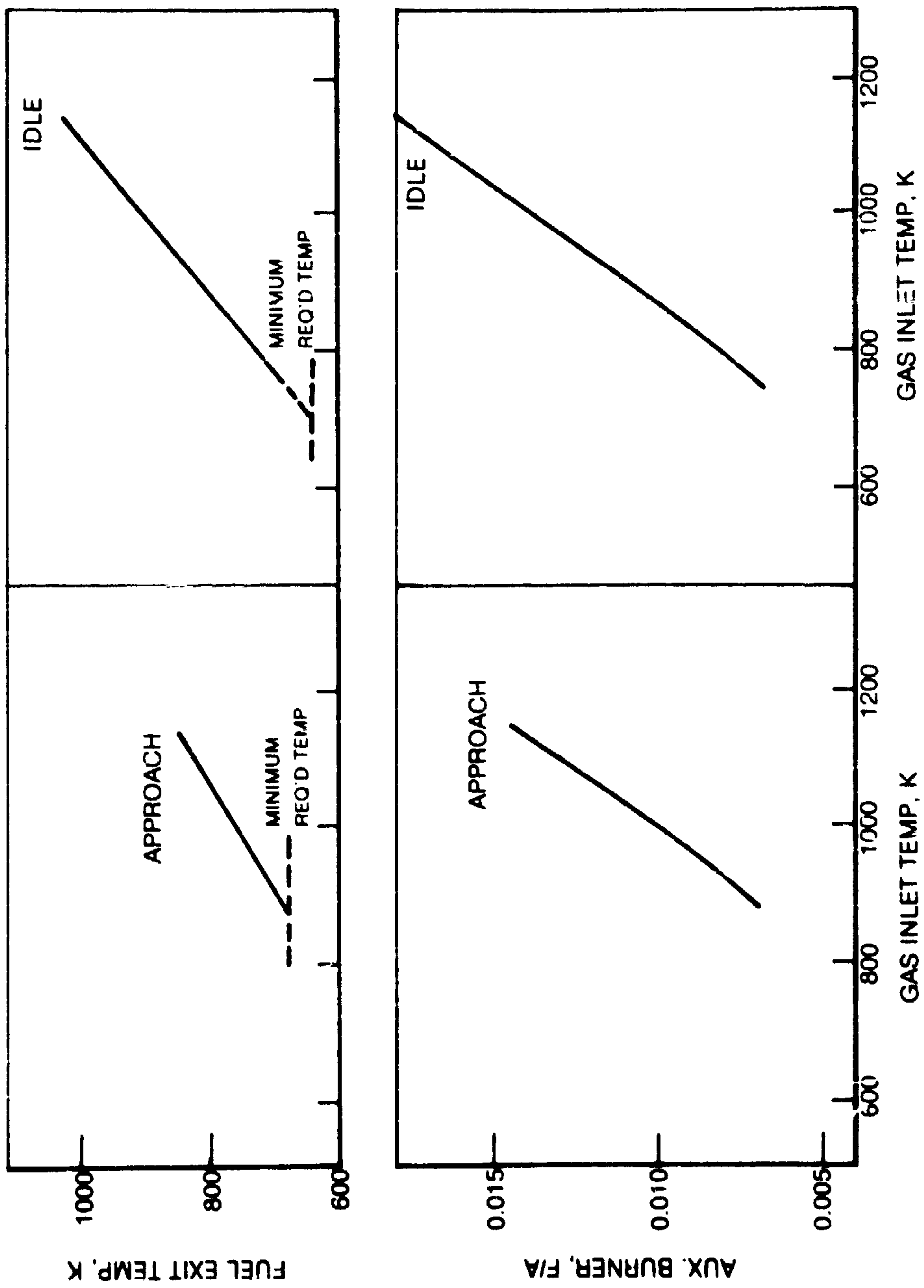

80-12-86-1

EFFECT OF MAXIMUM DEPOSIT THICKNESS

HEAT EXCHANGER DESIGN PARAMETERS

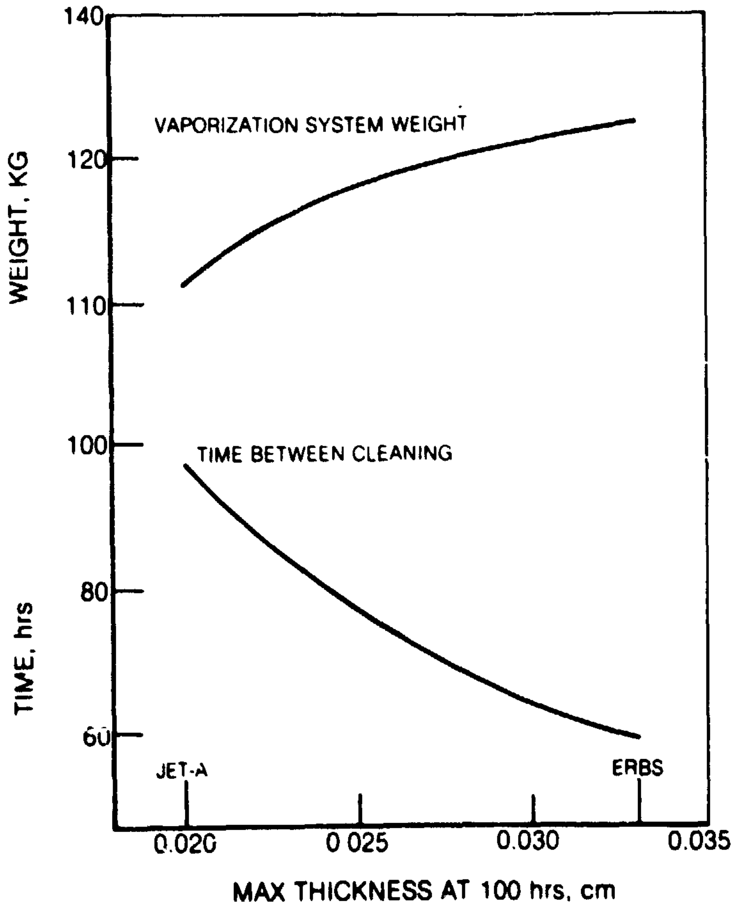

EFFECT OF CRITICAL TEMPERATURE ON WEIGHT

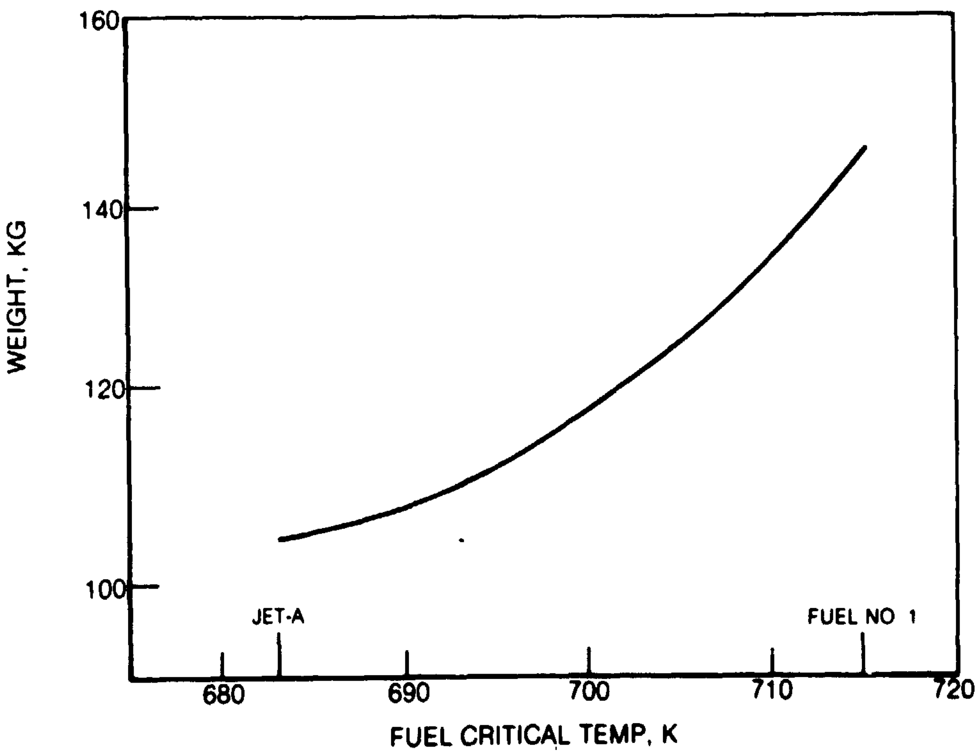

EFFECT OF ENTHALPY AT THE CRITICAL TEMPERATURE ON WEIGHT

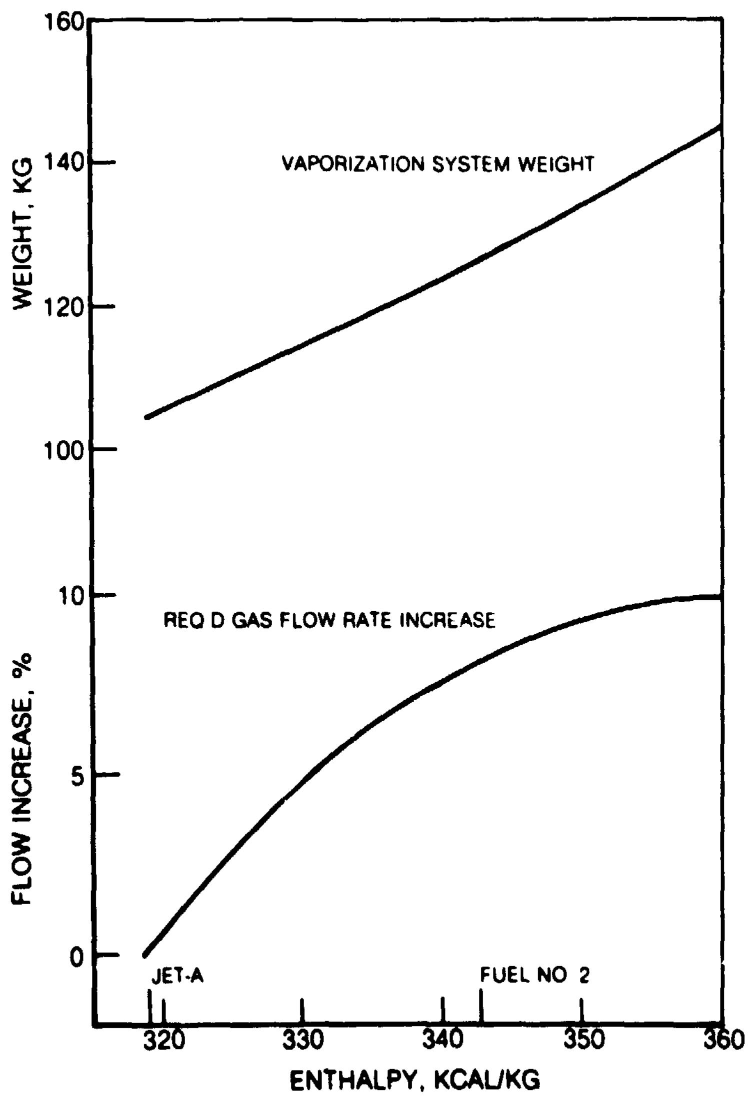

EFFECT OF FUEL VOLATILITY ON WEIGHT